UNIVERSITE DE LIMOGES

UNIVERSITE DE EREVAN

ECOLE DOCTORALE 521
FACULTE DES SCIENCES ET TECHNIQUES
INSTITUT DE RECHERCHE XLIM – DEPARTEMENT PHOTONIQUE

Thèse N° 44-2012

Manuscrit de Thèse
en vue d'obtenir le grade de

DOCTEUR DE L'UNIVERSITÉ DE LIMOGES
DOCTEUR DE L'UNIVERSITÉ DE EREVAN

Discipline / Spécialité : Electronique des Hautes Fréquences et Optoélectronique

Présentée et soutenue par

MERI KALASHYAN

Le 24 novembre 2012

NOVEL NONLINEAR-OPTIC METHODS FOR SIGNAL PROCESSING AND DELIVERY ON FEMTOSECOND TIMESCALE

Manuscrit de Thèse dirigée par Frédéric LOURADOUR et Levon MOURADIAN

JURY:

Rapporteurs

M. Aram Papoyan	Professeur, Directeur de Recherches, Institut de Recherche physique, Arménie
M. Ruben Zadoyan	Directeur de Recherche (Newport Technology & Applications Center)

Examinateurs :

M. Alain Barthelemy	Directeur de Recherches CNRS, Institut de Recherche XLIM, Département Photonique, Limoges
M. Frédéric Louradour	Professeur, Institut de Recherche XLIM, Département Photonique, Université de Limoges
M. Levon Mouradian	Professeur, Directeur de Recherche de laboratoire d'optique ultra-rapide, Université de Erevan

CONTENTS

INTRODUCTION 4

CHAPTER I. PULSE CONTROL ON FEMTOSECOND TIMESCALE 26

I.1. Prism-lens dispersive delay line for control of femtosecond pulses 27

I.1.1. Principle *29*

I.1.2. Fourier Transform spectral interferometry for shaped pulse characterization *33*

I.1.3. Spectral interferometric study of prism-lens dispersive delay line *35*

I.2. Synthesis of Fourier transform rectangular pulses in the process of spectral compression 41

I.3. Femtosecond pulse shaping based on 2D phase-only spatial light modulator 49

Conclusion to chapter I 54

CHAPTER II. FEMTOSECOND PULSE FIBER DELIVERY WITH OPTIMIZED DISPERSION CONTROL BY REFLECTION GRISMS AT 800 NM 55

II.1. Fiber delivery: basic features and numerical modelling 56

II.2. Delivery of 18 fs nanojoule pulses by large mode area photonic crystal fiber 64

II.3. Spatial light modulator-based pulse shaping and compression 74

Conclusion to chapter II 81

CHAPTER III. WIDEBAND SPECTRAL INTERFEROMETRY RESOLVED IN TIME 82

III.1. Pulse measurement by time-to-frequency conversion with a quadratic nonlinearity 84

III.2. SPIRIT for characterization of few-cycle femtosecond pulses 90

III.2.1. General description of SPIRIT *90*

III.2.2. Specificity of wideband SPIRIT *92*

III.2.3. Pulse reconstruction algorithm *94*

III.2.4. Experimental results *95*

III.2.5. Chirpogram *96*

III.2.6. Pulse measurements at the exit of fiber delivery scheme *98*

Conclusion to chapter III 100

SUMMARY 101

REFERENCES 104

MAIN DESIGNATIONS 116

ACKNOWLEDGEMENTS 117

Introduction

Since the advent of the laser over thirty years ago, there has been sustained interest in the quest to generate ultrashort laser pulses in the picosecond and femtosecond range. Over the last several years progress has been spectacular. Pulses of ~10 fs [1] and below (a few optical cycle pulses) [2] are now available directly from mode-locked titanium: sapphire lasers [3]. Even shorter pulses down to 6 fs [4] have been generated by using nonlinear optical pulse compression techniques. Turn-key femtosecond solid-state lasers are now commercially available; home-built as well as commercial femtosecond lasers and amplifiers are now present in laboratories around the world. This widespread access to femtosecond laser systems has accelerated the already considerable interest in this technology for studies of ultrafast phenomena in solid-state, chemical and biological materials, for generation and investigation of solid density plasmas, for fundamental studies of extremely high intensity laser-matter interactions and for high brightness X-ray generation, as well as for characterization of high-speed electronic and optoelectronic devices and systems, optical communications, medical imaging, and other applications. In the relatively near term one can also foresee the development of “practical”, power efficient femtosecond pulse systems, based either on semiconductor diode lasers, doped fiber lasers, or diode-pumped solid-state lasers, which will further extend the use of ultrashort pulses, particularly for commercial applications.

Femtosecond lasers constitute the world’s best pulse generators. However, many applications will require not only optical pulse generators, but also ultrafast optical waveform generators, in analogy with electronic function generators, which widely provide electronic square waves, triangle waves, and indeed arbitrary user specified waveforms. Over the past decade powerful optical waveform synthesis methods have been developed, which allow generation of complicated ultrafast optical waveforms according to user specification. Coupled with the now widespread availability of femtosecond laser systems, pulse shaping systems can potentially have a strong impact as an experimental tool providing unprecedented control over ultrafast laser waveforms for ultrafast spectroscopy, nonlinear optics, and high power amplification.

Many applications (such as multiphoton microscopy, nonlinear endoscopy) require also methods for the delivery of ultrashort pulses via an optical fiber [5]. The high peak power makes it difficult to deliver these pulses through conventional single mode fibers (SMFs) without pulse

broadening caused by group-velocity dispersion (GVD) combined with self-phase modulation. To overcome this problem, several types of optical fibers have been used.

From the other side the generation of pulse durations below 6 fs in the visible and near-infrared spectral range make characterization of these pulses a demanding task. Many years it was possible to generate ultrashort pulses but not to measure them. Although techniques such as spectrometry and autocorrelation were available, they provided only a vague measure of a pulse. Conventional autocorrelation techniques, which require the prior knowledge of the pulse shape, can be used to determine rough estimates of the pulse duration. For a more precise measurement, a variety of methods has been proposed allowing for a full reconstruction of pulse amplitude and phase from measured data only [6].

Review of the literature

Ultrashort lasers are an important tool to probe the dynamics of physical systems at very short timescales, allowing for improved understanding of the performance of many devices and phenomena used in science, technology, and medicine. In addition ultrashort pulses also provide high peak intensity and a broad optical spectrum, which opens even more applications such as material processing, nonlinear optics, attosecond science, and metrology. There has been a long-standing, ongoing effort in the field to reduce the pulse duration and increase the power of these lasers to continue to empower existing and new applications.

Efforts to control the temporal structure of individual laser pulses are almost as old as the pulsed laser itself. Femtosecond pulse shaping, pioneered by Heritage and co-workers over 15 years ago [7], has found excellent application in fundamental and applied science. Pulse shaping is the technique which controls the ultrashort pulse shape, and it became of great technological interest. Pulse shaping allows us to create modified and complex waveforms of pulses from optical sources of single pulse according to the user's specifications. Femtosecond pulses have extremely short duration, high peak power and large spectral bandwidth, so shaped femtosecond pulse is useful in different types of applications.

Techniques for the precise synthesis and control of the temporal shape of optical pulses with durations in the picosecond and subpicosecond regimes have been applied to diverse problems in, for example, spectroscopy [8], microscopy [9], laser control of matter [10], laser pulse compression

[11], telecommunications [12], and optical metrology [13]. To give a few examples, (sub-) picosecond flattop optical pulses are highly desired for nonlinear optical switching [14] and wavelength conversion applications [15], spectrotemporal imaging and time lens; picosecond parabolic pulse shapes are of interest to achieve ultra-flat self-phase-modulation (SPM) – induced spectral broadening in supercontinuum generation experiments [16]. The most commonly used technique for arbitrary picosecond and sub-picosecond optical pulse shaping is based on spectral amplitude and/or phase linear filtering of the original pulse in the spatial domain; this technique is usually referred to as “Fourier- domain pulse shaping” [17]. Drawbacks associated with this approach, including the need for a high-quality bulk-optics setup and limited integration with waveguide devices for incorporation in fiber optics systems, have motivated research on alternate solutions for optical pulse shaping. This includes the use of integrated arrayed waveguide gratings (AWGs) [18], and fiber gratings (e.g. fiber Bragg gratings [19], or long-period fiber gratings [20]). The main drawback of the fiber grating approach [19, 20] is the lack of programmability: a grating device is designed to realize a single pulse shaping operation over a specific input pulse and once the grating is fabricated, these specifications cannot be later modified. Recently, a new reconfigurable optical pulse shaping technique [21] which is based on synthesizing the desired output pulse shape by coherently combining a set of input pulse replicas with different time delays (e.g. using concatenated two-arm interferometers) was demonstrated.

Liquid crystal spatial light modulators (LC-SLMs) have been extensively used for femtosecond pulse shaping and nonlinear chirp compensation for the past ten years because of their flexibility for adaptive computer programming control [22]. Although acousto-optic modulators [23, 24] can also realize adaptive programming control as narrowband tunable filters and narrowband phase modulators. Moreover, the throughput efficiency of the acousto-optic modulator decreases rapidly with the increase of the spectral bandwidth, typically less than 10% over a 450 nm spectral width. In addition, the several-centimetres-long acousto-optic crystal [25] cannot bear the high peak power because of self-phase modulation, and the small aperture limits the achievable pulse energy, so it can not be applied to high-energy few-cycle-to-monocycle optical pulses. On the other hand, the LC-SLM has the advantage of a larger bandwidth, lower spatial dispersion, and higher efficiency compared with the programmable acousto-optic modulator. Therefore it is extraordinarily suitable for pulse shaping and nonlinear chirp compensation of an ultra-broadband octave-spanning spectra

[26]. The LC-SLM paves the way for coherent synthesis of single-cycle optical pulses and coherent control of atoms and molecules. Recently, 2.6 fs single isolated optical pulses, which contain only 1.3 optical cycle, were generated by nonlinear chirp compensation of the spectrum broadened by SPM as well as induced phase modulation in an argon-gas-filled hollow fiber by using an LC-SLM [27]. These are till now the shortest isolated optical pulses generated in the visible range, which shows the powerful capability of phase modulation of the LC-SLM. More recently a UV-transparent LC-SLM [28] was fabricated, and the UV pulses generated by frequency doubling of the laser pulses from a Ti:sapphire amplifier were shortened to their near-Fourier-transform-limited pulse duration through feedback chirp compensation [29], which means that the applicable spectral range of the LC-SLM has been extended to the UV region.

Besides phase modulation, the LC-SLM has an application for arbitrary amplitude modulation in the frequency domain to generate an arbitrary spectral shape. It can be used as a flexible band pass filter to optimize the ultra-broadband spectrum generated by SPM by removing the fine structure. Amplitude modulation using the LC-SLM is also very important in various fields such as pump–probe experiments to study selective absorption of organic or biological molecules. The ultra-broadband characteristics of the LC-SLM allow it to be applied for shaping few-cycle-to-monocycle intense pulses for driving single attosecond pulse generation [30].

The pulse shape optimization, which is of major importance for most applications, requires a precise, direct and reliable temporal characterization tool. The simplest and oldest pulse characterization method is to measure the pulse spectrum with a spectrometer. Since this measurement does not contain any information about the spectral phase, the temporal structure of the pulse remains undetermined. The techniques revealing some of the temporal structure of subpicosecond pulses are the intensity- and interferometric autocorrelations [31]. These techniques have been the standard pulse diagnostics for decades and still find widespread use in most ultrafast optics laboratories. Intensity autocorrelation comes in two different variants. In one variant, the autocorrelation signal is superimposed on a constant background [32]. The second variant records a background-free signal and therefore allows for a much higher dynamic range [31]. The first variant is only mentioned for the sake of completeness. Today, the second variant is used nearly exclusively.

For some analytic pulse shapes, a simple relation between the width of the autocorrelation function and the width of the input pulse can be found [33]. In all these cases, however, it is assumed that no or just a linear chirp is present on the pulse to be characterized. Since the autocorrelation function only depends on the pulse intensity, very limited information on the phase can be extracted. For example, assuming a linear chirp, the amount of chirp can be found by comparing the independently measured spectral bandwidth with the actually measured pulse duration. The sign of the chirp, however, remains undetermined. The intensity autocorrelation is rather insensitive towards the pulse shape. One should therefore restrict the application of intensity autocorrelation to cases in which the pulse shape is known a priori or in which only a rough estimate for the pulse duration is desired. Such a priori knowledge of the pulse shape is available, for example, for a wide range of passively mode-locked lasers with pulse durations well above 10 fs [34].

If two different instead of two identical pulses are correlated in a setup, one obtains an intensity cross-correlation trace (often simply referred to as cross-correlation). Cross-correlation of a short pulse with a replica that has propagated through a piece of glass with known dispersion was used together with an independently measured spectrum for an iterative pulse shape and phase reconstruction [35].

Another version of autocorrelation is interferometric autocorrelation, this time the two pulse replicas interact collinearly in the nonlinear medium. Interferometric autocorrelation contains more information than the intensity autocorrelation. Due to the interference terms it also reveals some information about the phase of the pulse. Additionally, the interferometric autocorrelation is more sensitive to the pulse shape than the non-interferometric one [36].

The fundamental quantity describing an ultrashort optical pulse is its real electric field. At optical frequencies, however, there exist no detectors capable of directly measuring the oscillating field. All detectors in the optical regime are energy detectors. The fastest electronic detection devices have response times on the order of one picosecond for photodiodes and of about 500 fs for streak cameras [37]. This is about two orders of magnitude longer than state-of-the-art optical pulses [38]. Therefore, all pulse characterization schemes have to rely on slow detectors. The solution to this measurement problem is to pass the pulses through filters of known response and record the average output energy with a slow detector as a function of the filters' parameters [39].

This is the basic idea behind all known pulse measurement devices. Based on the actual arrangement of the filters amplitude and phase characterization schemes have been divided into three classes: the spectrographic, the tomographic, and the interferometric techniques [39].

The interferometric methods are referred to as direct methods. Whereas the spectrographic and tomographic techniques require the acquisition of a relatively large two-dimensional set of data, the interferometric methods allow the reconstruction of the pulse from one-dimensional data if a train of identical pulses is assumed. In addition, this reconstruction procedure is generally non-iterative in nature.

New methods developed for amplitude and phase characterization, such as FROG [40-42], SPIDER [49], SORBETS [54] and SPIRIT [56, 57], have also been used for ultrafast pulse characterization.

In 1991 Kane and Trebino introduced the Frequency-Resolved Optical Gating (FROG) characterization method based on the measurement of a spectrally resolved autocorrelation signal followed by an iterative phase retrieval algorithm to extract the intensity and phase of the laser pulse [40-42]. FROG has been used for pulse durations from few femtoseconds to several picoseconds and for pulse energies ranging from the nJ- to the mJ-regime. Except one, all of the FROG techniques use an autocorrelator-like experimental setup measuring the spectrally resolved signal resulting from the interaction of two input pulse-replicas in a nonlinear medium for a series of different relative delays between the pulses. Transient grating FROG employs three interacting beams, but this variant is a rather uncommon implementation of FROG.

FROG based on second-harmonic generation (SHG-FROG) is possibly the most widely used FROG beam-geometry [43]. The signal recorded in SHG-FROG corresponds to a spectrally resolved intensity autocorrelation. SHG-FROG is the most sensitive FROG method and is the only one that can be easily applied to the characterization of unamplified pulses.

In the conventional non-collinear SHG-FROG, the finite beam-crossing angle between the two pulse replicas is the most important fundamental constraint on the achievable temporal resolution of the apparatus. In the sub-10-fs range, two serious problems with the FROG technique arise. The first is bandwidth limitation of the optics and the detection system involved, in particular the bandwidth limitation of the SHG process. This problem is reduced by using extremely thin nonlinear optical crystals. In contrast to autocorrelation, FROG allows us to correct for bandwidth

limitations to a certain extent. With this correction, measurements of 4.5-fs pulses have been successfully demonstrated [44]. Still, particular care has to be given to the accurate determination of the spectral calibration of the setup. The second more fundamental limitation is the reduction of temporal resolution caused by the finite beam-crossing angle in the nonlinear crystal.

Another class of modified FROG techniques measures the spectrally resolved cross-correlation between two different pulses. This class of methods is generally referred to as cross-correlation FROG (XFROG) [45, 46]. Although cross-correlation-like measurements can also be performed using higher-order nonlinearities, XFROG is usually based on second-order nonlinear interactions. Typically, one of the two cross-correlated pulses (the "reference" pulse) is significantly stronger than the second pulse (the "signal" pulse). Therefore, the use of second-order nonlinearities is dictated by the need for high sensitivity in order to measure weak signal pulses. The main advantage of XFROG is that the reference pulse is not required to spectrally overlap with the signal. XFROG has been demonstrated using sum-frequency generation as well as difference-frequency mixing. In contrast to normal FROG, XFROG even allows to spatially resolve the pulse shape of the signal beam. In principle, it is possible to simultaneously reconstruct both cross-correlated pulses from a single XFROG trace. In practice, however, this dual reconstruction algorithm is not very robust and requires an excellent signal-to-noise ratio.

One problem with using the FROG technique in the sub-10-fs regime is the extremely wide bandwidth associated with such short pulses. Strong spectral sensitivity dependence effectively reduces the dynamic range of the detection system and may lead to increased noise in the spectral wings. The FROG traces are not very intuitive. Usually, a simple visual inspection of the FROG trace is not sufficient to determine the type of phase distortions present on a pulse.

Spectral interferometry (SI) for pulse complete characterization has first been proposed by Froehly et al [47, 48]. The beam is split into two. Along one path, the beam acquires a spectral phase $\varphi_1(\omega)$, whereas the other beam acquires $\varphi_2(\omega)$. At the end of both paths, the two beams are collinearly recombined and sent into a spectrometer. The spectrometer measures the coherent superposition of the two electric fields with a square-law detector. Thus, one yields for the detected signal

$$I_{SI}(\omega) = \left|E_1(\omega) + E_2(\omega)\right|^2 = \left(E_1(\omega) + E_2(\omega)\right)\left(E_1(\omega) + E_2(\omega)\right)^*$$

And with some simple algebra

$$I_{SI}(\omega) = |E_1(\omega)|^2 + |E_2(\omega)|^2 + 2|E_1(\omega)E_2(\omega)|\cos(\varphi_1(\omega) - \varphi_2(\omega))$$

As can be seen, only the relative phase between the two interferometer arms appears in the interference term. If one is interested in the phase of one specific arm, the phase in the other arm has to be known. The interferometer arm with the known phase is referred to as the reference arm. For most experiments, one is only interested in the second and higher order dispersion contributions to the spectral phase. The knowledge of the reference phase can then be obtained either by keeping the amount of dispersion in the reference arm at a negligible level or by measuring the phase with a self-referencing measurement technique. The two beams in the spectral interferometry apparatus do not necessarily have to originate from a single initial beam. The only requirement is mutual coherence between the two interferometer arms. The maximum relative phase variation that can be measured with spectral interferometry is limited by the spectral resolution of the spectrometer. The range of applications for spectral interferometry is further limited by the requirement that the phase differences can only be extracted in the region of spectral overlap between the two interfering spectra. There are various methods for the extraction of the phase information from a spectral interferogram.

Spectral phase interferometry for direct electric-field reconstruction (SPIDER) is one of the most recent techniques for amplitude and phase characterization of ultrashort optical pulses [49]. SPIDER is a self-referencing variant of spectral interferometry. Conventional spectral interferometry measures the spectral phase differences between two pulses [47]. To access the spectral phase of a single pulse, SPIDER generates a spectral shear between the carrier frequencies of two replicas of this pulse. The phase information of the resulting interferogram allows the direct reconstruction of the spectral phase of the input pulse. With an independent measurement of the pulse spectrum one obtains the temporal structure of the pulse by a Fourier transform.

The idea of generating a spectral shear between two identical pulses to enable self-referencing spectral interferometric measurement of the phase of the input pulse was initially proposed for a technique named spectral shearing interferometry [50]. In this method an active phase modulator was used to provide the necessary spectral shear between the two pulse replicas. However, no active modulators exist, which are fast enough to provide the amount of spectral shear required for

measuring femtosecond pulses. The underlying concept of the SPIDER technique is the same as for spectral shearing interferometry. These two methods only differ in the way the shear is generated. Therefore, SPIDER can be understood as a variant of spectral shearing interferometry.

In SPIDER the spectral shear is generated by up conversion of the two replicas with a strongly chirped pulse using sum-frequency generation in a nonlinear optical crystal. It is convenient to directly derive the chirped pulse from the pulse to be measured by a dispersive element. The up-converter pulse has to be stretched in such a way that its instantaneous frequency can be considered constant for the duration of the pulse to be measured. Being separated by a delay τ much longer than the pulse duration, the two replicas are up converted by different portions of the chirped pulse with different frequencies. The resulting spectral interference pattern of the up converted short pulse replicas is of the form

$$S(\omega) = |E(\omega)|^2 + |E(\omega + \delta\omega)|^2 + 2|E(\omega)E(\omega + \delta\omega)| \times \cos[\phi(\omega + \delta\omega) - \phi(\omega) + \omega\tau]$$

where $E(\omega)$ is the frequency-domain representation of the electric field, $\phi(\omega)$ the spectral phase of the input pulse, ω denotes the angular frequency and $\delta\omega$ the spectral shear. The phase information contained in the cosine term can be extracted by a non-iterative, purely algebraic method. The constant delay τ is determined once by spectral interferometry of the two short-pulse replicas. After subtraction of the linear phase term $\omega\tau$, one obtains the spectral phase $\phi(\omega)$ at evenly spaced frequencies $\omega_i = \omega_0 + i \times \delta\omega$ by adding up the phase differences $\phi(\omega_n + \delta\omega)$- $\phi(\omega_n)$ (n =0…i -1). In the final step, the complex frequency domain representation of the electric field of the pulse is obtained from the reconstructed spectral phase and an independent measurement of the power spectrum. Temporal profiles are obtained by Fourier transforming these results. Because of the high speed of this algorithm and the fact that a single spectral measurement is sufficient to obtain the spectral phase, SPIDER can be operated at very high update rates.

SPIDER is an intrinsically fast technique. It requires acquisition of only two spectra and the pulse reconstruction consists of two Fourier transforms executed in the fraction of a second on a modest computer. SPIDER has been demonstrated for real-time single-shot characterization of a 10-Hz amplifier system and with update rates as fast as 20-Hz for a 1 kHz amplifier system [51]. SPIDER is particularly well suited for sub-10-fs pulse characterization for several reasons. In this regime, a short piece of a highly dispersive glass is sufficient for the generation of the strong chirp

of the up converter pulse. Use of sum-frequency mixing results in a more economic use of detection bandwidth, compared to SHG-based techniques. SPIDER allows for fast acquisition and its spectral phase reconstruction is insensitive to spectrally varying detection and conversion efficiencies. Another attractive feature of SPIDER is its simple non-iterative pulse reconstruction procedure.

A version of SPIDER that allows acquiring the fundamental pulse spectrum and the SPIDER interferogram in a single shot with a single spectrometer was demonstrated also [52]. For this purpose, the spectrometer was set to the second diffraction order of the SPIDER signal that coincides with the first diffraction order of the pulse spectrum. This technique is called HOT-SPIDER.

Another variant of SPIDER, a spatially-resolved SPIDER, allows for spatially resolved measurements of the pulse shape across the input beam [53].

SPIDER can be extended in a straightforward way to perform spatially resolved characterization of the input beam. No fundamental limitations of the SPIDER technique are known even for the characterization of spectra covering a full octave.

Superposition of optical radiations and beatings to extract the time signal (SORBETS) method is based on the superimposition of two slightly shifted replicas of the spatial representation of the pulse spectrum [54]. In this method, the beating signal due to the superimposition of the two spectra is recorded at each point of the spectrum. Knowledge of the phases of the beating signal allows to reconstruct the unknown spectral phase. An additional measurement of the spectral intensity leads to the complete characterization of the pulse. This setup does not involve any nonlinear optical process. They generate the beating signals of lower frequencies, so that these signals are easily recorded by fast linear detectors, thus avoiding the nonlinear step. A simpler one-step scheme is adopted, in which the beating signal is created at each point of the spectrum. The spectrometer was modified, so that two images of the spectrum are present in the Fourier plane, superimposed on the same line with a slight spatial shift. This spatial shift can be chosen as small as it is necessary. As a result, the frequency of the beating signal can be chosen small enough to resolve temporally the signal with an electronic detector.

The validity of the method was first demonstrated on a train of pulses with a repetition rate of 2.78 GHz. The setup that they used would be particularly suited to fully characterize ultrahigh repetition rate trains of identical pulses, at repetition rates below 50 GHz. This method could

efficiently be integrated in a setup to characterize, in amplitude and phase, the devices that are used in ultrahigh-speed telecommunication systems. A second demonstration of the same measurement scheme was performed on a single pulse, using a streak camera with a resolution of 10 ps.

Recently a similariton-based self-referencing method of spectral interferometry for the complete characterization of femtosecond signals was proposed [55]. In this method of similariton-based SI, the part of signal is injected into a fiber to generate the nonlinear-dispersive similariton-reference. The residual part of the signal, passing an optical time delay, is coupled with the similariton in a spectrometer. The spectral fringe pattern, on the background of the signal and similariton spectra, completely covers the signal spectrum, and the whole phase information becomes available for any signal. The known spectral phase of the similariton-reference allows to retrieve the signal spectral phase, and by measuring also the signal spectrum, to reconstruct the complex temporal amplitude of the signal through Fourier transformation. Thus, the method of similariton-based SI joins the advantages of both the classic SI and spectral shearing interferometry, combining the simplicity of the principle and configuration with the self-referencing performance.

Spectral interferometry resolved in time (SPIRIT) [56, 57] is a new technique that is capable of direct electric-field reconstruction that is not case sensitive, is fast, can be applied to single as well as to repetitive pulses, and offers a large degree of freedom. Like SPIDER and SORBETS, SPIRIT is based on spectral shearing interferometry. SPIRIT and SORBETS use geometrical shearing of two spatially dispersed twin spectra rather than shearing of their carrier wavelengths as in the case of SPIDER. The first published version of SPIRIT was only suitable for the characterization of high repetition rate trains of identical pulses. It involved a moving element and required relatively long measurement procedure that lasted several seconds. Later the new configuration of SPIRIT that can be used for repetitive pulse detection as well as for single shot measurement was demonstrated. A two-dimensional interferogram development, 2D-SPIRIT, offers a direct and intuitive characterization of short pulses [58].

Fiber optic delivery of femtosecond laser pulses is attractive due to several reasons. Fiber delivery enables pulse delivery at places difficult to reach using conventional mirrors and lenses such as in endoscopic multiphoton microscopy [59], which is an emerging medical diagnostic tool for in-vivo imaging [60]. The key challenge in a fiber-based pulse delivery for Ti:Sapphire femtosecond lasers are the dispersive and nonlinear properties inherent to fiber technology.

The nonlinearity and normal GVD of standard optical fibers at 800 nm restrict fiber delivery of 100-fs pulses to energies of ~20 pJ. This is less than 1% of the pulse energy for a standard Ti:sapphire laser and is uselessly low for many applications. A 1-nJ pulse is severely distorted after propagation through 1m of fiber. The natural length scale associated with dispersion is $L_D = \tau_0^2 / \beta_2$ (where τ_0 is the pulse half-duration at the 1/e level of the intensity for Gaussian pulses, and β_2 is the GVD parameter). Because the temporal broadening is caused by the different spectral components travelling at different phase velocities, it is useful to recognize that $L_D \sim 1/\Delta\omega^2$, where $\Delta\omega$ is the pulse bandwidth: a pulse with a larger bandwidth is affected more by dispersion. L_D for 100-fs pulses propagating through standard fiber (single-mode fiber at 800 nm) is roughly 9 cm. The nonlinear length is defined as $L_{NL} = \left[(\omega/c) n_2 I_{peak}\right]^{-1}$, where n_2 is the nonlinear refractive index and I_{peak} is the peak intensity of the pulse. For 100-fs pulses, at 800 nm and with energy of 1 nJ, L_{NL} ~ 1.3 cm. Thus, L_D / L_{NL} ~ 7, so nonlinearity initially dominates. The spectrum broadens significantly in the first few centimeters of fiber, after which GVD becomes the dominant effect. The pulse broadens, and the peak power drops proportionally. As a result, the propagation is nearly linear for all but the first few centimeters. The pulse at the output of a meter of fiber is broadened spectrally and temporally compared with the input and has an approximately linear frequency chirp.

To date, avoiding nonlinearity as much as possible has produced the best results for fiber delivery of 100-fs pulses from Ti:sapphire lasers. A large negative linear frequency chirp is imposed on the pulse (by the use of gratings or prisms), which increases the pulse duration to several picoseconds. Propagation through fiber with normal GVD restores the pulse to nearly the original duration; there is no attempt to compensate for nonlinear effects. This pre-chirping approach works reasonably well at low energies, but even with 20-pJ pulses substantial distortion occurs in the unavoidable nonlinear propagation at the end of the fiber, where the pulse is recompressed to some extent. When a negatively chirped pulse propagates in a medium with a positive nonlinear index of refraction, self-phase modulation compresses the spectrum and thus increases the pulse duration [61].

Several interesting fiber delivery schemes have been demonstrated in literature. The first approach concerns the normal dispersive fibers such as traditional large mode area (LMA) fibers,

microstructured endlessly single mode LMA fibers, and higher-order-mode (HOM) fibers [62]. They have either large mode fields (equivalent to a large effective area) or high dispersion to operate in a regime where $L_D << L_{NL}$, hence reducing the impact of nonlinear effects. However, since they are normal dispersive, they all require pre-chirping to provide a Fourier transform limited output at the end of a fiber delivery. Usually this is done by bulk optic gratings or prisms or combinations. A second category of potential delivery fibers are air-guiding fibers, which have a small n_2 in order to minimize the effect of nonlinearities and to enable high power applications. These are the so-called hollow core photonic band gab (PBG) fibers with anomalous dispersion [63] and chirped photonic band gab (CPBG) fibers with zero dispersion and zero dispersion slope [64]. Although both fiber types are intriguing due to a large nonlinear length they do have critical drawbacks such as a large positive dispersion slope and high transmission loss, respectively. When implementing such fibers in fiber deliveries one is forced to compromise on the system performance in terms of fiber length.

SMFs and single-mode photonic crystal fibers (PCF) have been successfully demonstrated for use in the imaging system. In standard SMFs, near-infrared femtosecond pulses are severely broadened because of chromatic dispersion and, in particular, power-dependent nonlinear effects, which become significant at pulse energies as low as 0.1 nJ [65]. Efficient multiphoton excitation, however, requires both high peak power and short pulse widths. In addition, single-mode propagation is necessary to preserve a spatial beam profile suitable for diffraction-limited focusing. However, in order to satisfy the single-mode condition, the core diameter of the step-index SMF is limited to ~5 μm. Relatively small-sized core makes SMF susceptible to generating nonlinear effects, e.g. SPM, which will reshape the spectra of laser pulses. SMF fiber was first tried for two-photon endoscopy, but it was demonstrated that such an endoscopy system has a low signal level because of the low numerical aperture (NA), the chromatic dispersion, and the nonlinearity [66]. The high peak power, about 10 kW, makes it difficult to deliver these pulses through conventional SMFs without pulse broadening caused by SPM and GVD [61]. To overcome this problem, researchers have used specialty fibers, such as hollow-core photonic bandgap fibers [67] and LMA fibers [68], but they are not readily compatible with standard optical components and are much more expensive than standard SMF. Pulse pre-chirping and post-chirping have been proposed to

mitigate the nonlinear distortion in standard SMF [69]. However, this scheme adds complexity and works best with a relatively short, predetermined, fiber length. Furthermore, because of strong chromatic dispersion of silica at wavelengths below 1 μm, it is nontrivial to transmit even low energy pulses over several meters of standard SMF.

Since their inception in the early 1990s, PCFs have revolutionized fundamental research on and development of optical fibers [70]. These PCFs, which are radically different from standard step-index fibers, are now becoming commercially available with great promise for providing highly flexible, easy-to-handle single-mode fibers suitable for high-energy pulse delivery. The superiorities of PCFs, such as endless single mode operation, dispersion engineering, and high nonlinearity have led to a broad range of applications, including the development of high-power fiber lasers [71]. In addition, double-clad PCFs made of pure silica have attracted research in biosensing and bioimaging to improve the system efficiency because of their dual function of single-mode and multimode delivery through the central core and the inner cladding region of high NA, respectively [72]. The detection efficiency of the nonlinear optical microscopy system based on the double clad PCF is approximately 2 orders of magnitude higher than that based on a standard SMF [72]. Although the dual function of the double-clad fiber makes miniature and flexible microendoscope probes possible, a further compact imaging system could be achieved by use of a multiport fiber coupler to achieve self-alignment and replace bulk optics for an all-fiber microscopy system [73]. Although the core diameter of PCF is larger than SMF (e.g. ~16 μm for large mode area PCF), the NA of PCF is usually small (e.g. ~0.06 for large mode area PCF) and, thus, results in difficulty and instability of laser coupling as well as small coupling efficiencies (< 30%) [74]. To address these issues, multimode fibers (MMF) may be a good candidate for delivery of ultrafast pulses for imaging. Compared to SMFs and PCFs, step-index MMFs have larger core diameters, larger NA, and larger coupling efficiency.

Solid core fibers, such as graded index multimode fiber or high order mode fiber, have been experimentally proven capable of merely nanojoule pulse energy capacity in the ultrashort pulse regime. The salient feature is the small area (about 1000 μm^2 or less) of the confined mode within the glass fiber core. The resultant high peak irradiance yields unrecoverable pulse distortion due to SPM or catastrophic damage from dielectric breakdown. Attempts to further expand the mode area have yielded severe multiple mode cross-coupling and distortion, and extremely high loss as a result

of weak mode confinement in low NA waveguides. Thus alternative optical fiber formats, such as hollow core waveguides, appear to be the most viable option for delivery. When the waveguide core comprises a gas at low to moderate pressure, the pulse train propagates with a much weaker nonlinear interaction. At atmospheric pressure, the nonlinear refractive indices (n_2) of air, argon, and helium are respectively ~4×10^{-23} m^2/W [75], ~1×10^{-23} m^2/W [76] and ~4×10^{-25} m^2/W [76]. These nonlinear refractive indices are three orders of magnitude weaker than a silica solid core with n_2~2.4×10^{-20} m^2/W [77]. Owing to the higher ionization potential and lower nonlinear refractive indices of argon and helium compared with that of air, pulses delivered through helium- and argon-filled hollow core photonic band-gap fibers (HC-PBGF) will experience lower nonlinear effects and higher damage threshold.

Hollow core waveguides have included metallic inner-surface fibers (capillaries) as well as HC-PBGF. Metal coated, hollow core fibers and capillaries have been utilized for infrared laser delivery where the guided mode diameter is fundamentally large, e.g. at the CO2 laser wavelength of 10 μm, or when multimode interference is not detrimental to the application. For near-infrared lasers neither of these conditions holds true. The requisite single mode propagation would require scaling the hollow core diameter down to a size that inhibits metal deposition on the inner surface. Near-infrared, single mode metallic hollow core fiber simply cannot be manufactured with current methods. Hollow core plastic one-dimensional (1D) Bragg fibers have shown their high potential for spatially and temporally distortion-free transmission of high peak power pulses. Nonetheless, due to fabrication complexities, it has been challenging for plastic Bragg fibers to achieve the low transmission loss domain of glass hollow core fibers. In these HC-PBGFs, SPM and other deleterious effects can be reduced by more than 1000 times as compared to solid core fibers, and delivery of microjoule level laser pulses has been demonstrated [78]. However, standard photonic bandgap hollow-fiber concepts provide guiding in relatively small wavelength bands that are inevitably accompanied by hard-to-compensate odd-order dispersion contributions [79]. The shortest pulse duration delivered with such standard hollow fibers with their constant cell size amounts to 170 fs at energy of 4.6 nJ [80]. To overcome the detrimental dispersion properties of standard hollow-core fibers, chirped photonic crystal fibers (CPCFs) [81] were recently demonstrated as an alternative, allowing for 25 fs pulse delivery over meter distances without the need for any further dispersion compensation measures.

Unsolved problems: Thus, successes of laser techniques in the field of generation of ultrashort pulses are conclusive. The researches directed to the management, control and registration of parameters of pulses are essentially advanced also. However, it is necessary to note, that the current stage of development of ultrafast optics and laser technologies imposes new, high requirements to the methods of signal processing and delivery. It stimulates intensive studies in the mentioned above directions with the purpose of research of the new physical approaches to the problems of high laser technologies. There are numerous of the important unsolved problems at the present stage of researches in these directions. Particularly:

- Despite the existing fiber delivery schemes, there are no schemes with simple and non-expensive solution for optimized and flexible dispersion compensation.
- High potential of spectral interferometry, makes demanded its improvements-modifications-extensions directed to increasing of accuracy and sensitivity of measurements and enlargement of the range of its applications.
- With the achievement of few-cycle femtosecond pulses the necessity of pulse complete characterization methods in this timescale became a demanded task.

Objectives of the work: The importance and practical significance of researches in the given directions together with a number of unsolved problems have defined the theme and the purpose of the work, including numerous important physical problems connected with signal processing and delivery. In particular:

- Experimental studies of nonlinear-dispersive self-interaction of pre-chirped pulses in view of shaping of transform-limited flattop pulses.
- Spectral interferometric investigations for femtosecond pulse complete characterization in view of development of new effective dispersive delay lines.
- Studies of pulse nonlinear-dispersive self-interaction in the fibers, for the pulses pre-chirped in the grisms, in view of development new effective methods of fiber delivery, for contemporary endoscopy.
- Studies of potential of spectral interferometry in view of development new, effective methods for complete characterization of a few optical cycle pulses.
- Investigations of femtosecond pulse shaping with new programmable spatial light modulators.

In the work, the basic method of studies was the physical experiment in conjugation with the numerical modelling of the processes under study.

This work consists of the introduction (including the review of the corresponding literature), three chapters, conclusion and the list of the literature. The work consists of 117 pages, including 52 figures and the bibliography containing 148 names.

In the introduction the urgency of the theme is proved, the review of the literature is presented and the purpose of dissertational work is formulated. In the end of the introduction the structure of the thesis, its summary, scientific novelty, the practical significance, statements to be defended, and the list of publications are presented.

Chapter 1 describes several methods for femtosecond pulse syntheses. A new dispersive delay line (DDL) based on prism-lens spectrometer is experimentally demonstrated. In comparison with traditional dispersive delay lines it has a compact and simple design, which is independent of the dispersive force. Only changing of one lens allows us to tune dispersion easily and significantly, as well as to change the dispersion sign. It is also important that new dispersive delay line is applicable for picosecond pulses due to the compact design. The setup consists of dispersive prism, lens for spectrum imaging in the focal plane, high-reflective mirror, and another lens as a phase mask. In the experiment, we use lenses with different focal lengths, i.e. we give to the pulse different parabolic phases. Collecting or diverging lenses were used to induce negative or positive chirps, respectively. To register the dispersion induced, we carried out spectral interferometric and autocorrelation measurements. We spectrally interfere the formed pulse with the initial laser pulse to determine the spectral phase induced. Our proposed dispersive delay line allows to shape pulses with various shapes. In the second part of this chapter we report on our experimental study of the dispersive regime of spectral compression, and particularly on the case of maximal spectral compression, when the combined impact of Kerr-nonlinearity and group velocity dispersion of single mode fiber (SMF) shape the transform limited rectangular pulses. We demonstrate ~3 times spectral compression of 100 fs pulses. By means of spectral interferometric measurements, we completely characterize these pulses. Numerical simulations and experiments show that ultrashort pulses with the rectangular envelope are formed when the relation DDL/SMF~2 takes place. Our results of pulse complete characterization obtained by spectral interferometry are in a good agreement with

the numerical simulations. An innovative and simplified direct space-to-time pulse shaper is also proposed. 2D liquid crystal spatial light modulator (SLM) acts as a pulse stretcher and amplitude-phase modulator. Accurate and simultaneous control of amplitude and phase is demonstrated.

In Chapter 2 we report a very compact system for femtosecond pulse fiber delivery from wide-band laser sources. We present the direct delivery of compressed ultrashort (sub-30 fs) nanojoule pulses at 830 nm through a large mode area photonic crystal fiber (LMA). Pulse fiber delivery pre-dispersing technique is developed, using LMA fiber and grism line. Simultaneous control of second order dispersion (SOD) and third order dispersion (TOD) is realized by compact grism line. 17.8 fs nanojoule pulse at the output of 2.7 m LMA fiber is demonstrated. Comparison between LMA fibers and standard SMF fibers is also discussed. Finally in the last part of this chapter SLM-based fiber delivery scheme is proposed. The capability of the SLM to generate arbitrarily shaped pulses is also illustrated.

Chapter 3 describes new methods for femtosecond pulse characterization. We experimentally propose a new method of real-time time-to-frequency conversion through aberration-free temporal lensing by sum frequency generation process. This all-optical time-to-frequency imaging allows direct, real-time pulse characterization in femtosecond time-scale. The new method is free of demand to differentiate the signal and reference radiation, self-referencing and aberration-free by self-shaping of nonlinear-spectronic reference pulse. We also present the experimental scheme of Wideband SPIRIT (Spectral Interferometry Resolved In Time), a method for the measurement of ultrashort and wideband pulses based on spectral interferometry. We report experimental results dealing with the characterization of few-cycle pulses. Third order dispersion measurement has been also possible with proposed system.

In the conclusion the basic results of the thesis are formulated.

Scientific novelty: In the result of our experimental studies (conjugated with the numerical modelling), the following new and original results are obtained to solve the urgent problems of ultrafast optics and photonics, particularly for signal processing and delivery:

- The capability of spectral interferometry for pulse complete characterization of sub-picosecond pulses is demonstrated for dispersively stretched and chirped pulses in the scheme of standard

spectrometer, and also for Fourier transform rectangular pulses shaped in the dispersive regime of spectral compression.

- It is shown that a laser, grism line and large mode area fiber, can serve as an effective femtosecond pulse delivery system. The delivery of 17.8 fs nanojoule pulse through 2.7 m large mode area fiber, by relevantly pre-chirping the pulses at the entrance, is experimentally demonstrated.
- A new programmable direct space-to-time femtosecond pulse shaper using phase-only liquid crystal spatial light modulators is demonstrated.
- Wideband SPIRIT, a new scheme of time resolved spectral interferometry, as a method for the measurement of few-cycle wideband pulses is experimented.

Practical significance: Studies carried out in the work expand understanding about ultrashort pulse processing and delivery on femtosecond timescale. Obtained results can be useful for development of new effective methods and devices for ultrafast optics and laser physics. Particularly:

- A compact and simple dispersive delay line for ultrashort pulse shaping, with the possibility to induce both negative and positive dispersion is experimentally demonstrated.
- An effective dispersive regime of spectral compression, when rectangular Fourier transform pulses are shaped, along with the achievement of maximal spectral compression ratio, is experimentally demonstrated, applying the spectral interferometry method of ultrashort pulse complete characterization.
- For femtosecond pulse delivery, a compact stretcher, which consists of a pair of grisms, and large mode area fiber compressor, is proposed and experimented.
- A new, simple and compact direct space-to-time femtosecond pulse shaper, with a single, programmable liquid crystal spatial light phase modulator (phase-only SLM) instead of grating and mask, is demonstrated experimentally.
- A new scheme of time resolved spectral interferometry (wideband SPIRIT), for complete characterization of few-cycle optical pulses, has been experimentally demonstrated. The capability of the new SPIRIT scheme to easily provide the data as a sonogram, which enables an intuitive representation of the pulse’s dispersion, is demonstrated.

Defending statements

1. Pulse relevant chirping at the input of LMA fiber, by dispersion management of the grism line, leads to the achievement of 18-fs pulse duration at the output of the fiber delivery scheme: consisting of grism line and LMA fiber.
2. A transverse modulation of a beam reflected from the diffraction grating under the Littrow condition leads to the pulse temporal modulation on the pico-femtosecond timescale and thus provides a way for space-to time conversion and for the ultrashort signal temporal shaping.
3. Self-interaction of negatively pre-chirped sub-picosecond pulses in fibers, due to the combined impact of Kerr-nonlinearity and group velocity dispersion, results in shaping of flattop, “rectangular” Fourier-transform pulses on the 100-femtosecond timescale.
4. Spectral interferometric information obtained via SPIRIT (Spectral Interferometry Resolved in Time) permits to completely characterise the few-cycle pulses (8 fs) and thus carry out temporal measurements on the few-femtosecond timescale.

Experimental works presented in this work are done at Yerevan State University and at University of Limoges. The scientific supervisors of the thesis are Prof. Frederic Louradour and Prof. Levon Mouradian.

List of publications related to the work

1. M.A.Kalashyan, K.H.Palanjyan, T.J.Khachikyan, T.G.Mansuryan, G.L.Yesayan, L.Kh.Mouradian, "Prism-Lense Dispersive Delay Line", Tech. Phys. Lett. 35 (3), 211-213 (2009).
2. М.Калашян, К.Паланджян, Г.Есаян, Л.Мурадян “Дисперсионная линия задержки на основе фурье синтеза” VIII Харківська конференція молодих науковців «Радіофізика та електроніка, біофізика» 25-27.11.2008, 117. (2008).
3. M.A.Kalashyan, K.A.Palandzhyan, G.L.Esayan, L.Kh.Muradyan, "Generation of transform-limited rectangular pulses in a spectral compressor" Quantum Electron. 40 (10), 868-872 (2010).

4. K.Palanjyan, M.Kalashyan, G.Yesayan, L.Mouradian “Synthesis of Fourier Transform Rectangular Pulses in the Process of Spectral Compression”- Proc. Conf. Laser Physics-2008, 150-153 (2009).
5. K.Palanjyan, M.Kalashyan, G.Yesayan, L.Mouradian “Spectral Interferometric Characterization of Spectral Compression: Dispersive Regime,” Proc. 4th Int. Conf. on Advanced Optoelectronics and Lasers 2008 (CAOL-2008), 428-430 (2008).
6. T.Mansuryan, M.Kalashyan, J.Lhermite, V.Kermene, A.Barthelemy, F.Louradour "Compact direct space-to-time pulse shaping with a phase-only spatial light modulator", Optics Letters, 36 (9), 1635 (2011).
7. T.Mansuryan, M.Kalashyan, J.Lhermite, A.Barthélémy, V.Kermene, F.Louradour "Direct Space-to-Time Femtosecond Pulse Shaping based on 2D Phase-Only Spatial Light Modulator", CLEO/Europe-EQEC 2011, paper CF.P.26 (2011).
8. C.Lefort, M.Kalashyan, D.Peyrot, T.Mansuryan, L.Mouradian, F.Louradour, A.Barthélémy “Pulse Compression and Fiber Delivery of Sub-30 fs Nanojoule Pulses at 830 nm” CLEO/USA 2011, CWR4 Ultrafast Pulse Generation II session (2011). / "Dispersion Compensation with a Grism-based Dispersive Line for Fiber Delivery of Sub-30 fs Pulses at 830 nm", CLEO / Europe-EQEC 2011, CD.P.4 (2011). / M.Kalashyan, C.Lefort, L.Martinez-Leon, T.Mansuryan, L.Mouradian, F.Louradour “Ultrashort pulse fiber delivery with optimized dispersion control by reflection grisms at 800 nm”, Opt. Express 20, Iss. 23, 25624–25635 (2012).
9. T.Mansuryan, A.Zeytunyan, M.Kalashyan, G.Yesayan, L.Mouradian, F.Louradour, A.Barthélémy "Parabolic temporal lensing and spectrotemporal imaging: a femtosecond optical oscilloscope"- J. Opt. Soc. Am. B 25, A101-A110 (2008).
10. A.Zeytunyan, M.Kalashyan, G.Yesayan, L.Mouradian, F.Louradour, A.Barthélémy, "Similariton-based spectral interferometry for femtosecond signal characterization", European Conference on Optical Communication 2011 (ECOC’11), 978-1-4577-1918-9 (2011).
11. M.A.Kalashyan “Wideband SPIRIT for characterization of few-cycle femtosecond pulses”, Armenian Journal of Physics 5/2, 81-85 (2012).
12. L.Martínez-León, T.Mansuryan, M.Kalashyan, J.Lhermite, F.Louradour, Ch.Hazera, S.Petit, E.Cormier, A.Barthélémy "Complete Measurement of 8 fs Pulses with Wideband SPIRIT", CLEO/Europe-EQEC 2011, paper CF.P.17 (2011). / "Characterization of 8 fs pulses through

wideband SPIRIT", 10th Euro-American Workshop on Information Optics, 10.1109/WIO.2011.5981475 (2011).

Patents:

1. Լ.Մուրադյան, Տ.Մանսուրյան, Ա.Զեյթունյան, Մ.Քալաշյան, Գ.Եսայան, Ֆ.Լուրադուր, Ա.Բարթելեմի, «Գերարագ օպտիկական օսցիլոգրաֆ», ՀՀ արտոնագրի հայտ No. AM2009044, G01 D 5/26 (2009):

2. Ա.Ա.Կիրակոսյան, Ք.Հ.Փալանջյան, Մ.Ա.Քալաշյան, Ա.Ս.Զեյթունյան, Գ.Լ.Եսայան, Լ.Խ.Մուրադյան "Դիսպերսային հապաղման գիծ''- AM N. 2178 A2, G02F 1/01, G02B 5/00 (2008):

CHAPTER I

PULSE CONTROL ON FEMTOSECOND TIMESCALE

Ultrashort pulse generation has always been an urgent area of research in the field of laser pulse applications. Modern applications of ultrashort pulses provide new and advanced opportunities for commercial purposes. An ultrashort pulse can be defined as one with picosecond and femtosecond duration. Ultrashort optical pulses can be produced from longer pulses using optical pulse compression techniques [82]. Ultrashort pulse optical sources are of great technological interest due to their distinguishing features, which include 1) ultrashort duration; 2) ultra-large spectral bandwidth; 3) high peak power. Ultrashort optical pulses can be used in optical communication systems with long-distance and high bit rate.

However, many applications will require not only optical pulse generators, but also ultrafast optical waveform generators. Over the past decade powerful optical waveform synthesis methods have been developed which allow generation of complicated ultrafast optical waveforms. To apply ultrashort pulses in suitable applications it is necessary to control their temporal shapes. This shaped pulse can be used in different optical applications. However, it is difficult to control ultrashort pulses from available laser sources. Therefore, it is necessary to use a pulse shaper which produces more modified shapes of ultrashort pulses. Pulse shaping is the technique which controls the ultra-short pulse shape and phase, and it became of great technological interest because of its potential applications in laser pulse compression, fiber communication, signal processing, laser spectroscopy, device characterization, solid state physics, etc [83].

During the past two decades, a number of devices for shaping ultrashort pulses have been developed. The predominant method relies on manipulating the phase of the pulse in the spectral domain to produce complex pulse shapes in the temporal domain.

Recent advances in the area of ultrafast optics and, in particular, the area of optical communications, demand also new techniques for the generation of ultrashort rectangular optical pulses. Ultrashort rectangular optical pulses are desirable for a wide range of ultrafast pump-probe experiments, studies of carrier dynamics or coherent excitation and control of optically induced quantum states. The use of the Fourier synthesis technique [84], which was first applied to produce

ultrashort rectangular pulses, has such problems as the use of the lossy and expensive, bulky, optical elements. To avoid these problems, recently the superstructured fiber Bragg gratings were used to generate a rectangular pulse and a 20 ps rectangular pulse was demonstrated experimentally by using a 2.5 ps soliton. However, in this method a well-defined input pulse shape is needed. Moreover, the width of the generated rectangular pulse becomes much wider than the input pulse width. The generation of a powerful rectangular light pulse is obtained by insertion of a pulse shaper into a laser system. This shaper device is conveniently set between the laser oscillator and amplifiers. The oscillator delivers very short (less than 1-ps) Gaussian pulses; the shaping system transforms those pulses into pulses with a predetermined waveform. Systems for manipulating subpicosecond pulses with the aim of generating complicated ultrafast optical waveforms and relatively long square pulses according to user specifications have been studied and tested for a number of years [85].

In this chapter we propose and experimentally demonstrate new methods of ultrashort pulse shaping with different temporal profiles.

¢1.1. Prism-lens dispersive delay line for control of femtosecond pulses

In this section a new, alternative dispersive delay line for ultrashort pulse shaping is demonstrated. The proposed scheme gives possibilities to shape pulses with different temporal profiles and phases.

Dispersive delay lines (DDLs) are well-known devices that have various designs and operate on different principles, including diffraction gratings and prisms [86,87], metal vapour [88], Fabry–Perot interferometer [89], optical filters [90], electro-optical phase modulators [91], with nonlinear dispersive crystals [92], scanned grating-based phase control [93], liquid crystals [94], etc. These devices are now widely used in laser techniques and optics as pulse stretchers and compressors both outside and inside laser resonators.

Most frequently, DDLs employ a pair of gratings or prisms. A pair of two parallel gratings acts as a DDL (see Fig.1.1.1 (a)). Optical pulses propagating through such a grating pair behave as if they were transmitted through an optical fiber with anomalous GVD. When an optical pulse is

incident at one grating of a pair of two parallel gratings, different frequency components associated with the pulse are diffracted at slightly different angles. As a result, they experience different time delays during their passage through the grating pair. It turns out that the blue-shifted components arrive earlier than the red-shifted components. In a positively chirped pulse, blue-shifted components occur near the trailing edge of the pulse whereas the leading edge consists of red-shifted components. Thus, the trailing edge catches up with the leading edge during passage of the pulse through the grating pair, and the pulse is compressed. Disadvantage of the grating pair is related to the diffraction losses associated with it. Typically, 60 to 80% of the pulse energy remains in the pulse during first-order diffraction at a grating. This results in an energy loss of about a factor of 2 during a single pass through the grating pair, or a factor of 4 in the double-pass configuration. The use of diffraction gratings also does not provide dispersion easily adjusted through zero value.

A pair of prisms can be used instead for the same purpose. Unlike the grating pair, the prism sequence can produce a net group delay which can be adjusted from positive to negative. Although a number of prism arrangements can be devised, one arrangement is especially advantageous (Fig.1.1.1 (b)). The two prisms are used at Brewster's angle incidence at each surface. When a short pulse is sent into a prism, e.g. its spectral components are angularly dispersed and sent into different directions. A second prism of opposite alignment can then be used to make the spectrally dispersed beams parallel again. On their propagation between both prisms, the outer rays experience a delay relative to those at the centre. It is important to note that this parabolic spectral delay is equivalent to negative group velocity dispersion. It can therefore be used to compensate for positive material dispersion. Pairs of Brewster-cut prisms can compensate dispersion without introducing losses and have been very successfully used inside laser cavities. Combinations of four and more prisms have been investigated. Prism-based compressors exhibit low losses, but their application is restricted to pulse durations in the femto or subpicosecond range [95]. In the standard DDL scheme, the magnitude (slope) of the induced chirp depends on the distance between prisms (or gratings), which implies large size of the device.

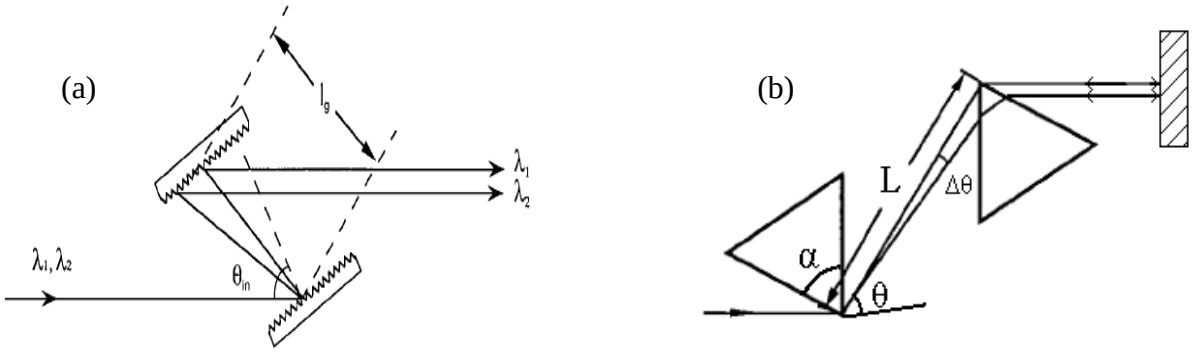

Fig. 1.1.1. (a) Gratings-based DDL; (b) prisms-based DDL.

We have designed and experimentally tested a new prism–lens DDL, which is based on the direct control of the spectral phase of pulses. Advantages of the proposed device are the compact design and the possibility of controlling both magnitude and sign of dispersion.

This section describes a new prism–lens DDL scheme, which makes possible a compact design. In this scheme, the magnitude and sign of the dispersion-induced chirp are determined by the lens strength and, hence, do not directly depend on the device dimensions. The chirp magnitude and sign can be changed without changing the pathways of rays in the system and, hence, without need in additional correction (adjustment) of the setup.

1.1.1. Principle

The proposed device has been tested for standard femtosecond laser pulses. In terms of classical radio physics, a DDL (representing a dispersive medium) is characterized by the phase transmission function $D(\omega) = \exp[i\phi(\omega)]$, which allows the Fourier transform $F(\omega)$ of the slowly varying complex amplitude to be written as follows:

$$F_{out}(\omega) = D(\omega) \times F_{in}(\omega) \,, \tag{1.1.1}$$

Here, $\omega = \Omega - \Omega_o$ is the shift of the current frequency Ω relative to the central frequency Ω_o, $\phi(\omega) = -d\sum k_j \omega^j / j!$ is the dispersion-induced spectral phase, $k_j \equiv k_\omega^{(j)}$ is the parameter characterizing the dispersion of group velocities in the *j*-th approximation of the theory of

dispersion, $d = z / L_D$ is the length of the medium normalized to the dispersive length $L_D \equiv \tau_o^2 / |k_2|$, and τ_o is the initial pulse duration [96].

The dispersion-induced spectral phase obeys the parabolic relation in the second-order approximation of the dispersion theory ($k_3 << k_2 \tau_o$), in the temporal analogy of diffraction, and accordingly, it is described by a parabolic equation:

$$\phi(\omega) = \frac{-\omega^2 k_2 d}{2}. \tag{1.1.2}$$

The above considerations imply that the DDL function can be realized by imparting radiation a spatial phase in a spectrometric device capable of expanding the frequency components with respect to the transverse spatial coordinate. A lens can serve as a spatial parabolic phase modulator. In the paraxial approximation, the phase induced by a lens can be expressed as follows [97]:

$$\phi(x) = \frac{-x^2 k_0}{2f}, \tag{1.1.3}$$

Where f is the focal distance, x is the transverse spatial coordinate, $k_o \equiv 2\pi / \lambda$ and λ is the radiation wavelength.

For a spectrometric system comprising m prisms (with a refractive index n and its frequency derivative n') and a lens (with a focal distance f_0), the radiation frequency ω and the transverse spatial coordinate x in the focal plane are linearly related as $x = \alpha\omega$, where $\alpha \equiv (dx/d\omega)_o = 2 f_o n' m / \sqrt{4 - n^2}$ for a prism with an apical angle of $\varphi = 60^o$ [98]. Then, an additional lens (with a focal distance f placed at the output of this system will lead to the modulation of the radiation phase according to the law $\phi(\omega) = -\omega^2 \alpha^2 (k_o / f)/2$ instead of the relation (1.1.2) provided by the usual DDL. Thus, for a device schematically depicted in Fig. 1.1.2, the transmission function is as follows:

$$D(\omega) = \exp[-i\omega^2 \alpha^2 (k_o / f)/2]. \tag{1.1.4}$$

Let a Gaussian pulse arriving at the input of this prism– lens DDL to have a spectral width $\Delta\omega_o$, an initial spectral phase $\phi_o(\omega) = -\beta\omega^2/2$, and the corresponding duration

$$\tau_{in} = \frac{\sqrt{1+(\beta\Delta\omega_o{}^2)^2}}{\Delta\omega_o}$$

The output pulse has the amplitude

$$F_{out}(\omega) = |F_{in}(\omega)| \times \exp[-i(\beta + \kappa_o\alpha^2 / f)\omega^2 / 2]$$

and the duration

$$\tau_{out} = \frac{\sqrt{1+\Delta\omega_0{}^4\left(\beta + \kappa_0\alpha^2 / f\right)^2}}{\Delta\omega_0}$$

so that the ratio τ_{out} / τ_{in} is

$$\left(\frac{\tau_{out}}{\tau_{in}}\right)^2 = \frac{1+\Delta\omega_0{}^4(\beta + \kappa_0\alpha^2 / f)^2}{1+\beta^2\Delta\omega_0{}^4}. \qquad (1.1.5)$$

The proposed prism–lens DDL scheme has been experimentally tested using a Ti:sapphire laser as a source of light pulses. The radiation parameters were as follows: wavelength, λ = 800 nm; pulse duration (full width at half maximum), ~100 fs; pulse average power, p ~ 1.5 W; pulse repetition rate, 76 MHz. The device according to Fig. 1.1.2 consists of the dispersive prism P and lens L_0 as the simplest spectrometer, an additional lens L as the phase mask, and a high-reflecting mirror M. The dispersive prism (P) and the phase mask (L) are placed at the focuses of lens L_0. In this scheme, prism P converts the frequency spectrum into an angular distribution and lens L_0 expands the spectral components with respect to the transverse spatial coordinate x at the mirror, which allows the spectral phase to be controlled using a spatial phase mask. We use lens L as the phase mask, which gives to the radiation a spectral phase according to relations (1.1.3) and (1.1.4). The experiments were performed with lenses possessing various optical strengths. The negative and positive chirps were realized using convergent (convex) and divergent (concave) lenses, respectively.

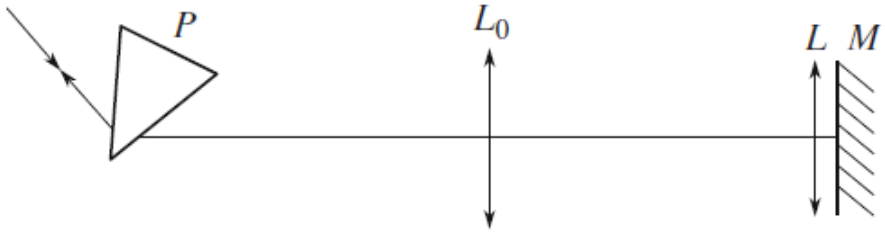

Fig. 1.1.2. Schematic diagram of the prism–lens DDL.

In these experiments, the intensity correlation functions were measured at the input and output of the proposed prism–lens DDL using an APE PulseCheck correlator. Fig. 1.1.3 shows the normalized correlation functions of pulses stretched in the DDL in comparison to the initial pulses. As can be seen, the stronger the lens, the greater the pulse stretching. Since the pulse spectrum remains unchanged, the pulse stretching is completely related to the dispersion-induced spectral phase.

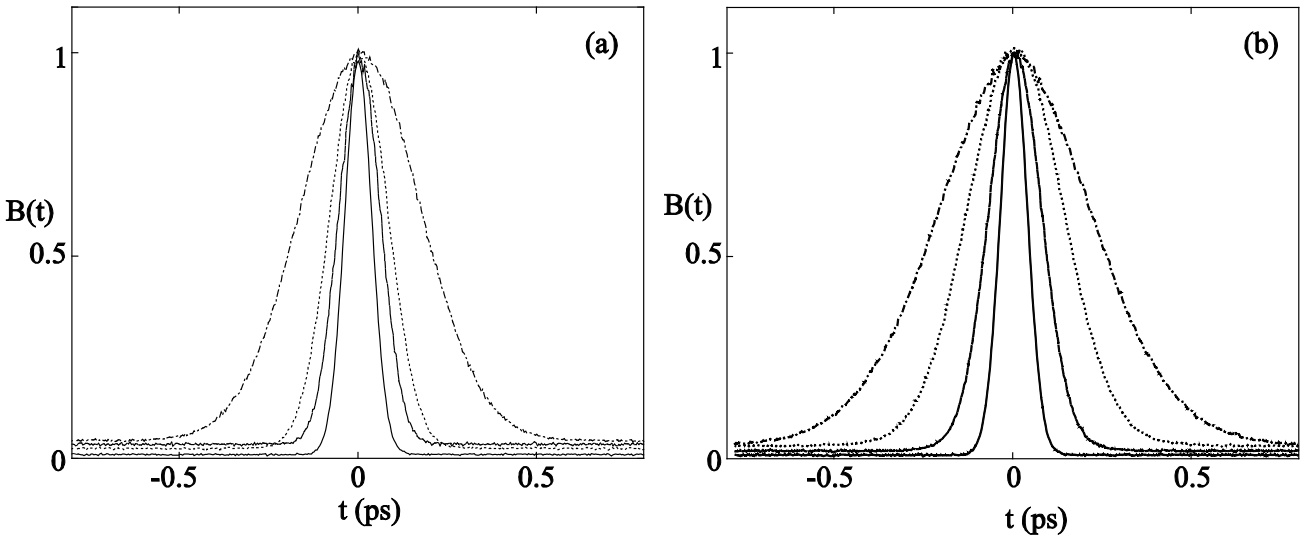

Fig. 1.1.3. Normalized intensity autocorrelation functions $B(t)$ of initial pulses (solid curves) in comparison to those of the output pulses stretched in the DDLs with various optical strengths of lenses: (dashed curves) f = 1.7 m (a) and –2.8 m (b); (dotted curves) f = 1.3 m (a) and –1.4 m (b); (dash–dot curves) f = 0.6 m (a) and –0.6 m (b).

The major problem of autocorrelation is that it does not uniquely determine the pulse characteristics. It cannot even accurately determine the pulse length, since to do that requires prior information about the pulse shape, which in fact is impossible to obtain. The disadvantage of the intensity autocorrelation measurement is in the fact that it does not contain complete information on the pulse shape. Moreover, the same autocorrelation trace can correspond to pulses of different shapes. Thus, intensity autocorrelation is not sufficient to determine the intensity. Below another more informative method for pulse characterization will be described.

1.1.2. Fourier Transform spectral interferometry for shaped pulse characterization

Interferometry provides a very sensitive and accurate means to measure the phase of an optical field. This approach can be considered as classical in the field of optical testing.

Fourier-transform spectral interferometry is a version of interferometry where the signal is measured in the frequency domain relative to a reference pulse [48]. Typically this is recorded with a detector array placed in the focal plane of a grating spectrometer, to yield a spectral interferogram. The schematic apparatus is in the case when the pulse under test is derived from the reference pulse by propagation in a device under test. The data set is a function of only a single variable frequency, rather than of two variables as in time–frequency methods. This means that the second dimension of a two-dimensional detector array may be used to record spatial variations in the spectral phase, for example.

The spectral phase is extracted via a direct inversion that is both rapid and robust. The test and reference pulse are delayed in time with respect to one another by τ by using a linear time-stationary filter $\tilde{S}_L^P(\omega) = e^{i\omega\tau}$. The detected signal (interferogram) is then $D(\omega;\tau) = |\tilde{E}_R(\omega) + \tilde{E}(\omega)e^{i\omega\tau}|^2$, where $\tilde{E}_R$ is the reference field and $\tilde{E}$ the test pulse field. The spectral phase difference between the test and reference pulses is encoded in the relative positions of the spectral fringes with respect to the nominal spacing of $2\pi/\tau$.

The phase difference can be extracted by using a three-step algorithm involving a Fourier transform to the time domain, a filtering operation, and an inverse Fourier transform. The interferogram may be written as

$$D(\omega;\tau) = D^{(dc)}(\omega) + D^{(ac)}(\omega)e^{i\omega\tau} + [D^{(ac)}(\omega)e^{i\omega\tau}]^*, \tag{1.3.1}$$

where

$$D^{(dc)}(\omega) = \tilde{I}(\omega) + \tilde{I}_R(\omega), \tag{1.3.2}$$

$$D^{(ac)}(\omega) = |\tilde{E}(\omega)\tilde{E}_R(\omega)|\, e^{i[\phi(\omega)-\phi_R(\omega)]}: \tag{1.3.3}$$

The dc portion of the interferogram, Eq. (1.3.2.), is the sum of the individual spectra of the pulses and contains no phase information. The ac term, Eq. (1.3.3.), contains all of the relative phase information.

There are three steps for reconstructing the spectral phase from the interferogram. First, isolate one of the ac terms, and hence $\phi(\omega)-\phi_R(\omega)+\omega\tau$, by means of a Fourier transform and filter technique (Fig. 1.1.4). Let *t* be the conjugate variable to ω and $\tilde{D}$ be the Fourier transform of Eq. (1.3.1). If τ is sufficiently large, the dc and ac components (located at *t*=0 and $t=\pm\tau$) are well separated in time, and the phase-sensitive component $D^{(ac)}$ can be filtered. For this purpose we use a filter $H(t)$ centered at $t=\tau$. The filtered signal, $\tilde{D}^{(filtered)}(t)= H(t-\tau)\tilde{D}(t)$, is simply the Fourier transform of the positive ac portion ($t=+\tau$) of the interferogram. The spectral phase difference is the argument of $IFT[\tilde{D}^{(filtered)}]$, i.e., the inverse Fourier transform of $\tilde{D}^{(filtered)}(t)$,

$$\phi(\omega)-\phi_R(\omega)+\omega\tau=\arg[D^{(ac)}(\omega)\exp(i\omega\tau)]=\arg\{IFT[\tilde{D}^{(filtered)}](\omega)\}. \quad (1.3.4)$$

The next steps include removing $\omega\tau$ by subtracting a calibration phase and reconstructing $\phi(\omega)$ by subtracting the reference phase $\phi_R(\omega)$. In cases when the test pulse is obtained by linear propagation in a device under test, the extracted phase difference $\phi(\omega)-\phi_R(\omega)$ completely characterizes the dispersion properties of the device.

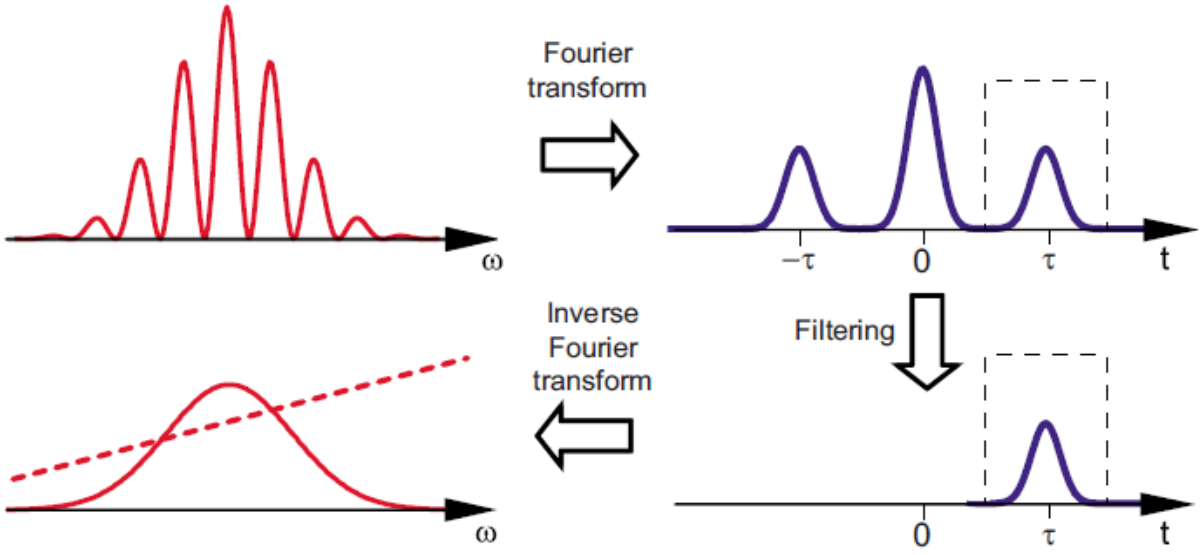

Fig. 1.1.4. Diagram of the inversion algorithm for Fourier-transform SI. After an initial Fourier transform to the time domain, an ac sideband is digitally filtered to isolate the interference term. An inverse Fourier transform is made, and the amplitude (solid curve) and phase (dashed line) of the interferometric component are extracted.

The above analysis refers to an idealized version of an experiment. The spectrometer has a finite spectral resolution that depends on its optics and detector, which leads to a decreased fringe contrast when the fringe period becomes comparable with the spectral resolution. Furthermore, sampling of the interferogram of Eq. (1.3.1) is performed at a finite rate (e.g., with the array of finite-size photodetectors that compose the detector located at the Fourier plane of the spectrometer). The interferogram is sampled at frequencies that are not necessarily evenly spaced. Finally, the quickly varying fringes that allow the extraction of the spectral phase difference from a single interferogram can make Fourier-transform spectral interferometry sensitive to frequency calibration of the optical spectrum analyzer. These effects are not detrimental to most applications of SI, and can be accounted for.

Fourier-transform spectral interferometry has applications in cases where one wishes to characterize a weak modulated pulse whose spectrum overlaps completely with that of a known, and usually more intense, reference pulse. This is not an uncommon situation in ultrafast optics, arising wherever linear filters (such as a pulse shaper or stretcher and compressor) are used to manipulate the pulse. It also pertains to some nonlinear optical processes that are used in time-resolved spectroscopy, such as degenerate four-wave mixing. Since the Fourier transform of the optical spectrum can also be measured directly by using temporal scanning, versions of SI based on this principle have been applied in wavelength ranges where direct spectral measurements are difficult.

The key features of interferometry that make it useful for pulse characterization are the rapidity of data acquisition, the direct and fast reconstruction of the field from the data.

1.1.3. Spectral interferometric study of prism-lens dispersive delay line

In order to check that the lenses give parabolic phases to the input pulses, we recorded the spectral interference patterns as superposition of the input and output pulses. For this purpose, the Ti:sapphire laser radiation was split into two beams, one of which passed through the DDL and the other served as a reference. The interference patterns were recorded using an Ando AQ6315 optical spectrum analyzer. Using these patterns, it is possible to recover the spectral phase of radiation. Fig. 1.1.6 illustrates the interference patterns recorded for different diverging and collecting lenses. As we can see, in case of collecting lenses the oscillations on the interferogram's left side are thicker

than on the right side. The pulse has a negative chirp in this case. Using diverging lenses, we have the opposite image. Oscillations are thicker on the right side because of positive chirp. These interferograms allow us to retrieve spectral phases induced by collecting and diverging lenses. Furthermore, we can retrieve corresponding pulses.

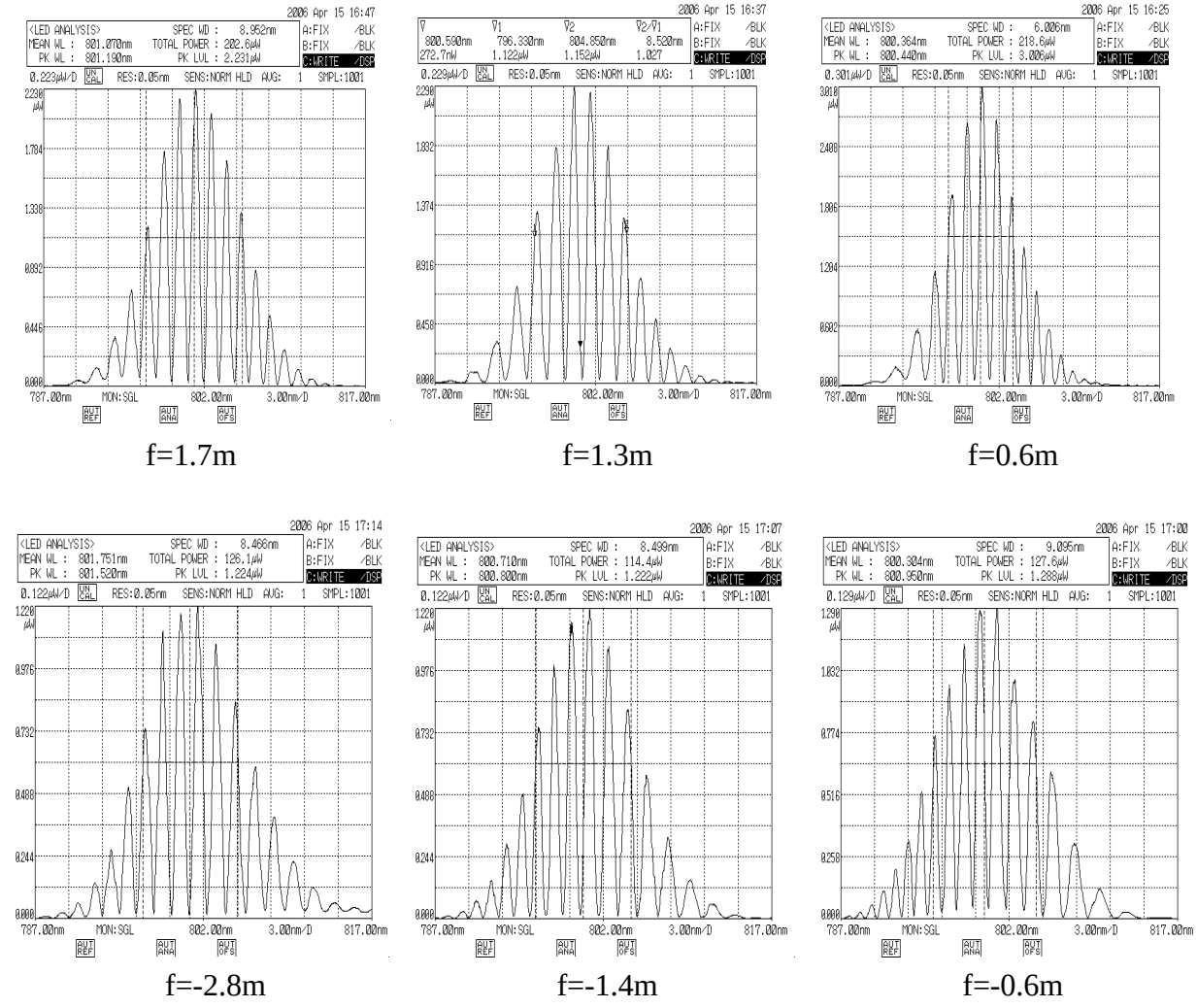

Fig. 1.1.6. Spectral interferograms for various lenses.

Fig. 1.1.7 (a) shows the typical patterns of the recovered spectral phases, where dots correspond to the maxima and minima of the interference pattern (with a phase difference of π), while solid lines show the fitted curves. The dashed curve is the spectral profile of the intensity. As can be seen, the recovered spectral phases are parabolic in the energy-carrying part of the spectrum. Fig. 1.1.7 (b) presents a plot of the square of pulse stretching ratio versus $1/f$ (experimental dots) and a

parabolic fit to the experimental points. As can be seen, the experimental data agrees well with the relation (1.1.5).

In conclusion, we have described and demonstrated a prism–lens DDL as a simple spectrometer and an additional lens as the phase mask. In contrast to the traditional DDLs, the sign and magnitude of dispersion in the proposed DDL are determined by the optical strength of the lens serving as the phase mask.

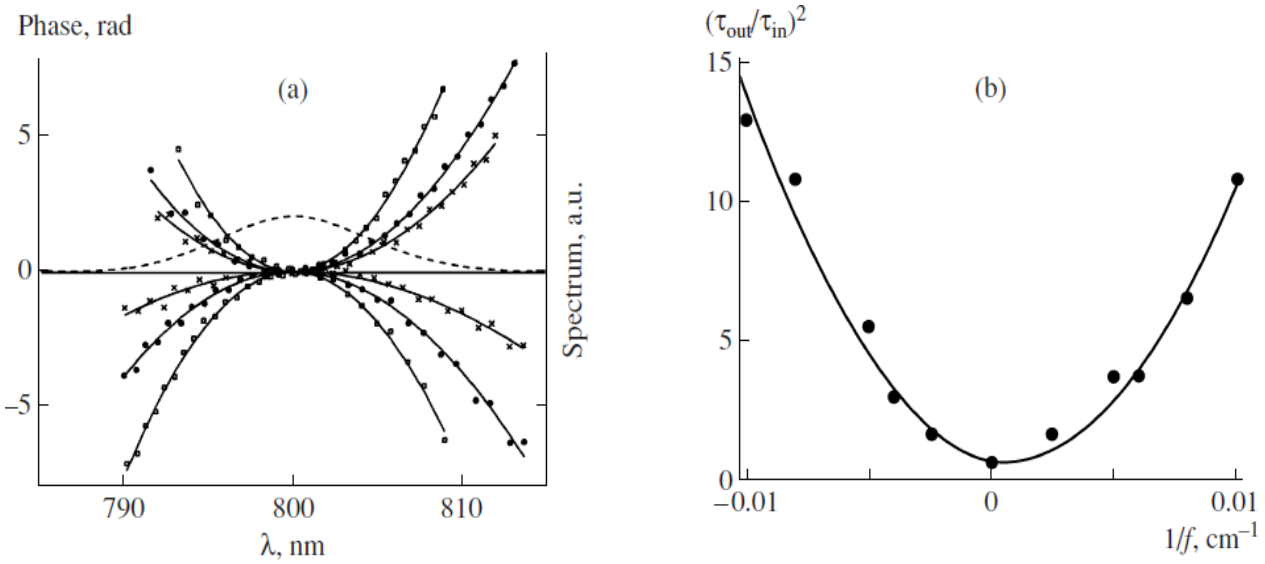

Fig. 1.1.7. (a) Recovered patterns of spectral phases and (b) plot of the pulse duration versus 1/*f* (points). Curves show parabolic fit to the experimental points.

We have also used the prism-lens dispersive delay line to shape pulses with the different temporal profiles. Below we will describe the shaping of ultrashort pulses with different temporal profiles.

First, we simply place a thin glass plate in front of a part of the widened laser beam. The part of the beam passing through the glass plate obtains a time delay with respect to the other free-propagated part. This way we shape pulses with two- or three-peak structures. Moving the plate along the vertical axis, we adjust the power proportion. The thickness of the plate determines the time delay between the peaks. For example, 250 fs delay corresponds to a 0.15mm thick glass plate.

To shape pulses with more complex shape we have used the prism-lens dispersive delay line as a simple spectrometer. As it was described above, in this scheme at the mirror we have spatial

distribution of spectral components. We shape complex pulses by placing amplitude and phase masks at the focal plane of the lens. We use lenses with different focal lengths and thin glass plates with inhomogeneous surfaces as the phase masks. This way we shape pulses with complex substructure.

To shape two peaks pulses we use again this scheme by placing the glass plate near the mirror, thus we have the phase shift between the different parts of the spectrum. The power proportion is determined by the thickness of the plate and the part of the spectrum. To have an idea about the shaped pulses we record the autocorrelation traces of pulse passed trough the spectrometer.

Three and more peaks pulses are shaped by giving the phase shift to the central part of the spectrum. Again we record the corresponding autocorrelation traces at the exit of the scheme.

We carried out the numerical modelling of the experiment also, and compared the results of experiments and simulations. The calculated autocorrelation traces were compared with the experimental ones. We have qualitative agreement between the recorded and calculated auto-correlation traces.

The recorded autocorrelation traces of shaped pulses are demonstrated in Fig.1.1.8. Pulses are shaped by using the glass plates with 0.1-0.125 mm thickness.

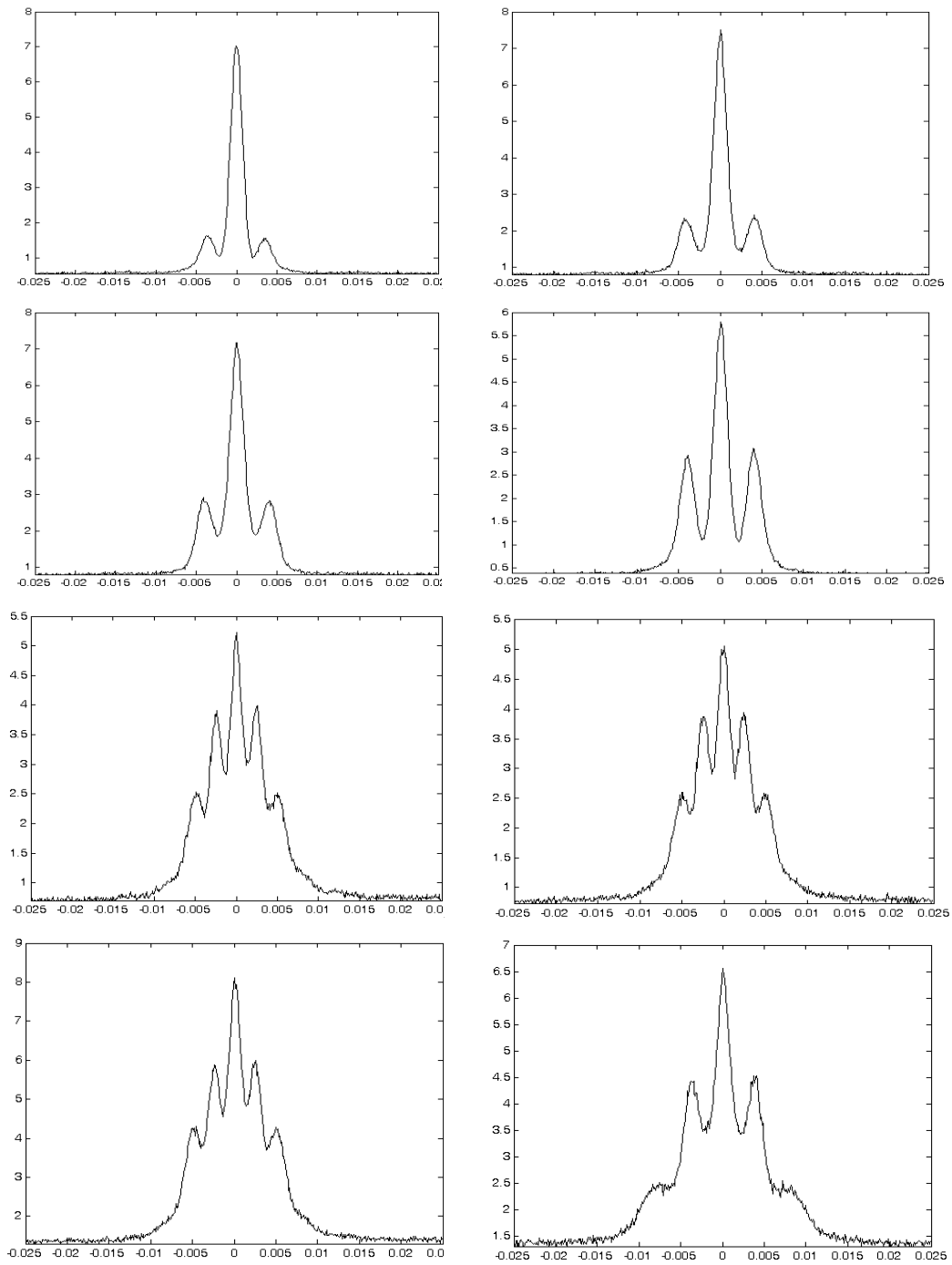

Fig.1.1.8. Recorded autocorrelation traces of shaped complex pulses.

Fig.1.1.9 illustrates the calculated autocorrelation traces and pulse temporal profiles, also for comparison are presented recorded autocorrelation traces of shaped pulses. As we can see, the recorded and calculated autocorrelation traces are in good accordance with each other.

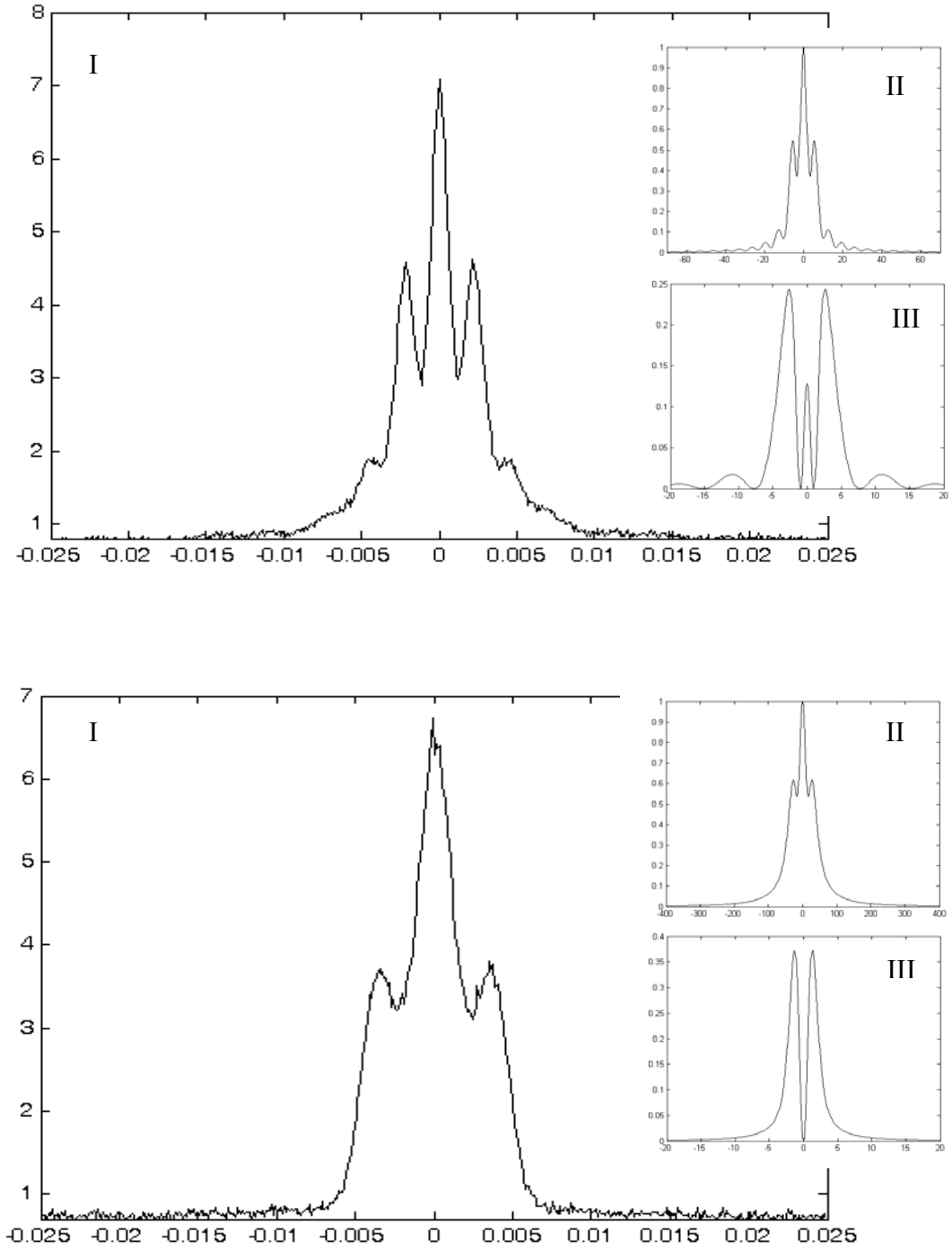

Fig.1.1.9. (I) - recorded autocorrelation traces, (II) - calculated autocorrelation traces, (III) – calculated pulse temporal profiles.

§1.2. Synthesis of Fourier transform rectangular pulses in the process of spectral compression

In this section the generation of 100-fs transform-limited pulses with a rectangular envelope in a spectral compressor is experimentally demonstrated. The pulses are characterised by the spectral interferometry method described in the previous section.

Interest in the formation of ultrashort pulses with a rectangular envelope is caused by their wide application, in particular, in optical communication for calibrating devices for ultrashort pulses formation [61], in control of light-induced quantum states [99], and so on. Such picoseconds pulses are formed by splitting the initial pulse into multiple replicas and delaying them in a set of birefringent crystals [100] or fiber optic couplers [101]. In an alternative approach, rectangular pulses are formed using spectral amplitude-phase masks placed into a femtosecond laser system [102] or in waveguides with a *sinc* transfer function [103]. It should be noted that pulses formed by these methods have a super-Gaussian or trapezoid temporal profile, but in the literature they are usually called rectangular due to a flat top and steep fronts.

The need for special devices [100-103] for formation of such rectangular pulses stimulates the development of new approaches to the problem. From the viewpoint of simplicity, it seems attractive to form rectangular pulses in a waveguide due to nonlinear-dispersive self-action. However, the pulse formed as a result of the mutual effect of the Kerr nonlinearity and the group velocity dispersion is positively chirped [104]. Transform-limited rectangular pulses can be achieved by negative chirping of pulses at the entrance to the waveguide. Such a system is actually a spectral compressor consisting of DDL and SMF [105, 106]. The analysis of the role of GVD in the spectral compression [107] showed the possibility of formation of transform-limited ultrashort pulses with a rectangular envelope.

This work is aimed at experimental investigations of the formation of transform-limited rectangular pulses in a spectral compressor, on the basis of the numerical analysis of the process [107]. The experiments were performed using spectral interferometry, which allows total characterization of the complex radiation field [108].

The experimental setup (Fig. 1.4.1) consisted of a Coherent Verdi 10 Mira 900F Ti : sapphire femtosecond laser (wavelength 800 nm, pulse duration at FWHM 100 fs, bandwidth 10.5 nm, pulse repetition rate 76 MHz, average power 1.5 W, peak power 2×10^5 W), a spectral compressor with a

DDL consisting of a pair of dispersion prisms P made of SF11 glass and a reverse mirror M3, a Newport FSE (780 nm) SMF, and a recording system [Ando AQ6315 optical spectrum analyzer (OSA) and APE Pulse-Check autocorrelator].

In the course of the experiment, the laser radiation was delivered to a Mach - Zehnder interferometer, in which the beam was split into two parts by a semitransparent mirror M1. The low-power part (20 %) was used as a reference for spectral interferometry. The powerful part of the radiation (80 %) was directed to the spectral compressor. The prisms were placed so that the beam was incident at the Brewster angle and propagated through their vertices. In the DDL with an anomalous dispersion, the spectrum does not change, while the pulse becomes longer and negatively chirped. After passing the DDL, the beam was coupled by a microobjective into the SMF, where the SPM leads to quenching of the chirp and to spectral compression of the pulse. The output spectrally-compressed pulse and the reference pulse were delivered to the OSA, which recorded the spectral-interference pattern: the overlap of the spectral harmonics of the signal and reference waves resulted in a total spectral pattern with beatings due to the difference in their spectral phases. Computer processing of the recorded spectral-interference pattern allowed us to reconstruct the spectral phase of the pulse under test formed in the spectral compressor by a method described in [109]. The measured spectrum of this pulse, together with its reconstructed spectral phase, makes is possible to completely reconstruct the pulse temporal amplitude and phase using the Fourier transform, i.e., to completely characterize the pulse under study. For temporal measurements in the course of experiments we also recorded the intensity autocorrelation functions. The experimental stages are illustrated in Fig. 1.4.2. We performed checking spectral and auto-correlation measurements at the entrance and exit of the DDL, which confirmed the spectrum stability and the expected degree of pulse stretching.

The experiments were combined with the numerical simulation of the process based on the nonlinear Schrodinger equation, taking into account the Kerr nonlinearity and the GVD, which adequately describes the process under study for pulse durations of about 100 fs [104]. The equation was numerically solved by the split-step fast-Fourier-transform algorithm.

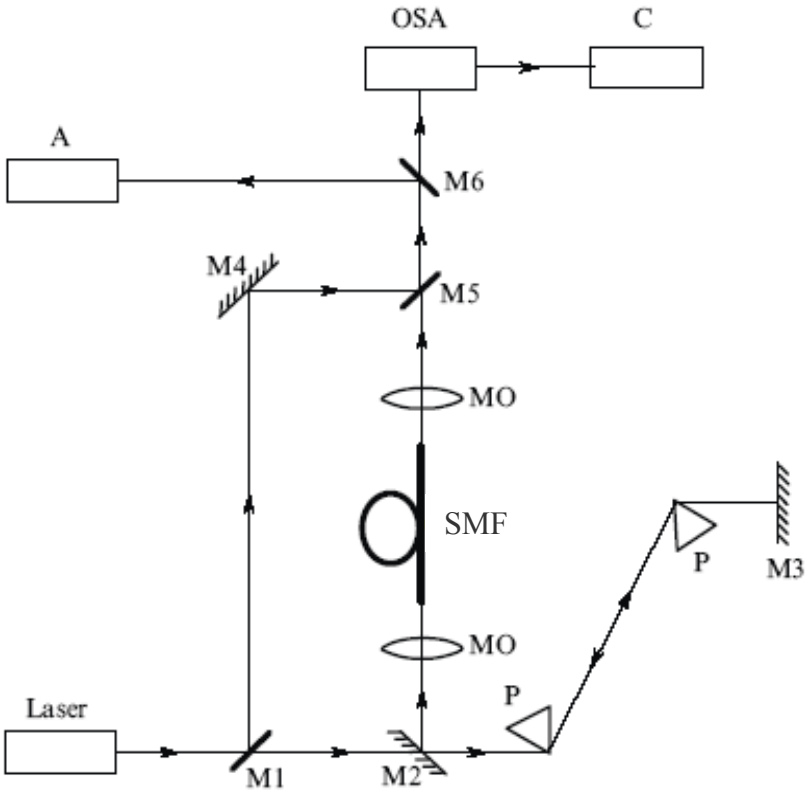

Fig. 1.4.1. Scheme of the experimental setup: (M1-M6) mirrors, (P) prisms, (MO) microobjective, (A) autocorrelator, (OSA) optical spectral analyser, (C) computer.

Our numerical investigations performed for different lengths of DDL and fiber confirmed the statement that the formation of rectangular pulses depends only on the ratio of the prism separation d (further called the DDL length) and the fiber length f [107]: rectangular pulses are formed at $d/f \approx 1.6 \cdot k_2^{(f)}/k_2^{(d)}$, $k_2^{(f)}$=10^3 fs^2/cm and $k_2^{(d)}$=6.5 $\times 10^3$ fs^2/cm are the second-order group velocity dispersion coefficients for SMF and DDL, respectively. In dimensionless variables, this condition has the form $Z/\varsigma \approx 1.6$, where $\varsigma = f/L_D^{(f)}$, $Z = d/L_D^{(d)}$, $L_D^{(f)} = \tau_o^2/k_2^{(f)}$, and τ_0 is the initial pulse duration [104]. Under these conditions, we achieve the maximal spectral compression.

The experiment was performed for the DDL length $d = 90$ cm (Z=5.4) and the fiber length $f = 22$ cm (ς=3.2). The degree of spectral compression at the exit of this system was 2.8, i.e., the bandwidth in this case was 3.7 nm. The compressed spectrum with small satellites has a shape of a sinc-like function which is the Fourier transform of a rectangular function (Fig. 1.4.2 (b)).

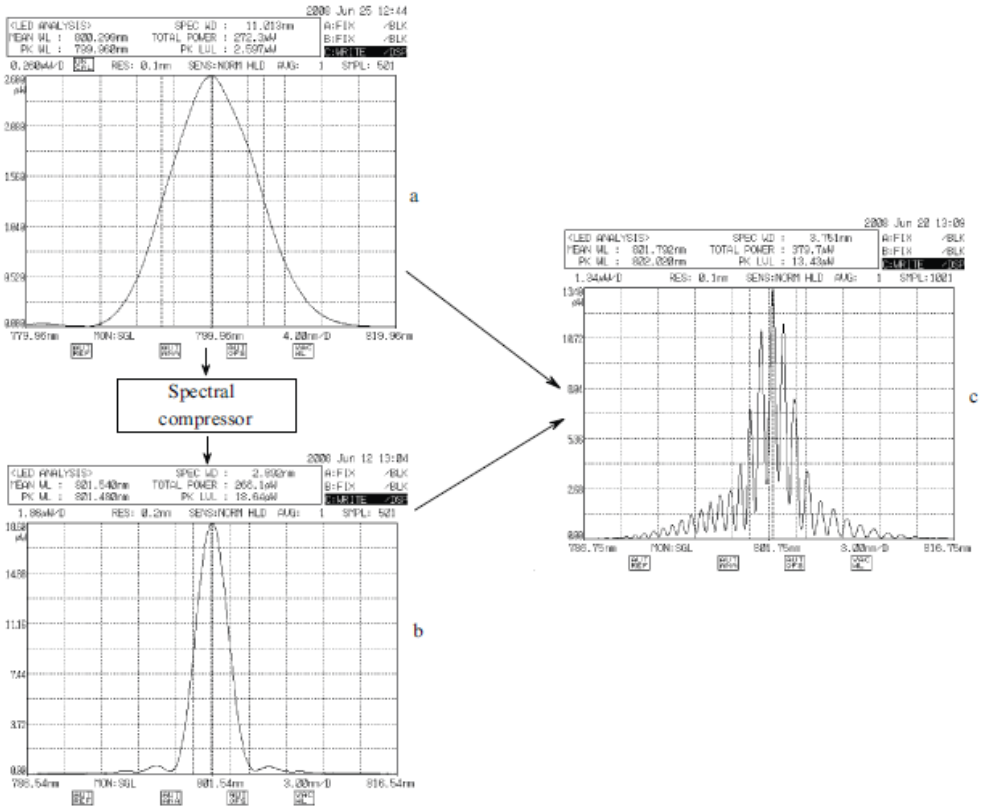

Fig. 1.4.2. Illustration of experiment through spectrograms: spectral profile of the initial pulse (a), spectrum at the exit from the spectral compression system (b); and spectral interference pattern (c).

The measurement results are shown in Fig. 1.4.3. From Fig. 1.4.3 (b) and 1.4.3 (d), one can see that phase modulation of the obtained rectangular pulses is almost absent, i.e., the pulses are transform-limited. The dashed curve in Fig. 1.4.3(c) corresponds to the results of numerical simulation with the corresponding radiation and setup parameters: we can see that calculated pulse temporal profile well agrees with the experimental one.

The reconstructed pulse profiles were used to calculate the intensity autocorrelation functions, which were compared with the measured autocorrelations. Fig. 1.4.4 shows the intensity autocorrelation traces of a rectangular pulse. The measured and calculated correlation functions quantitatively agree with each other.

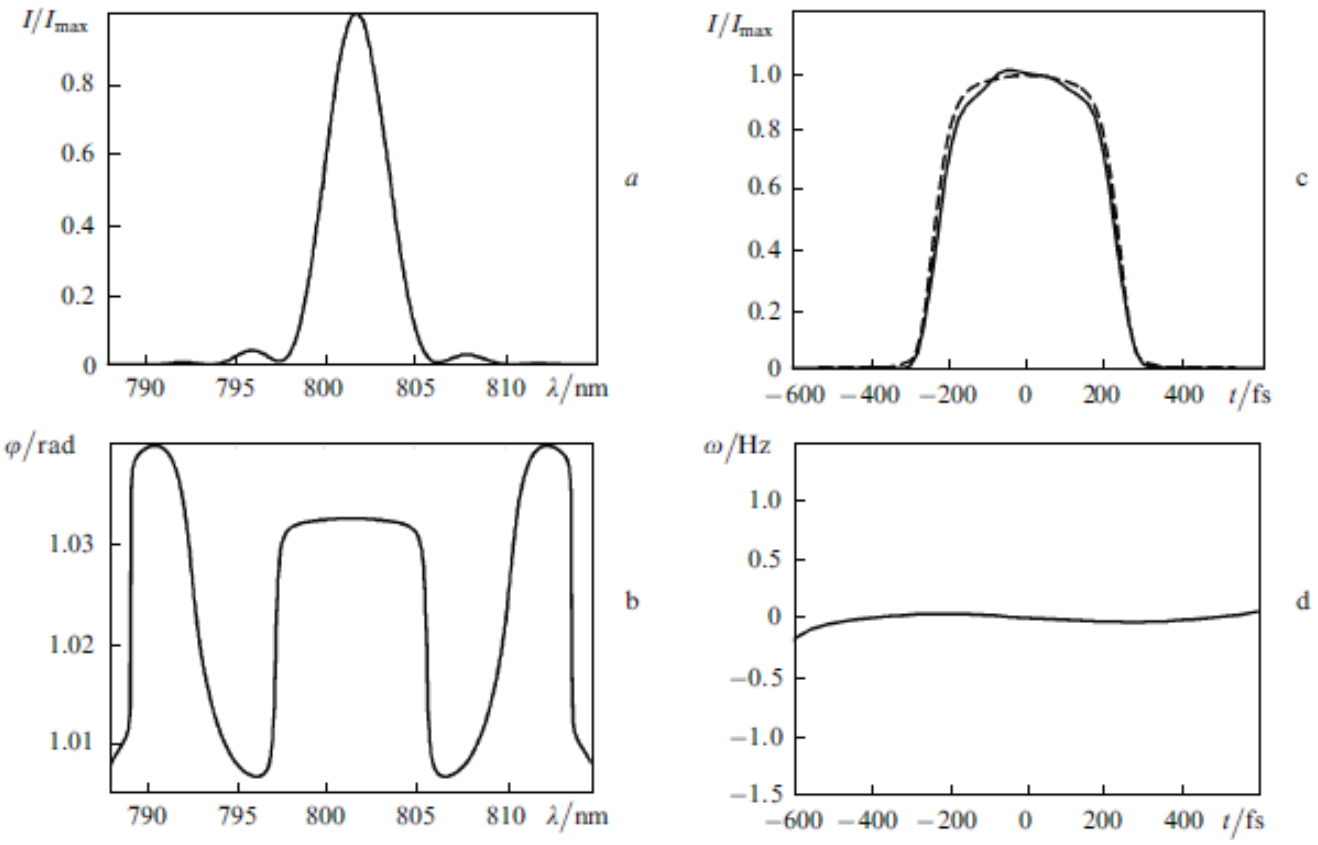

Fig. 1.4.3. Measured spectrum (a), reconstructed spectral phase (b), temporal profile (c), and chirp (d) of a pulse for $d = 90$ cm and $f = 22$ m. The dashed curve corresponds to the temporal pulse profile obtained in the numerical experiment.

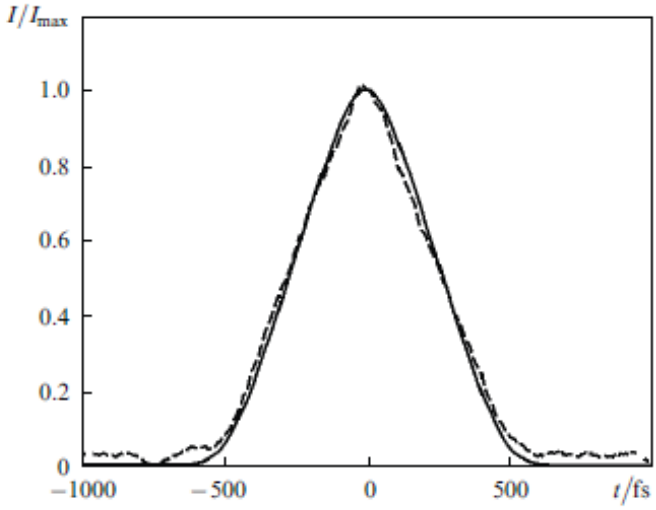

Fig. 1.4.4. Intensity autocorrelation traces of a rectangular pulse: measured (dashed curve) and calculated from the recovered pulse profile (solid curve).

Fig. 1.4.5 presents the dependence of the degree of spectral compression on the average radiation power in the fiber for $d =$ 90 cm and $f =$22 cm. The power was changed by changing the efficiency of coupling into the fiber. One can see that the pulse bandwidth narrows with increasing power, but widens again at powers exceeding 120 mW. The experimental results agree with the calculations. The experimental and numerical investigations showed that rectangular pulses are formed in the region of the maximum spectral compression. The numerical investigation also revealed that for other DDL and fiber lengths with the same ratio $Z/\varsigma \approx 1.6$, the dependence of the spectral compression on the average power in the fiber has the same shape but a different scale. For example, for longer DDL lengths, one observes an increase both in the degree of the maximum spectral compression and in the corresponding power.

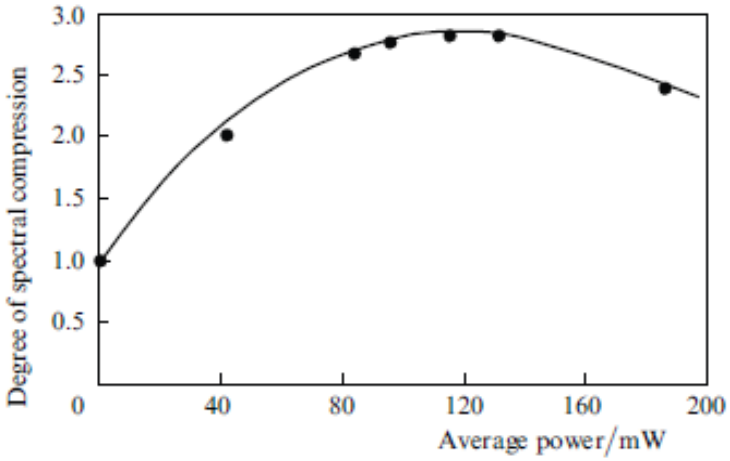

Fig. 1.4.5. Dependence of the degree of spectral compression on the average radiation power in the SMF for $d =$90 cm and $f =$22 cm. The dots and the solid curve correspond to the experimental and calculated data, respectively.

At powers that do not correspond to the maximum spectral compression, the pulse profile differs from rectangular. The temporal profiles of pulses at the exit from the spectral compression system at different average powers in the fiber are shown in Fig. 1.4.6.

The formation of rectangular pulses at the same ratio $Z/\varsigma \approx 1.6$ but different DDL and fiber lengths [$d =$ 142 cm (Z =10.3) and $f =$44 cm ($\varsigma =$ 6.7)] is demonstrated in Fig. 1.4.7. One can see that the reconstructed pulses also have a rectangular shape. The bandwidth in this case was 3 nm,

i.e, the spectrum was compressed by a factor of 3.5. Our investigations showed that, as well as in [100-103], the steepness of the pulse edges is determined by the initial Gaussian pulse duration and does not depend on the compressor parameters. However, at long DDLs, when the spectral compression is high, the formed pulses are longer. Taking the duration ratio of the pulse edge and peak as a rectangularity criterion [100], we can say that the shape of pulses obtained at longer DDL and fiber is closer to the rectangular.

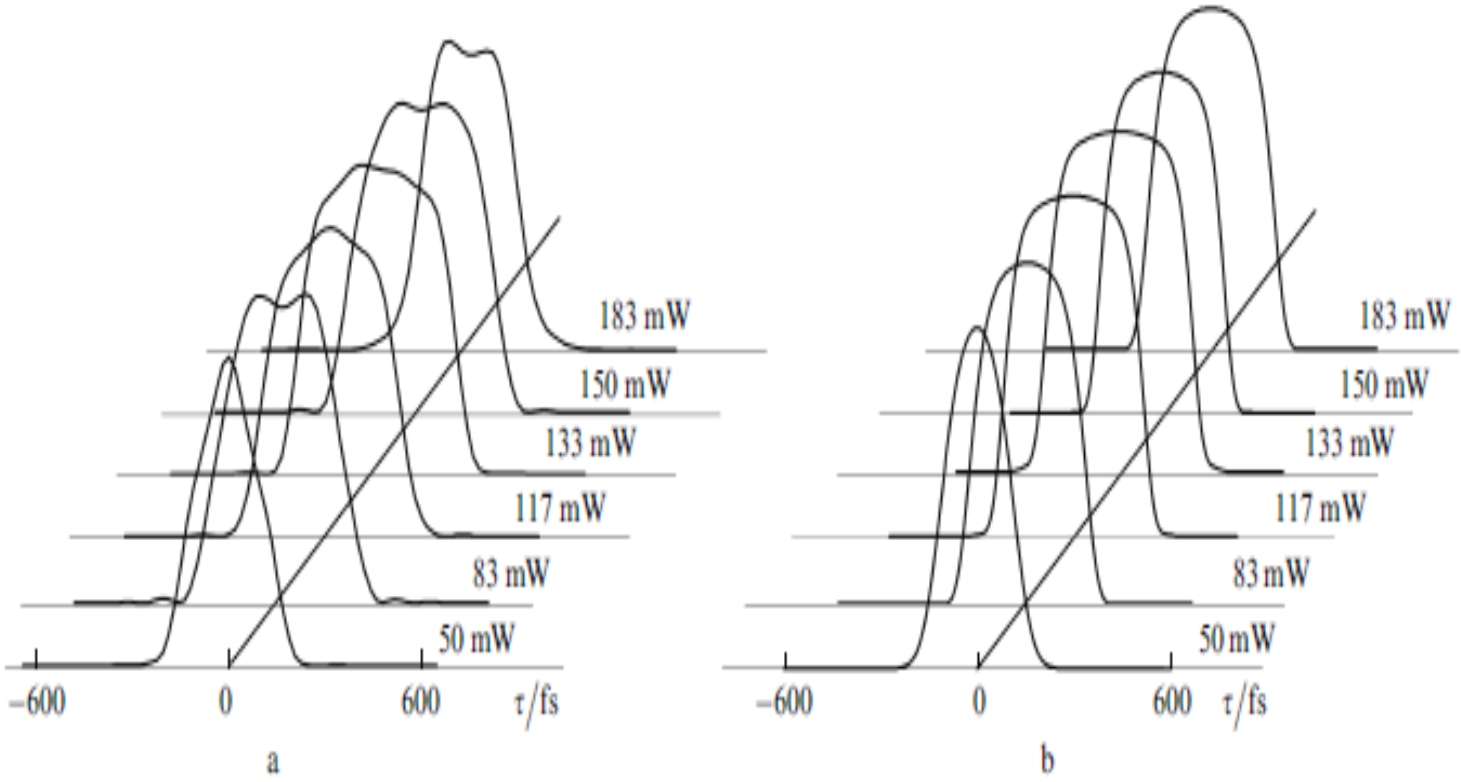

Fig. 1.4.6. Experimental (a) and calculated (b) temporal pulse profiles at $d = 90$ cm and $f = 22$ cm and different average powers in the fiber. The pulse amplitudes are normalised to their peak values.

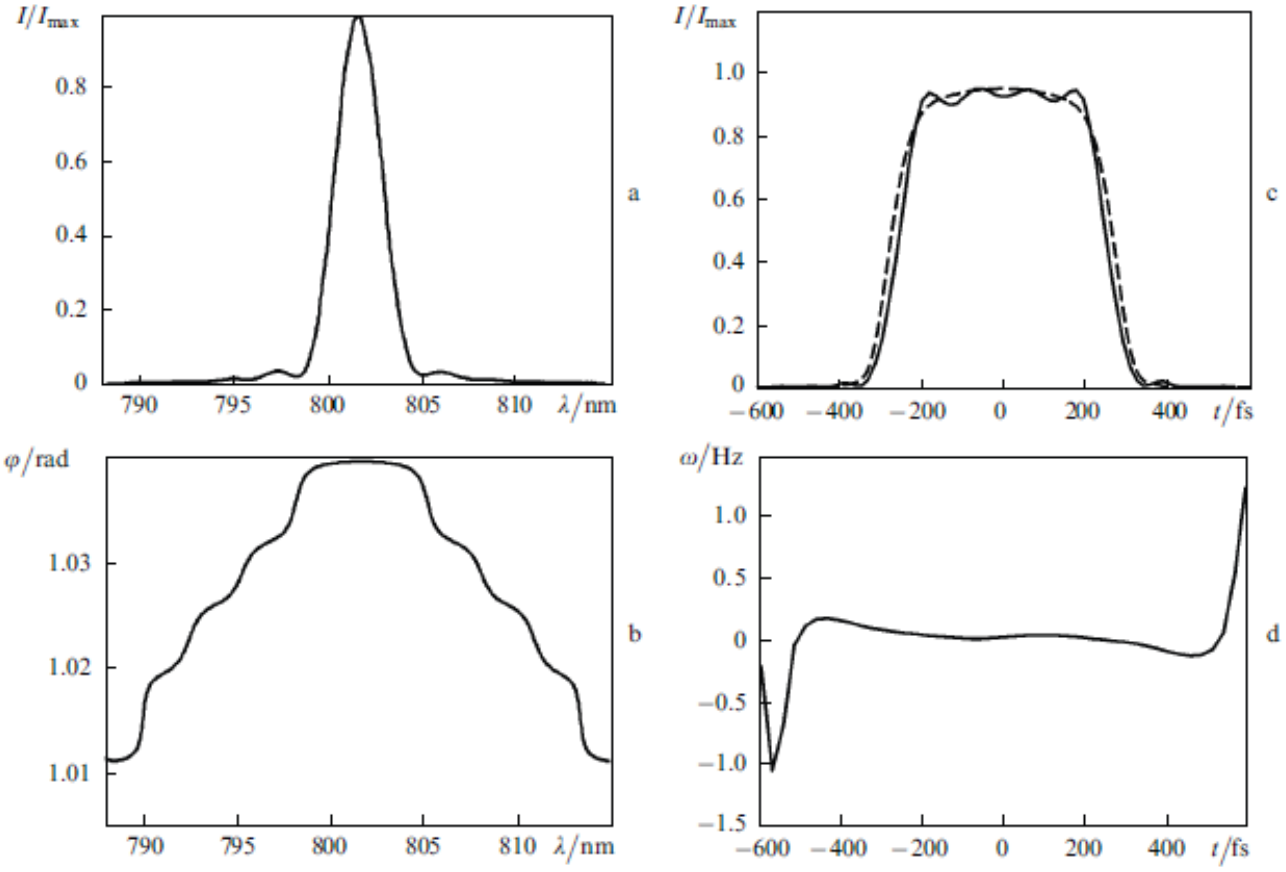

Fig. 1.4.7. Measured spectrum (a), reconstructed spectral phase (b), temporal profile (c), and chirp (d) of a pulse for $d = 142$ cm and $f = 44$ cm. The dashed curve corresponds to the temporal pulse profile obtained in the numerical experiment.

It should be noted that, in addition to the maximum spectral compression, a more necessary condition for the formation of rectangular pulses is $Z/\varsigma \approx 1.6$. To confirm this, we studied the spectral compression for the ratio $Z/\varsigma \approx 1$. In particular, for $d =$ 90 cm (Z = 5.4) and $f = 44$ cm ($\varsigma = 6.7$) (see Fig. 1.4.8), the temporal pulse profiles, as expected, have non-rectangular shape. In this regime, the pulse stretching in the DDL is decreased due to the dispersion in the fiber, which blocks the spectral compression [107]. In the experiment, the maximum degree of spectral compression in this case was 1.2.

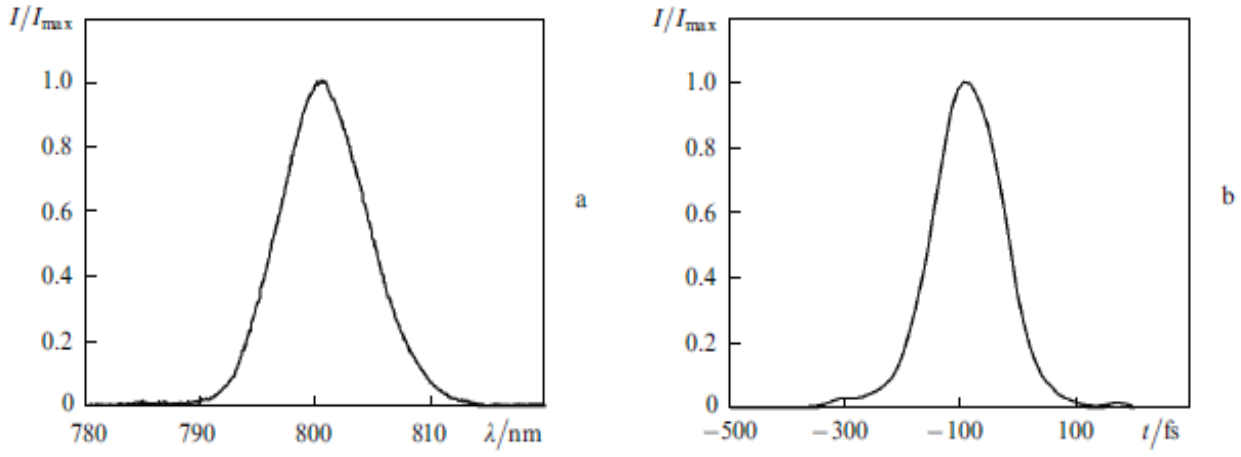

Fig. 1.2.8. Spectrum (a) and temporal profile (b) of a pulse in the regime of blocked spectral compression for $d = 90$ cm and $f = 44$ cm.

It is obvious that our results also agree with the data reported in [106]. This study was not aimed at obtaining pulses of a particular shape, but, due to the used ratio $Z/\varsigma \approx 1.7$, the pulses at the exit of the spectral compressor also had a flat top and a sinc-like spectrum.

In conclusion the formation of transform-limited rectangular pulses in a spectral compression system was studied experimentally. It is shown that the formation of such pulses does not depend on the DDL and fiber lengths separately, but depends on the ratio of the distance between the prisms and the fiber length. GVD in an optical fiber can change the physical image of the spectral compression process. The investigations showed that rectangular pulses are formed at the DDL-to-fiber lengths ratio $Z/\varsigma \approx 1.6$ in the region of the maximal spectral compression. At DDL lengths shorter than fiber lengths, spectral compression is blocked.

¢1.3. Femtosecond pulse shaping based on 2D phase-only spatial light modulator

With the advancement of electronics technology and the ability to manipulate anisotropic media electronically via computer interfaces, user-defined, programmable spectral windows and masks were developed, beginning the era of active pulse shaping. These programmable devices, such as SLMs [110] and acousto-optic modulators [111], allow one to manipulate the phase and amplitude of an ultrashort pulse by writing the desired phase function in real-time. This opened the door for

such areas of research as coherent quantum control and optimization of other ultrafast processes with computer feedback algorithms.

Despite the fact that programmable devices can achieve a very wide range of modulation functions, there are always some limitations of the pulse shaping apparatus. Primarily, pulse shaping is performed by manipulation of the spectral amplitude and phase of the pulse in the Fourier domain. Thus the fidelity of waveforms generated is limited by the spectral resolution of the device, i.e., how accurately the device can manipulate a single frequency of light. However, other limiting factors include the maximum phase modulation of the pulse shaper (as well as the resolution of the phase modulation), the bandwidth of the input pulse, and the throughput of the pulse shaper. The throughput (or efficiency) of pulse shaping apparatuses has continued to increase as advances in technology allow for more efficient SLMs. In the case of SLMs, the majority of the losses in a pulse shaping apparatus are due to the dispersive element, typically a grating. Several techniques have been proposed to produce complex modulation of an electromagnetic field with an SLM for encoding computer-generated holograms [112, 113]. In both cases, two neighboring pixels with a single-dimension modulation capability are coupled to provide the two degrees of freedom required for independent phase and amplitude modulation. It has been demonstrated that a SLM can be used to compensate for the thermal phase distortion occurring in high-energy glass amplifiers. SLMs have been used also in a wide range of applications, including in high-energy laser applications for intracavity beam shaping [114] and focal spot control [115], in digital holography for the optical reconstruction of digital holograms [116], in modern optical technology as real-time refractive lenses [117]. Recent advances in the fabrication of high-resolution SLMs have extended the use of SLMs into various disciplines, especially in the field of adaptive optics. Most frequently SLMs have been extensively used for femtosecond pulse shaping and nonlinear chirp compensation. That’s why we decided to use SLM based femtosecond pulse shaper to control fourth and fifth orders of dispersion. Our goal is to combine the shaper with the pulse delivery scheme to be able to obtain maximally compressed pulses.

Here, we report a simplified and very compact direct space-to-time pulse shaping (DST-PS) setup by using for the first time to our knowledge a phase-only high resolution liquid crystal (LC) SLM, without additional mask, relay optics, and diffraction grating as in conventional DST-PS [118], this experiment is done together with the Tigran Mansuryan. Furthermore, we show that it is

possible to perform high-fidelity pulse shaping both in amplitude and in phase with a single phase-only LC-SLM. We introduce a single phase-only high resolution SLM simulating an inhomogeneous blazed phase grating. This computer-controlled element plays the role of both the spatial mask and of the dispersive element of the spectroscope. Amplitude and phase modulation of the wave diffracted in the first order by the synthesized grating are performed independently controlling respectively the blaze angles and the absolute phases of the local phase gratings that are displayed along the SLM. Experimental setup is shown in Fig.1.3.1.

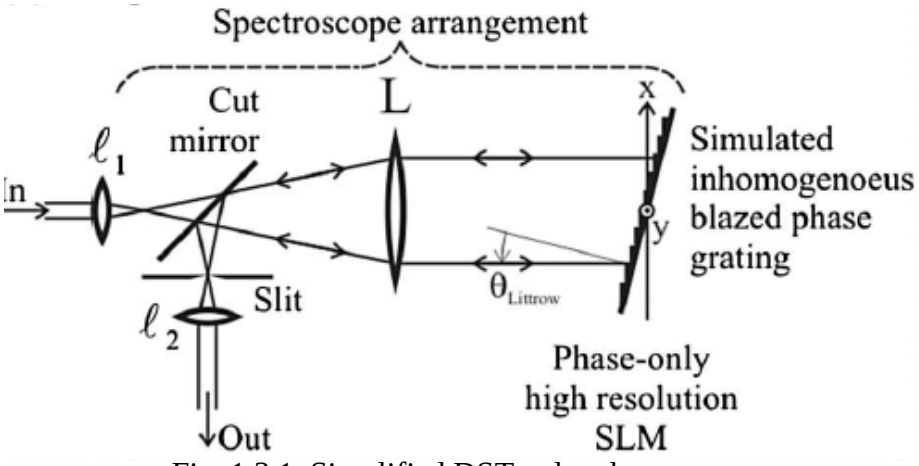

Fig. 1.3.1. Simplified DST pulse shaper.

A Ti:sapphire oscillator centered on 803 nm producing pulses with 200 fs autocorrelation duration (FWHM) fed the setup depicted in Fig. 1.3.1. A 2D HOLOWEYE phase-only programmable LC-SLM was used (reflective LCOS microdisplay; 1920 × 1080 pixels; 8:0 μm pixel pitch; ≈3π phase-shift at 800 nm; 60 Hz frame rate). The grating periodic modulations were set parallel to the small dimension of the device [i.e., y direction in Fig. 1.3.1]. Each three pixels of the LC-SLM were associated as one grating groove (i.e., p ¼ 24μm). The resulting blazed grating (15.36 mm width, 41.66 grooves/mm) gave a calculated space-to-time scale factor amounting to 111 fs/mm and a time window close to 1.62 ps. This is in very good agreement with measured data, which amounted respectively to 110 fs/mm and 1.61 ps [see Fig. 1.3.2(a)]. For those measurements, we used an intensity cross-correlator, using a fraction of the oscillator as reference. In order to test the shaper flexibility for amplitude modulation, various pulse doublets were synthesized with pulses having different amplitudes and/or different durations [Fig. 1.3.2(b) and 1.3.2(c), respectively). More generally, Fig.1.3.2(d) illustrates a pulse sequence involving five equidistant pulses.

The ability of the phase-only SLM to induce about 3π phase-shift has been used for phase modulation demonstration. A pulse doublet was synthesized with first identical and then opposite phase relationship. The registered spectra (see Fig.1.3.3) of the two sequences clearly show the phase control. Spectral fringes are shifted by half-period when the π phase-shift is added. Phase modulation can be achieved working with two different absolute phases for the two related local gratings. A contribution to this phase-shift can also come from the translation along the x direction of one of the two local gratings by one or two pixels that results respectively in 2π=3 or 4π=3 additional phase-shift. We have checked that both phase and amplitude modulations can be independently achieved without couplings. The diffraction efficiency in the first order of a uniform blazed phase grating synthesized by the LC-SLM was measured to be 36%. It is rather close to what would result from the association of a dual mask amplitude-phase LC-SLM and a diffraction grating inside a standard DST-PS setup (i.e.≈60% for the amplitude -phase LC-SLM and≈80% for a conventional diffraction grating). In spite of this, the overall efficiency was small, amounting to few percents depending on the desired pulse profile. Indeed, it is known that DST-PS basic principle results in rather low throughputs [119].

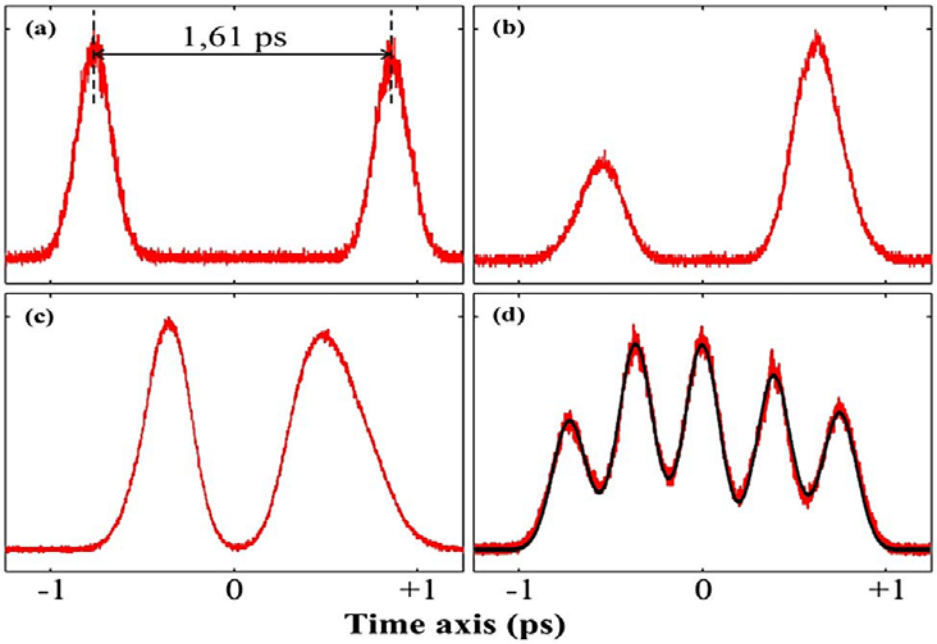

Fig. 1.3.2. Cross-correlation signals measured at the output of the DST shaper in case of amplitude modulation. (a) Doublet with maximal time separation. The time window of the shaper amounted to 1.6 ps. (b) Double pulse with different amplitudes. (c) Double pulse with different durations. (d) Sequence of five equidistant pulses: measured and calculated cross-correlations, the difference between measured and calculated curves is 2.6%.

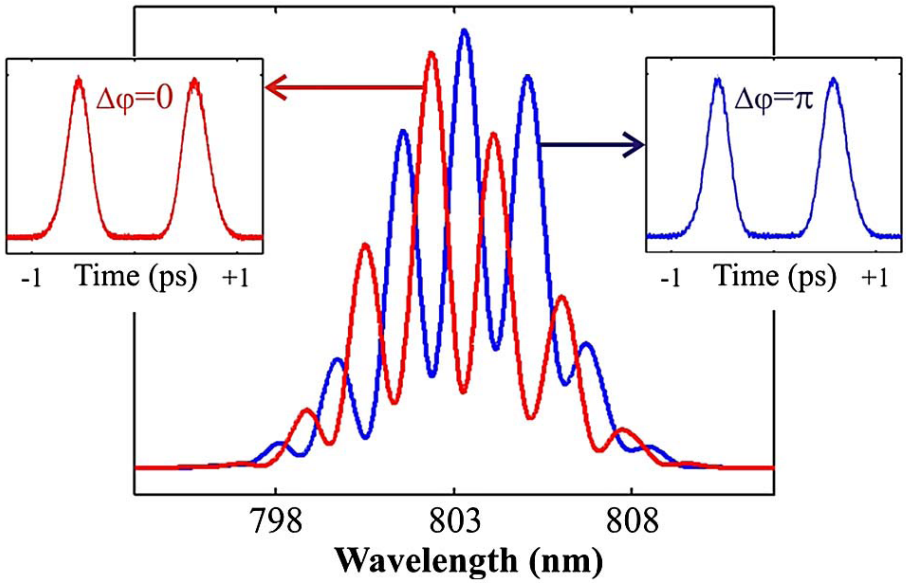

Fig. 1.3.3. Phase modulation. A double pulse sequence was synthesized with two different phase relationships: 0 and π. As a consequence, the two related spectra are shifted by half a fringe.

In conclusion, a new, very simple and compact DST femtosecond pulse shapers, where the grating and mask are replaced by a single programmable LC phase only SLM. The flexibility of the shaper for amplitude or/and phase control is demonstrated by double pulse generation with different amplitude and phase (in range of π) characteristics. Shaped pulse sequence, consisting of five peaks, demonstrates the prospective of this shaper in telecommunication. For other applications it has an advantage of fast (real time) and visually controllable device, as well; the pulse form can be directly observed on DVI monitor. The disadvantage of the shaper is the small total efficiency, which makes difficult to use this shaper inside others schemes. Optimization and development of "time windowing" and energetic characteristics, as well as performing for short pulse (10 fs) range and polarization state shaping, are the subjects of future studies.

Obtained results can be useful for the problems of control, transfer, and recording of optical signals.

Conclusion to chapter I

1. We propose and experimentally demonstrate an alternative dispersive delay line for ultrashort pulse shaping with the following advantages:
   - compact and simple design, independent of dispersive force;
   - possibility to induce both negative and positive dispersion;
   - easy tunable dispersion;
   - possibility to shape pulses with different temporal profiles
   - applicable for picosecond pulses due to compact design.

   Obtained results are in good accordance with the numerical simulation.

2. We experimentally demonstrated that the fiber group velocity dispersion together with the principal factor of Kerr nonlinearity becomes important for spectral compression. The group velocity dispersion impact is controllable, it can:
   - block spectral compression by temporal recompression of pulse in the fiber;
   - lead to an effective dispersive regime of spectral compression when rectangular Fourier transform pulses are formed along with the achievement of maximal spectral compression ratio.

   These pulses are Fourier transform limited, in contrast to the well known rectangular pulses generated in the fiber due to the combined impacts of self-phase modulation and dispersion. Our results of pulse complete characterization obtained by spectral interferometry are in a good agreement with the numerical simulations.

3. A new programmable direct space-to-time femtosecond pulse shaper using phase-only liquid crystal spatial light modulators has been demonstrated. The experimental setup is very simple and compact. The flexibility of the shaper for amplitude and phase control has been demonstrated by the generation of various pulse sequences with tailored intensity and phase (in the range of π).

CHAPTER II.

FEMTOSECOND PULSE FIBER DELIVERY WITH OPTIMIZED DISPERSION CONTROL BY REFLECTION GRISMS AT 800 NM

Femtosecond optical pulses have found a large spectrum of applications in contemporary science and technology. In many cases it would be advantageous to deliver the femtosecond pulses to the system under investigation with optical fiber [120]. Delivery of nJ, sub-100-fs laser pulses via an all-fiber distribution link has many applications in multi-photon microscopy [121], terahertz spectroscopy [122] and terahertz imaging [123], as well as in other areas where beam delivery of fs-pulses via optical fiber is of an advantage.

For example, fiber delivered coherent anti-Stokes Raman scattering (CARS) imaging system has increasingly attracted research attention, because of its flexibility for optical alignments as well as the importance for in vivo microendoscopy applications [123, 124]. As a nonlinear optical imaging technique, CARS imaging has been demonstrated as a powerful tool for label-free optical imaging. This technique offers many advantages including chemically selective contrasts based on Raman vibrational activity, high sensitivity and rapid acquisition rates due to the coherent nature of the CARS process, and sub-wavelength spatial resolution [125, 126]. Because of its highly-directional coherent property, the CARS signal is several orders of magnitude stronger than the conventional Raman signal; therefore, CARS offers ultrafast imaging capability in video rate in vivo [127]. Endoscopy has revolutionized modern medicine by allowing clinicians to visualize internal organs to screen for diseases such as colorectal cancer [128], lung cancer [129] and Barrett's esophagus [130]. Endoscopes are widely used in modern medical practice, making clinical procedures less invasive and saving time and cost, while providing physicians with valuable information from within the body. While current state-of-the-art clinical video endoscopes transmit excellent image quality, their overall size is capped by the dimensions of their sensors and electronics. Smaller and more flexible endoscopes have recently become available for clinical practice using optical fiber bundles, where each individual fiber is used to transmit one pixel in an image [131,132]. Maintaining acceptable image quality with small diameter fiber bundles is challenging, however; each optical fiber has a finite size, and therefore only a limited number of

fibers can be packed into an endoscope with a given diameter. Multiphoton microendoscopy enables visualization of cellular layers and intracellular organs with deep penetration depth and provides valuable information for early diagnosis of diseases and understanding complex mechanisms of biophenomena in living animals for research [133]. In vivo multiphoton microendoscopy can be used to directly observe molecular mechanisms of life without the need for sacrificing animals or removing tissue from the body, which is essential for practical applications. Multiphoton endoscopy uses an optical fiber for providing a comfortable distance between a target and optical and electronic hardware and a small sized probe for imaging internal organs in vivo [133].

Therefore, the goal is to develop a flexible, stable, and easy-to-use optical fiber delivery system as those used in confocal fluorescence endoscopy, optical coherence tomography, and in vivo endoscopy imaging systems. Many applications require methods for the delivery of pulses via an optical fiber over extended distances without significant pulse distortion.

¢2.1. Fiber delivery: basic features and numerical modelling

Femtosecond optical pulses are now involved in a wide range of applications. Frequently it is desirable to deliver those pulses with a flexible optical fiber without losing their basic specificities, i.e. shortness and intensity. However, because of their large bandwidth and high peak power, femtosecond pulses are not easy to deliver with an optical waveguide. They suffer from temporal and spectral broadenings because of respectively group-velocity dispersion and nonlinear self-phase modulation. This is particularly true operating near 800 nm carrier wavelength where normal dispersion is large. Several types of innovative optical fibers were proposed with the aim of reducing the waveguide dispersion or reducing its nonlinearity or more interestingly both of them. An attractive recently published solution relies on a kagome lattice argon filled hollow-core photonic crystal fiber [134]. Such fiber has a very weak nonlinearity and it has been predicted that its dispersion could be cancelled, controlling the pressure of the gas introduced in it. However, the experimental demonstration of this concept is still missing. Up to now the shortest pulse ever delivered by an optical fiber in the 800 nm range has been achieved using an air filled hollow-core fiber with a cladding made of a chirped photonic crystal [135]. This kind of innovative air-silica

microstructured fiber has a much larger bandwidth than those of previously experimentally validated hollow-core fibers [136]. Its very low and flat dispersion allowed for the delivery of sub-20 fs pulses. However chirped photonic crystal fibers have high guiding losses (> 5 dB/m) so that the previously published result involving this concept relates to only 0.13-nJ and 6.5-kW pulses at the output of a relatively short fiber (i.e. 80 cm).

Most applications of femtosecond fiber delivery, such as multi-photon endomicroscopy or fibered femtosecond terahertz generation, require more powerful excitations and longer fibers. T. Le and co-workers from Femtolasers Productions GmbH have demonstrated [135] that it was possible to efficiently deliver 800-nm 1.1-nJ 26.5 fs pulses through a 1.6-m long flexible waveguide working with LMA solid-core microstructured fiber. This kind of commercial fiber has a very low attenuation (i.e. <0.01 dB/m @ 780 nm at a moderate bending radius of 20 cm) in addition of being endlessly single mode over a broad bandwidth. It has a small nonlinearity because of a large core. However its dispersion is high so that the key issue relies in this case on fiber dispersion pre-compensation. Dispersion compensation can be achieved by means of an anomalous stretching device located before the fiber that acts as a compressor. For wide-bandwidth pulses cancellation of only second order dispersion (SOD) is not sufficient. One has to make efforts to compensate also for third order dispersion (TOD). For this reason T. Le worked with a specific SOD and TOD compensation system made of a combination of an expanded two prism-pair stretcher with two pairs of custom-made TOD optimized chirped mirrors. Authors reported that this scheme was sensitive to chirped mirrors manufacturing tolerances. Additionally this rather complex arrangement was not tunable which is rather detrimental for applications in biophotonics for example. That’s why a simpler and cheaper solution for optimized and flexible dispersion compensation is still desirable.

For this purpose we have focused our interest to a device associating a compact stretcher made of two grisms with a LMA fiber compressor. A grism-pair stretcher is composed of two identical grisms each of them being the assembly of a diffraction grating in close contact with a prism [137]. A grism-based stretcher has a negative SOD and its TOD can be set negative too providing suitable conditions for LMA fiber dispersion cancellation at 800 nm. Inside a grism-pair stretcher there exist enough geometrical freedom degrees to adjust the SOD and TOD continuously and simultaneously at desired values. Conventional prism or grating stretchers do not allow for such optimized

dispersion control. It has been demonstrated that grism-pair stretcher is a compact and simple solution for accurate dispersion control. The use of a grism-pair was first proposed for dispersion control by P. Tournois [137] to give high negative SOD with zero TOD. Later, E. A. Gibson and co-workers [138] showed that a grism-pair can simultaneously compensate for both second and third dispersion orders of material at 800 nm with high throughput working with reflective gratings near Littrow configuration. More recently it has been successfully involved in several ultra-wideband amplified systems [139]. Our group has also recently reported preliminary results about the use of a grism line for fiber delivery and pulse compression [140]. Here we will show with a grism-pair stretcher it is possible producing 1-nJ pulses with duration well below 30 fs at the direct exit of a 2.7 meter long LMA fiber.

Propagation of femtosecond light pulse inside an optical fiber at 800 nm is mainly governed by chromatic dispersion. In case of nanojoule-pulse Kerr type nonlinearity can also play an important role. The relative impact of those two physical phenomena can be evaluated looking at their respective characteristic lengths. The characteristic length that is associated to dispersion is $L_D = \frac{\Delta t_o^{\,2}}{4 \log 2 . \beta_2}$, where Δt_o is the pulse full width at half maximum in intensity (FWHM) duration and β_2 the fiber SOD parameter [61]. The dispersion of a LMA fiber is very close to the one of pure fused silica that composes the core with a weak contribution to dispersion coming from the waveguide [141]. At 800 nm β_2 of fused silica amounts to $\approx +\,35000$ fs^2/m so that for a 30-fs pulse L_D is ≈ 9 mm. The nonlinear length is defined as $L_{NL} = \left[(\omega / c) n_2 I_{peak} \right]^{-1}$, where $n_2 \approx 3.10^{-20}$ m^2/W is the nonlinear coefficient and I_{peak} is the peak intensity of the pulse [61]. For a 1-nJ and 25-fs pulse, propagating in a LMA fiber having a 16-μm mode field diameter corresponding to 200 μm^2 mode effective area, the nonlinear length is ≈ 2 3 mm at 800 nm, meaning that $L_D < L_{NL}$. As a consequence nonlinearity is strongly mitigated by dispersion that becomes the more important issue that has to be addressed first. As will be discussed later, nonlinearity induces some amount of spectral compression but its contribution can be considered as a secondary effect. As a consequence, the performances of the device are mainly related to the accuracy of the balance between the stretcher and the fiber compressor dispersions.

To help to design the stretcher, we have first performed numerical modeling of the [stretcher-compressor] system. Our grism-stretcher is made of an anti-symmetrically positioned reflecting grism pair (see Fig. 2.1.1). Its dispersion has been evaluated as a function of wavelength from group delay geometrical calculation [137]. The following characteristics were used as calculation inputs: (i) for the optical components, grating groove period d, prism apex angle α, prism glass refractive index Sellmeier law $n(\lambda)$; (ii) for the geometrical adjustment freedom degrees (see Fig. 2.1.1), the incidence angle θ upon the stretcher, the distance $L_{prism}=OT_2$ between the two prisms, the distance $L_{tip}=OT_1$ between the two tips of the two prisms. $L_{in}=T_1C_1$ is in another input parameter; however it can be demonstrated that, at fixed L_{tip}, the value of L_{in} has no impact upon stretcher dispersion.

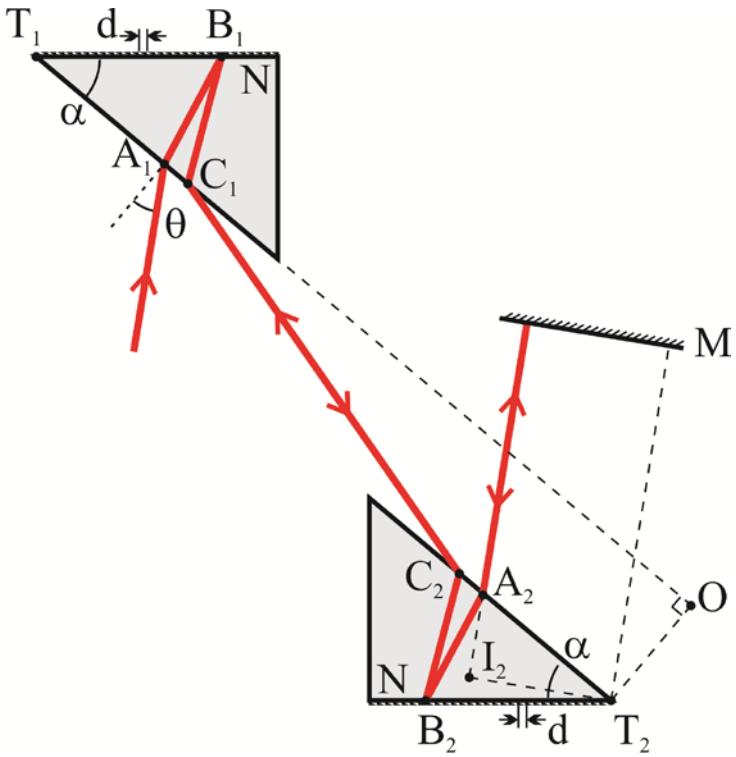

Fig. 2.1.1. Monochromatic optical path inside the grism-stretcher. M denotes a retro-reflecting plane mirror, N is the group index of the prism glass, α the prism apex and d the grating groove period . $L_{prism} = OT_2$ and $L_{tip} = OT_1$.

The group delay t_g of the stretcher is calculated by adding up the path lengths of an individual frequency component:

$$t_g = \frac{2}{c}\left[N(C_1B_1 + B_1A_1) + A_1A_2 + N(A_2B_2 + B_2C_2) - C_2I_2\right]$$

N is the group index of the prism glass while c denotes the light velocity in vacuum. Path lengths were calculated through conventional laws of optics and geometry. Group delay calculation is an original alternative to spectral phase calculation [139]. Our approach brings equivalent results with the advantage of being more direct.

The dispersive properties of the LMA fiber that plays the role of the compressor were assumed to be the one of pure fused silica (i.e. β_2=+34560 fs^2/m, β_3=+28220 fs^3/m and β_4=-13430 fs^4/m @ 820 nm). The data provided by the manufacturer of the LMA fiber [NKT Photonics] that was used during our experiments confirmed that this assumption was safe. Finally, input temporal and spectral intensity shapes were described with squared hyperbolic secant functions while durations and bandwidths were measured at half maximum in intensity. Spectral filtering that could result from diffraction grating spectral transmission variation has not been included in the model.

The adjustment of the stretcher begins with the search for the incidence angle θ onto it that provides the suitable ratio r_{32}=TOD/SOD. θ controls $r_{32}^{stretcher}$ while this ratio is slowly dependent on the distance L_{prism} between the two grisms. In our experiment we worked with grisms made of 600-grooves/mm-gratings and 40°-BK7-prisms. This choice provides the desired r_{32} parameter (i.e. $r_{32}^{stretcher} = r_{32}^{fused\ silica}$ = +0.817 fs @ 820 nm) at θ=38.884°. In this position the incidence onto the diffraction grating inside the two grisms is equal to 15°. The blaze angle of the grating that has been used during our experiments was 13.9° and the angular deviation induced by the grating is small ($\Delta\theta = \theta_4-\theta_3$ =12°@ 820 nm) conditions which ensure that the energetic efficiency of the stretcher is high (>30 % across the entire bandwidth).

Now, at fixed θ, SOD and TOD of the stretcher increase approximately linearly with distance L_{prism} between the two grisms so that the desired SOD and TOD can be reached simultaneously adjusting L_{prism}. During our experiments we worked with a 2.7-meter-long LMA fiber having φ_2^{fiber}=+9.332e+4 fs^2, φ_3^{fiber}=+7.627e+4 fs^3 @ 820 nm. The fiber SOD and TOD cancellations are performed simultaneously at θ=39.884° with L_{prism} =14.404 mm and L_{tip}=59 mm. In this position the stretcher-compressor is limited by uncompensated higher orders of dispersion. Calculations revealed that fourth order of dispersion (FOD) was the limiting factor with a negligible impact coming from the fifth and higher orders. Stretcher and fiber FODs amounted respectively to $\varphi_4^{stretcher}$=-4.42e+5 fs^4 and φ_4^{fiber}=-3.64e+4 fs^4 @ 820 nm. The two contributions have the same sign

meaning that they cannot compensate for each other and the net FOD is largely dominated by the stretcher contribution. When applied to a signal with 50-nm-bandwidth it results in a in a pulse with duration equal to 40 fs (see Fig. 2.1.2a) which is twice the Fourier limit (i.e. 19.4 fs for a Gaussian shape pulse having a 50-nm-bandwidth). Changing for a grating with a different groove density and/or for a prism with a different apex and/or material could represent solutions for smaller FOD while preserving SOD and TOD cancellations. However our calculations showed that those alternative choices could result in deviation from the Littrow configuration inside the grisms and as a consequence to deleterious reduction of the stretcher throughput. We believe that the above mentioned parameter set involving readily available commercial components (see next section) represents a good trade-off between optimized dispersion compensation with moderate FOD and high throughput.

Else, exact cancellation of the net SOD is not optimum in term of compressed pulse duration. Indeed it is advantageous to work with some amount of positive net SOD (i.e. +620 fs2 in the particular conditions that were described above) that is able to partially mitigate the negative net FOD coming namely from the grism-stretcher. Calculations confirm that a significantly shorter and brighter pulse can be obtained for different adjustments of the stretcher. The minimal duration is obtained with θ= 38.925 ° and L_{prism}= 14.385 mm. It amounted to 26.6 fs (FWHM) (see Fig. 2.1.2c) which corresponds to 1.4 times the Fourier limit while the peak power exceeds 30 kW for a 1-nJ pulse which corresponds to 62% of the peak power of the Fourier transformed pulse having identical bandwidth and energy. In case of exact cancellation of net SOD, a 1-nJ pulse having the same bandwidth has a peak power amounting to only 19 kW.

In the same conditions (i.e. with the same fiber, the same bandwidth, the same pulse energy), working with a grating-pair stretcher would relate to a delivered pulse with a much larger duration (i.e. 3 times larger for 600 grooves/mm gratings separated by 12.5 cm).

Because of very high uncompensated TOD, numerous secondary pulses would appear in the trailing edge of the compressed pulse. The peak power and the ability of producing at the fiber exit a second order nonlinear signal, such as two-photon fluorescence, would be respectively 6 and 9 times smaller. Working with a prism-pair stretcher would result in very similar performances in comparison with gratings, except for the secondary pulses that would appear now in the leading

edge, but with the additional drawback of requiring a very large distance between the two components (i.e. more than 2 meters between two SF11 prisms inside a 4-pass-stretcher).

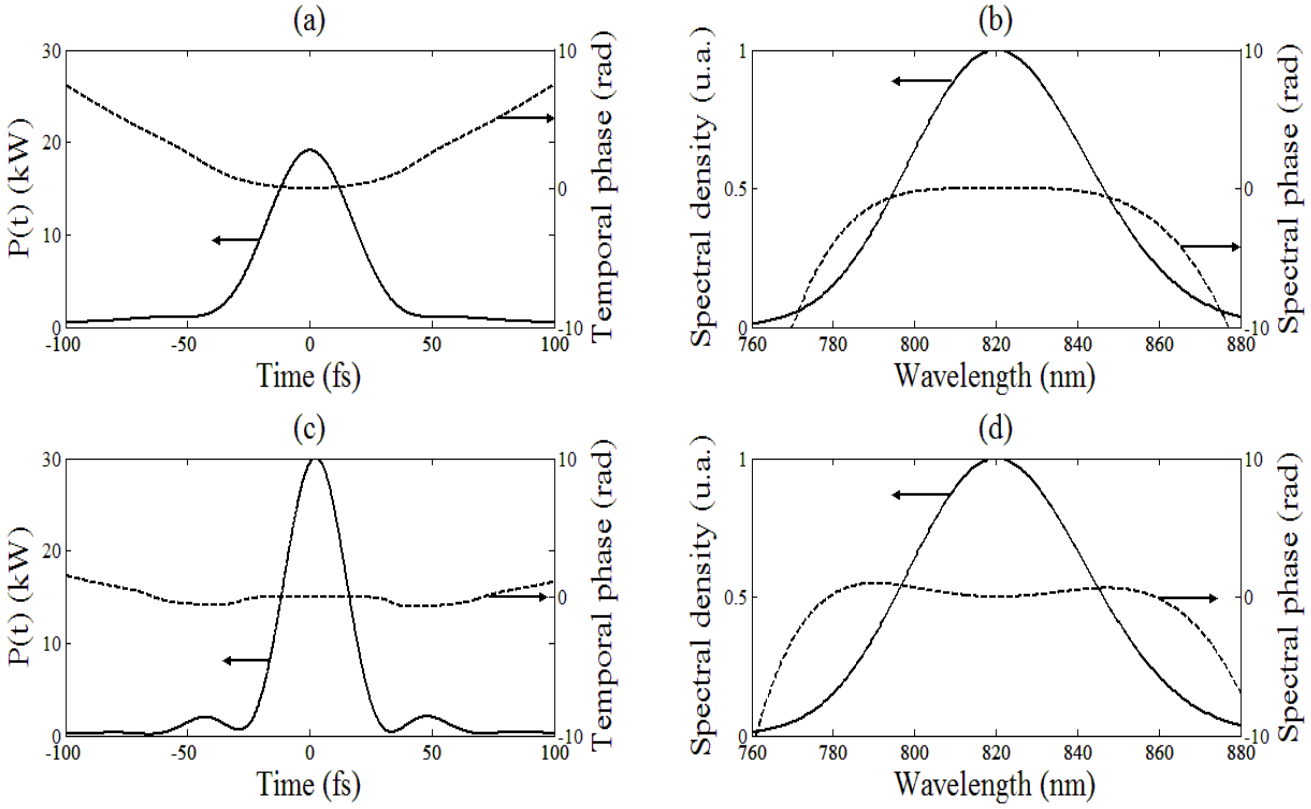

Fig. 2.1.2. Calculated pulse and spectrum at the direct output of 2.7-m long LMA fiber for two different adjustments of the grism-based stretcher at fixed L_{tip}=59 mm: (a) and (b), θ=39.884° and L_{prism} =14.404 mm; the stretcher perfectly compensates for both SOD and TOD of the fiber; the stretcher brings a large amount of FOD which is clearly seen on (b); the compressed pulse duration is equal to 40 fs (FWHM) with a peak power amounting to 19 kW for a 1 nJ pulse - (c) and (d): θ= 38.925 ° and L_{prism}= 14.385 mm; now the stretcher is adjusted so that TOD is compensated and that net SOD and net FOD partially compensate for each other; spectral phase variation amplitude across the spectrum is somewhat smaller; as a consequence the pulse duration is smaller (i.e. 26.6 fs) and the peak power is higher (i.e. more than 30 kW for a 1 nJ pulse).

Our device gives also very interesting results with long fibers. For example we have performed simulations increasing the fiber length to 10 meters (i.e. 3.7 times the previous one), all other characteristics being unchanged. With this long fiber SOD and TOD exact cancellations were

obtained for the following parameters: L_{prism} =61.21 mm, θ=39.48° and L_{tip}=150 mm. In this situation the stretcher FOD increased by a factor 3.2 (i.e. $\varphi_4^{stretcher} = -1.4e+6\ fs^4$) with respect to the case of a 2.7-meter-long fiber what resulted in a longer compressed pulse. However the delivered pulse is still very short. Its duration amounted to 57 fs (FWHM) which is only 1.4 times longer than the one for the 2.7-meter-long fiber and the pulse shape was unchanged. As previously, the shortest pulse has been performed when SOD partially mitigated FOD. It was obtained when L_{prism} =61.15 mm and θ=39.50° and the shortest duration amounted to 34 fs (FWHM) at the end of the 10-meter-long LMA fiber.

Now it is important to check that the performances of the stretcher-compressor are preserved at high power when nonlinear effects happen in the last few centimeters of the fiber compressor. For this purpose the nonlinear pulse propagation inside the dispersive LMA fiber has been modeled using the split-step method proposed by G.P. Agrawal [61]. Our model accounts for dispersion at all orders coming from the grism-based stretcher and from the fiber, for Kerr self-phase modulation, self-steepening and Raman scattering coming from fused silica third order optical nonlinearity inside the fiber core. At the largest energy level that has been achieved experimentally (i.e. 1 nJ at the fiber exit), the calculated total nonlinear phase-shift amounted to 3.7 radians meaning that nonlinear effects do have some impact. At this power level we have observed numerically and experimentally a noticeable spectral compression at the fiber exit amounting to 18% of the initial spectral width. However the compressed pulse duration does not increase proportionally as it would be the case for a Fourier limited compressed pulse. For a 1-nJ-pulse exiting the LMA fiber, the final duration increases to only 27.4 fs corresponding to a 3%-increase with respect to the linear regime. In presence of nonlinearity the calculated peak power amounted to 26 kW. This can be understood as follows; because it acts upon negatively chirped pulse, nonlinearity removes frequencies in the spectrum wings resulting in spectral narrowing [142] instead of more common spectral broadening when acting upon unchirped pulse. Those lateral spectral components are more affected by FOD. That is why by removing the spectral components that are affected the most by FOD, nonlinearity somehow tends to reduce the negative impact of FOD. Simulations reveal that self-steepening has a negligible impact while Raman scattering induces slight spectral modulations in the summit of the spectrum without modifying the pulse shape in a noticeable manner. As a conclusion we can

confirm that the system is weakly influenced by nonlinearity of a LMA fiber. The scalability of the device to higher energy levels and the use of more nonlinear fibers with smaller core such as standard SMF will be discussed below.

¢2.2. Delivery of 18 fs nanojoule pulses by large mode area photonic crystal fiber

In this section a very compact system for femtosecond pulse fiber delivery from wideband laser sources is experimentally demonstrated. Pulse fiber delivery pre-dispersing technique is developed, using large mode area photonic crystal fiber and grism line. Simultaneous control of SOD and TOD is realized by the compact grism line. 18 fs nanojoule pulse at the output of 2.7 m LMA fiber is demonstrated. To our best knowledge, obtained 18 fs pulse is the shortest pulse ever delivered directly by an optical fiber. 18 fs pulse durations were achieved by using a grism compressor. We used also conventional polarization maintaining single mode fiber (PM-SMF) to compare with LMA. For both fibers we adjusted the distance between the grisms to produce the shortest possible output pulses. Under similar conditions, a standard SMF delivers pulses about 10 fs longer than those delivered by LMA.

We started from a commercial femtosecond Ti: Al_2O_3 oscillator (MICRA from COHERENT, Inc.) having the following parameters of radiation: adjustable spectral bandwidth from 20 nm to 110 nm; 80 MHz for the repetition rate; 400 mW average power; 805 nm central wavelength in case of 110 nm bandwidth; central wavelength tunable in the range of 750-850 nm @ 20 nm bandwidth; rectilinear polarization within the setup plane. At the direct output of the MICRA oscillator the pulse is not compressed. However it is rather negligible with the dispersions induced later by the grism-based stretcher and by the fiber. The pulses emitted by this femtosecond source were negatively stretched by our grism-based stretcher that was made of two home-assembled grisms before being launched into the delivery fiber (see Fig. 2.2.1.). Each grism was composed of a 40° antireflection coated BK7 (ref. H-K9L from Union Optics) prism separated by a 30 μm air gap from a 600 grooves/mm gold coated blazed diffraction grating from Richardson Gratings (ref. 53066BK02-351R). The stretcher had a net energetic efficiency amounting to 36% (i.e. 78% for one grism) for an incident rectilinear polarization within the setup plane. The total spatial footprint of

the device is equal to 100 cm^2 square. Then light was launched into a 2.7 meter long endlessly single-mode LMA fiber from THORLABS, Inc. (ref. LMA-20) that has been cleaved by ourselves. A self-made cleave mostly produces a small angle (1-2°) between the normal of the fiber input face and the incoming beam, which deflects the reflected beam enough to not disturb significantly the oscillator anymore. For this reason there was no isolator within the setup. Nevertheless, we have never had problem of reinjection in the oscillator. The pure fused silica core of the LMA fiber had a mode field radius equal at 1/e to 8.3 μm (i.e. an effective mode field area equal to 215 μm^2) with a low numerical aperture equal to 0.04 @ 780nm. An achromatic lens with f = 15 mm focal length served to inject light into the fiber with a coupling efficiency amounting to 68% at best. The LMA was not polarization maintaining but it was slightly birefringent. A half-wave plate was located before the fiber in order to excite only one polarization mode. At the exit the polarization was approximately rectilinear. The fiber bending radius was equal to 30 cm so that the fiber transmission was close to 100%. As a result, the energy of the pulse that exited the fiber could reach at best 1 nJ. After the fiber a noncollinear second order autocorrelator with a 10-μm-thin doubling crystal and an interferometric autocorrelator with a two-photon-absorption photodiode were used for temporal characterizations while an optical spectrometer performed simultaneous spectral analysis. Coherent pulse measurements were also performed by using time resolved spectral interferometry through the SPIRIT technique [57] that has been specially adapted to broadband pulses. During our experiment for comparison besides LMA fiber we used also conventional PM-SMF. First we will discuss the results obtained with the LMA fiber.

Experimental setup is shown in Fig.2.2.1. It consists of three main parts: laser source, dispersive element, delivery fiber. The best result that we have obtained experimentally is reported in Fig. 2.2.2, proving the delivery of pulses having sub-20-fs duration and 1-nJ energy at the direct exit of a 2.7-meter-long LMA fiber. The corresponding output spectrum width was equal to 51 nm. The actual time-bandwidth product amounted to 0.46 assuming Gaussian shape pulse. The Fourier-transform limited pulse having the same spectrum and the same energy (i.e. 1 nJ) would correspond to 48-kWpeak power. We have estimated that the pulse peak power was in the range of 30-40 kW. The previous pulse duration is notably smaller than calculation predictions (see Fig. 2.1.2. (c)). This could be explained perhaps by the fact that our broadband oscillator (MICRA from COHERENT,

Inc.) could deliver highly chirped pulses. There exists a specific laser operation regime during which a large positive FOD imparts the emitted pulse. In this situation the oscillator could contribute to strongly reduce the uncompensated FOD of the whole system.

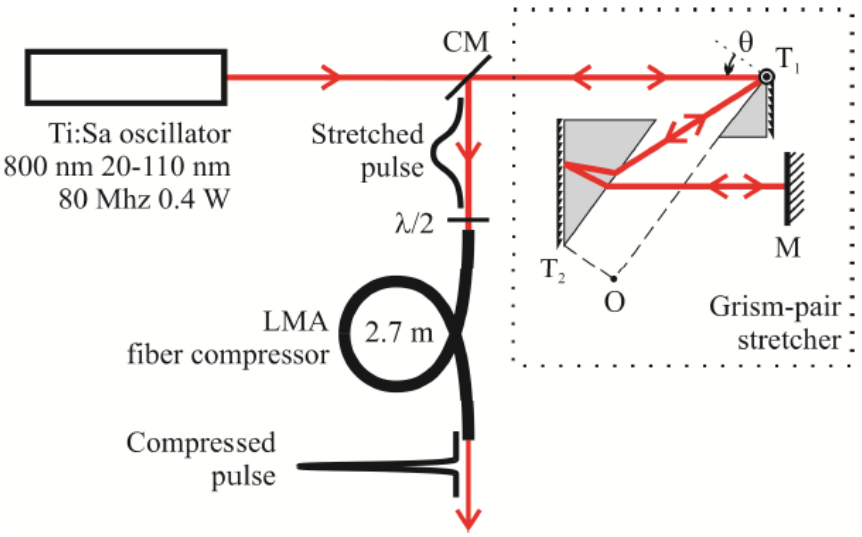

Fig. 2.2.1. Experimental setup. The system was composed of three main elements: a Ti:Sa femtosecond oscillator, an anomalous stretcher made of two antiparallel grisms each of them being the assembly of a prism in close contact with a reflective diffraction grating, and a 2.7- meter-long large mode area microstructured (LMA) fiber. The stretcher was adjusted so that the pulse was optimally compressed at the direct exit of the LMA fiber. The main freedom degrees are θ, L_{Prism}=OT2 and L_{Tip}=OT1; CM ≡ cut mirror; M ≡ plane retro-reflecting mirror.

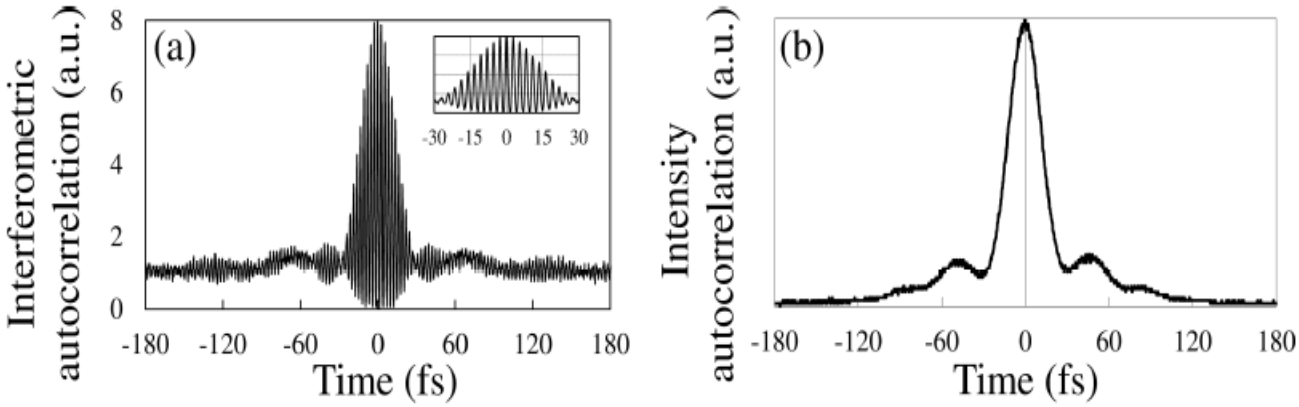

Fig. 2.2.2. (a) Interferometric autocorrelation (inset: central part of interferometric autocorrelation) and (b) intensity autocorrelation indicate very short durations for 1 nJ pulses at the direct exit of a 2.7-meter-long LMA fiber. Both of the two autocorrelations are related to sub-20-fs (FWHM) duration (respectively 17.8 fs or 19.9 fs for secant hyperbolic square or gaussian shape pulses).

During more common operation regimes (e.g. just after cleaning and/or readjusting the laser cavity) the oscillator FOD returns to moderate values so that this contribution vanishes. In those more usual and more reproducible cases, we have measured sub-30-fs pulses accordingly to what was predicted by the model (see Fig. 2.1.2.(c)). The compressed pulse duration was equal to 29 fs (FWHM) what corresponded to 0.65 for the time-bandwidth product. The compressed pulse duration was equal to 29 fs (FWHM) what corresponded to 0.65 for the time-bandwidth product. Coherent pulse characterization is done using SPIRIT apparatus which will be described in more details in the next section.

At the direct exit of the laser, the initial spectrum width was 71 nm. After the grism stretcher it was 62.5 nm. At the LMA fiber exit, in case of low power the bandwidth was equal to 62.5 nm, while in case of high power it was reduced to 51 nm (see Fig.2.2.3.(a)) corresponding to 18% spectral compression. In order to study the spectral compression inside the LMA fiber, we have registered bandwidths for different power levels at the exit of the LMA fiber. Spectral compression is clearly seen on Fig.2.2.3.(b).

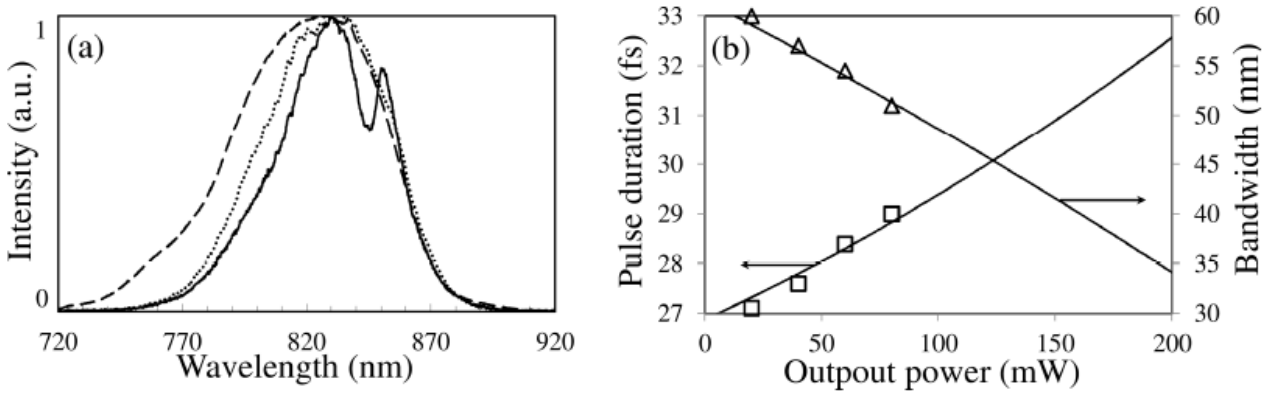

Fig. 2.2.3. (a): Spectral densities at the oscillator output (dotted line), at the grism-stretcher output (dashed line) and at the LMA-PC fiber output (solid line) for 1 nJ pulses. For those three locations the bandwidths were respectively equal to 71 nm, 62.5 nm and 51 nm. Grism stretcher filtering and spectral compression coming from nonlinear propagation inside the fiber are the reasons for bandwidth variations. (b): Pulse duration and spectral bandwidth at the output of the 2.7-meters-long LMA fiber as a function of output power. Triangle and square represent experimental measurements while solid lines relate to calculations.

The red-shifting filtering effect introduced by the grism-stretcher (see Fig.2.2.3.(a)) can be attributed to the grating spectral transmission. At low power, the spectrum exiting the fiber is close to the one at the fiber input. It proves the high spatial quality of the beam exiting the grism-stretcher which is exempt from spatial and angular chirp.

The MICRA oscillator which is bandwidth adjustable offers the opportunity to investigate the influence of the initial spectral bandwidth. We measured pulse durations and profiles for different spectral bandwidths: 110, 100, 90, 80, 70, 60, 50, 40, 30 and 20 nm. We were trying to find an optimum in term of main lobe duration, but also satellite lobe contribution (as less as possible). Fig. 2.2.4 shows the corresponding spectra and autocorrelations traces. For narrow bandwidths, dispersion is easily compensated leading to clean Fourier transform limited compressed pulses. In this case the pulse is long (i.e. 55 fs @ 20-nm-bandwidth). For broad bandwidths, time aberrations coming from uncompensated FOD distort the signal which contains satellite pulses. The shortest autocorrelation duration has been obtained in case of 70 nm spectral bandwidth.

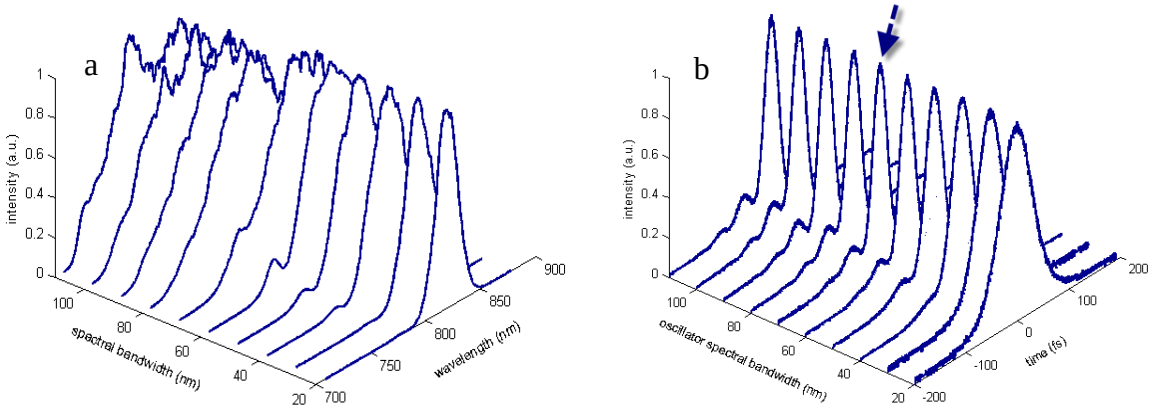

Fig. 2.2.4. (a) – spectra after oscillator, (b) - autocorrelations traces.

The influence of the variation of bandwidth at a constant 820 nm carrier wavelength is presented in Fig. 2.2.5. The duration measurements are done at FWHM (Fig.2.2.5(a)) and at 10% from the ground (Fig.2.2.5(b)), to take into account the satellite lobe contribution.

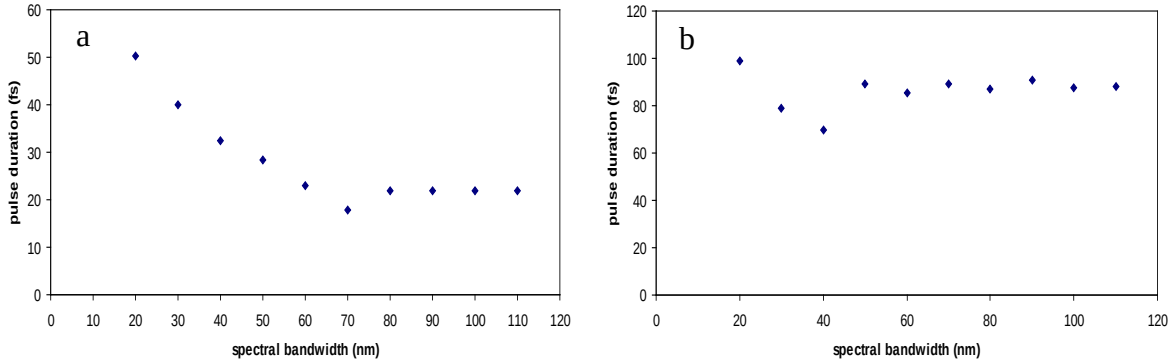

Fig. 2.2.5. Registered pulse durations vs. the spectral bandwidth: (a) - pulse durations at FWHM, (b) -pulse durations at 10% from the ground.

Another way to underline the satellite lobe contribution is the calculation of Strehl ratio for the beams. Strehl ratio is the ratio between the surfaces of the main lobe divided by the total surface of the autocorrelation trace. Fig.2.2.6 illustrates Strehl ratio calculated with the frontier at 2*FWHM.

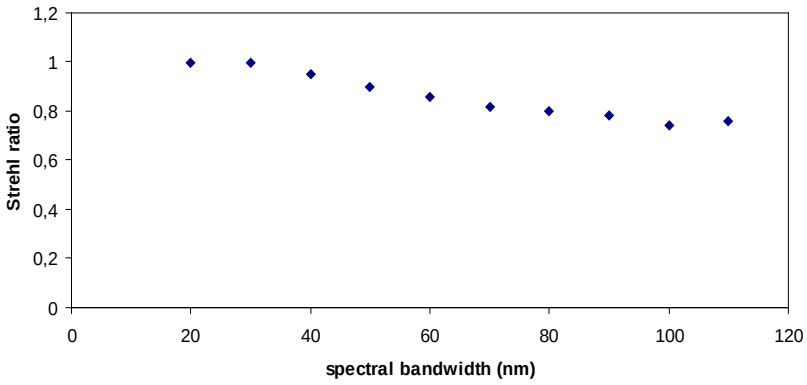

Fig. 2.2.6. Strehl ratio vs. the spectral bandwidth calculated at 2*FWHM.

We have measured also the nonlinear signal from two photon photodiode in case of constant average power (Fig.2.2.7). This curve gives the optimum at 50 nm and shows that proposed pulse delivery system does not require wideband sources.

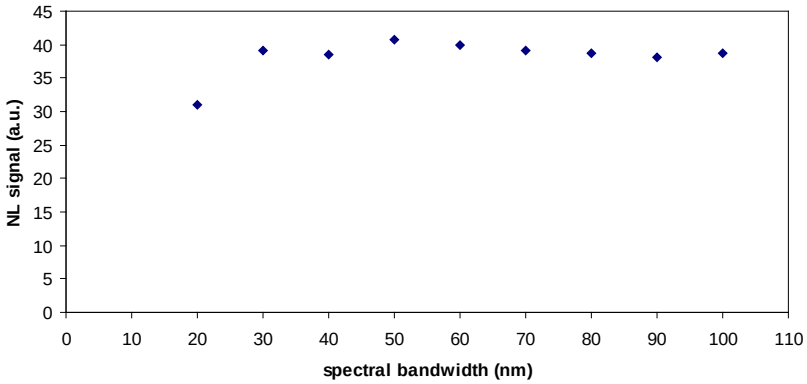

Fig. 2.2.7. Nonlinear signal from two photon photodiode.

Carrier frequency tuning of our fiber delivery system has also been investigated. This study has been performed working with 20-nm-bandwidth pulses what allowed us to tune the carrier wavelength over 100 nm (see Fig.2.2.8). This wide tunability is an advantageous feature namely towards biomedical applications for which optimization of operating wavelength is an important issue. The optimal carrier wavelength in terms of pulse shortness appeared to be equal to 820 nm.

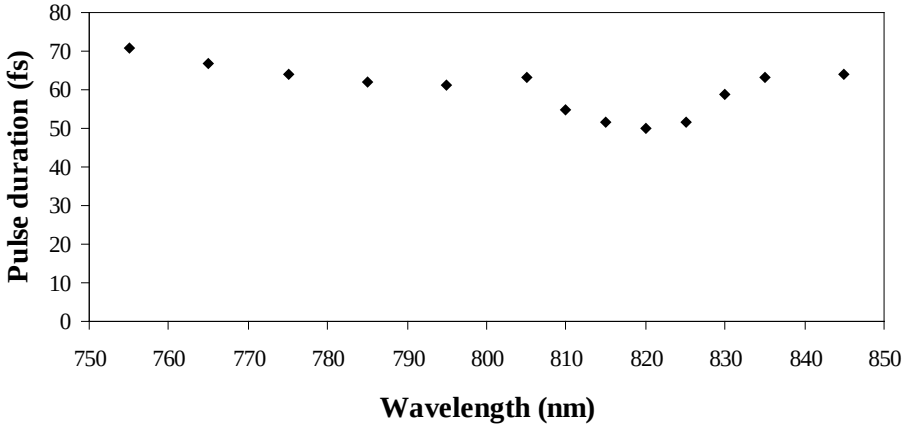

Fig. 2.2.8. Output pulse duration as a function of carrier wavelength varying across the full tunability range (i.e. 100 nm) of our MICRA-5 oscillator when adjusted with 20-nmbandwidth. The tunability of our femtosecond fiber delivery system expands across more than 100-nm-bandwidth from 750 to 850 nm.

Despite the advantageous feature of being weakly nonlinear because of their large core, LMA fibers offer poor spatial resolution when used inside an imaging device such as a multiphoton endomicroscope. This is true for air-silica microstructured LMA fibers and also for higher-order-

mode LMA fibers that were also successfully involved in powerful femtosecond pulse fiber delivery demonstrations. From the point of view of spatial resolution, standard single mode fibers (SMF) with small fundamental mode size could be preferred. In order to prove that our dispersion compensation scheme also brings benefits with this kind of more nonlinear fibers, we replace the LMA fiber by a standard single mode fiber having 6- μm-mode field diameter corresponding to 28-μm^2-mode effective area. This type of fiber is approximately 7 times more nonlinear than the LMA-20 that was used during our previous experiments, while its SOD is 1.2 times greater (i.e. β_2=+392 fs^2/cm; β_3=+320 fs^3/cm and β_4≈-150 fs^4/cm @ 820 nm). For a 1-nJ-energy 25-fs-duration pulse propagating in it, the nonlinear length is LNL = 6 mm what leads to $L_D \approx L_{NL}$. Dispersion is still mitigating nonlinearity but in a smaller extent than in the case of LMA fiber where $L_D << L_{NL}$. Some nonlinear spectral compression is now predicted at the SM fiber exit. However it is much smaller than in the case of narrowband pulses which relate to $L_D >> L_{NL}$. For this reason, we have obtained short compressed pulses at the output of the SM fiber too. By using a 2.7-meters-long standard polarization maintaining single mode fiber (PM-SMF), in case of 820nm carrier wavelength, for a 60-nm initial bandwidth and 80-mW power injection (i.e. 1-nJ energy delivered pulse) we have recorded autocorrelation with 39-fs-duration corresponding to Gaussian pulse with 28-fs-duration (see Fig.2.2.9) consequently 10 fs longer pulse in comparison with LMA fiber. In this situation spectral compression inside the standard SMF amounted to 36%.

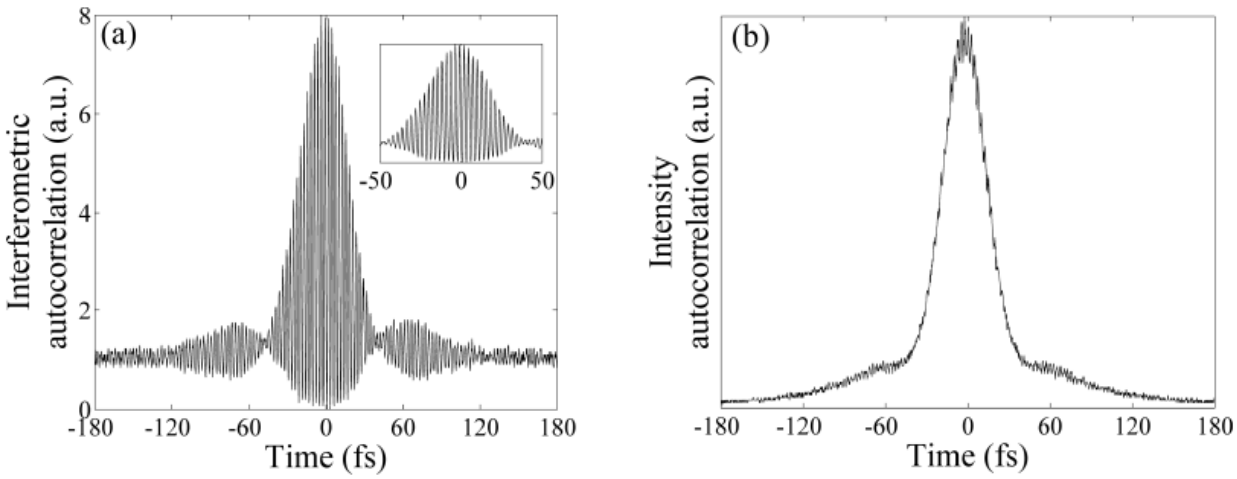

Fig. 2.2.9. Pulse delivered at the output of a 2.7-meters-long standard PM-SM fiber. Interferometric (a) and intensity (b) autocorrelations are both related to 28-fs-duration (FWHM) pulse having 1-nJ-energy.

As in case of LMA fiber, the shortest pulse durations were measured during the particular operation regime during which the laser oscillator brought a non-negligible contribution to FOD. Without this favorable circumstance we have obtained 32.5-fs-duration pulses having 1- nJ-energy. Comparison between LMA and PM-SM fibers and scalability to higher power levels are evidenced on Fig.2.2.10. With the standard SMF spectral compression is much stronger (see Fig.2.2.10 (b)) and the pulse is longer with a more complex shape (see Fig.2.2.10 (c)). However it is worth noticing that even at energy levels as high as 2.5 nJ the pulse duration is still much smaller than 50 fs at the output of the standard SMF.

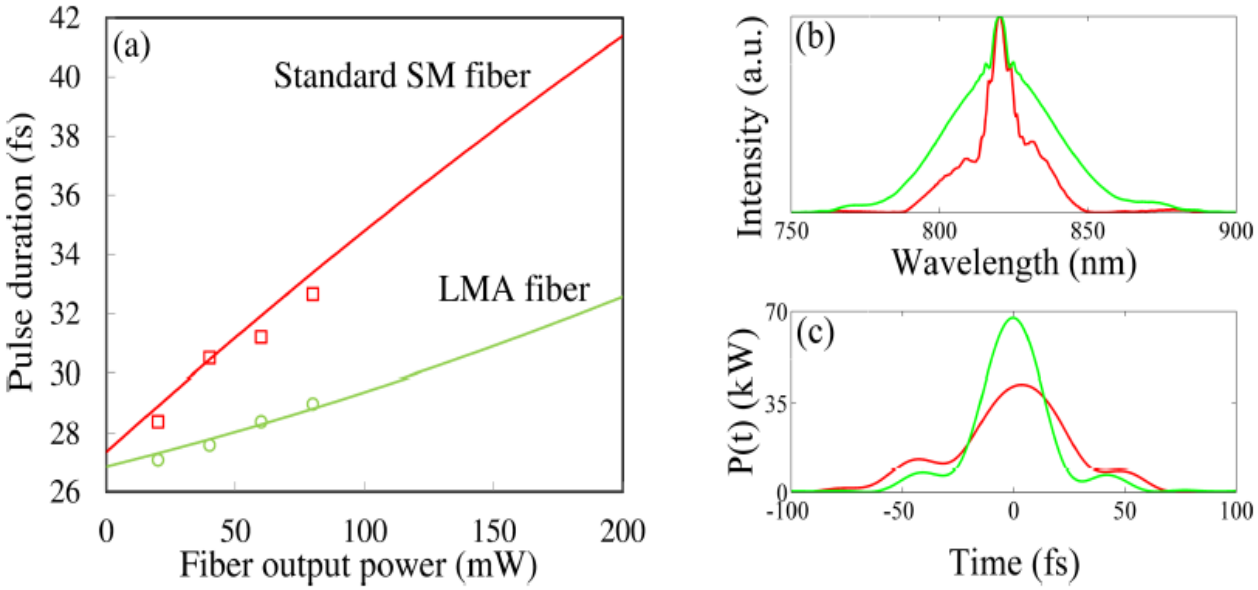

Fig. 2.2.10. (a): Measured pulse duration as a function of output average power at the output of a 2.7-meter-long fiber, squares with a standard PM-SM fiber, circles with a LMA fiber. Solid lines are corresponding calculations (for the standard SMF and for the LMA SMF). (b): Calculated spectra at the fiber exit for 200 mW average power @ 80 MHz (i.e. 2.5 nJ). Spectral compression is much stronger in the standard SMF which has increased nonlinearity. (c): Calculated pulse temporal profiles. LMA SMF gave a cleaner and brighter pulse.

Also we have studied the spectral compression/ broadening and the pulse duration vs. dispersion variation in the grism line. Fig. 2.2.11 shows that the maximal spectral compression point and the maximal pulse compression point are shifted from each other. Maximal spectral compression is inside the fiber, when the pulse duration is minimal.

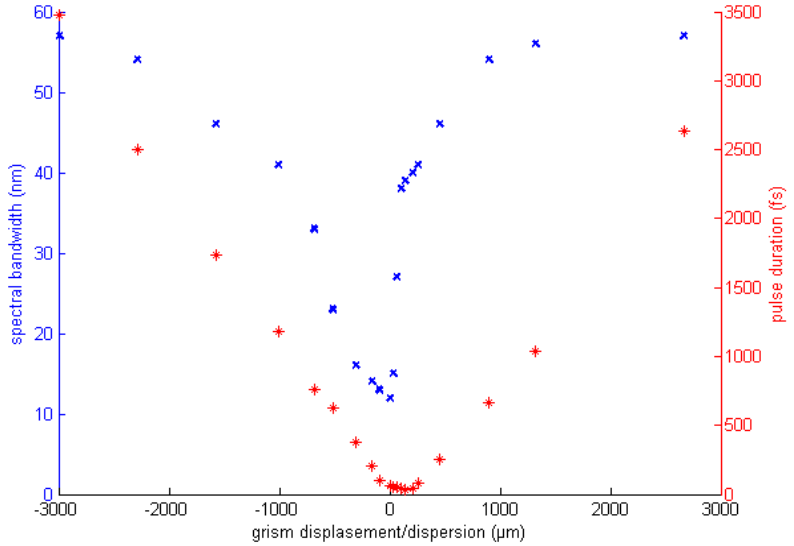

Fig. 2.2.11. Spectral bandwidth and pulse duration vs. grism's separation.

Thus, our comparison of LMA and PM-SMF fibers shows that obtained pulse durations are not so far (only 10fs difference), therefore SMFs are more preferable, because of the following properties of LMA fibers: LMA fibers require the special cleaving procedure, these fibers are sensitive to the bendings, the beam size is large which means that the process of delivering require special optics and finally LMA fibers are much more expensive than standard SMFs.

In conclusion, we have numerically and experimentally demonstrated an efficient femtosecond fiber delivery setup with improved fiber dispersion precompensation thanks to a high throughput grism-pair stretcher. Sub-30-fs-duration 1-nJ-energy pulses were compressed at the direct exit of 2.7-meters-long large mode area fiber. The proposed device that involves only readily available commercial components is compact in addition of being wavelength tunable over a 100-nm-badwidth around 800 nm. Large mode area fibers gave the best performances in terms of pulse shortness and brightness. But surprisingly standard single mode fibers also gave short and powerful pulses despite their increased nonlinearity. It is also highlighted that the proposed pulse delivery system does not require wideband sources (more than 40 nm). With the additional dispersive device (Dazzler, Fourier phase shaper), which can control fourth and fifth orders of dispersion, a few femtosecond transform limited pulse delivery can be realized by the proposed scheme. This task is the one of the subjects of our future studies. Our final objective is to apply this technique to nonlinear endomicroscopy.

¢2.3. Spatial light modulator based pulse shaping and compression

In the last section a very compact system for femtosecond pulse fiber delivery was demonstrated. Pulse fiber delivery pre-dispersing technique was developed, LMA fiber and grism line. It was demonstrated that by simultaneous control of SOD and TOD by the compact grism line it is possible to obtain 18 fs pulses at the output of 2.7m LMA fiber. To go further and obtain more compressed pulse, we decided to put SLM inside the grism line (see Fig. 2.3.1) and compensate the high orders of dispersion. This experiment is done together with the Claire Lefort.

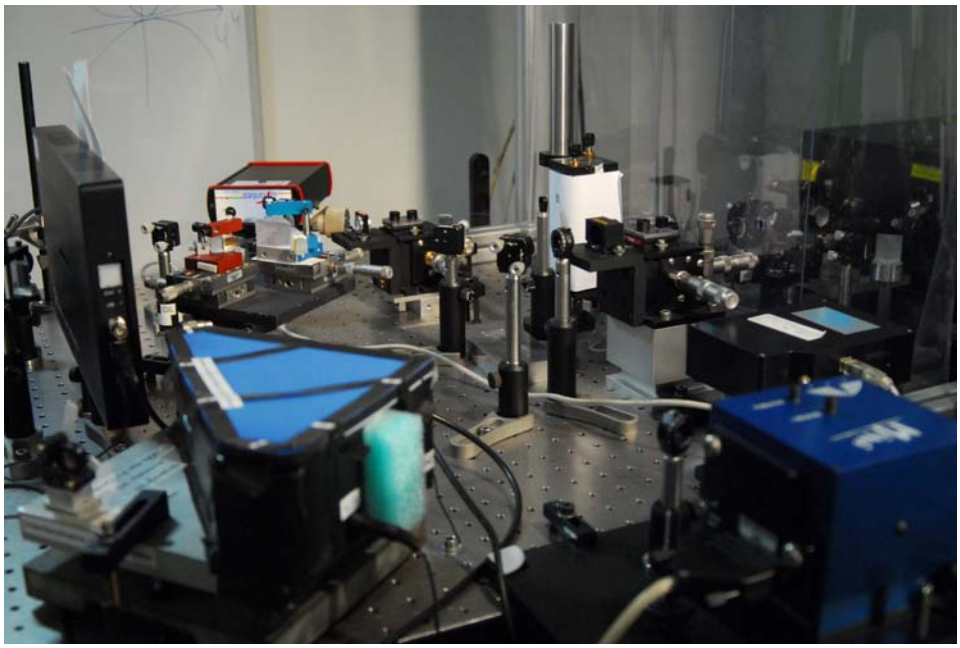

Fig. 2.3.1. Picture of the setup with the SLM inside the grism line.

We were using the SLM-640 liquid crystal modulator arrays, which provided independent control of each element in a linear array of 640 pixels. The arrays are 5 mm high, and the pitch is 100 μm, resulting in total array apertures of 64 mm for SLM-640 models.

Single-array models are configured at the factory for phase or amplitude modulation, while dual-array models consist of two precisely aligned modulators, providing a unique and convenient method for simultaneous modulation of both the phase and amplitude at each pixel. The patented dual-mask configuration can operate either as a phase and amplitude modulator of specifically polarized incident light or as simply a phase modulator of arbitrarily polarized incident light. The

three modulation schemes can operate in either transmissive or reflective mode. The reflective mode is enabled by replacing the output polarizer with an optional mirror, which causes light to pass through the system twice, and thus doubles the optical action of the modulator.

The SLM optics use nematic liquid crystal to alter the phase or polarization state of light. The basic principle is that the liquid crystal material provides an electrically variable index of refraction for light that is polarized along the crystal's extraordinary axis. Light polarized along the orthogonal axis, termed the ordinary axis, does not see a change in refractive index with voltage.

The phase (P) models of the SLM modulate phase at each pixel by introducing light that is polarized along the extraordinary axis. This is shown in Fig.2.4.2 (a). A polarizer at the output of the SLM removes any residual vertically polarized light to ensure the device operates as a pure phase modulator and does not alter the polarization state of the beam.

The amplitude (A) models modulate intensity at each pixel by introducing light through a horizontal polarizer, then into a liquid crystal cell whose extraordinary axis is at 45 degrees, so it acts as an electrically variable wave plate, to transform the polarization state of light. The light then passes through as exit polarizer that analyzes the polarization state and thus effects an intensity modulation as the wave plate varies over the range from zero to one-half wave. This is shown in Fig.2.3.2 (b).

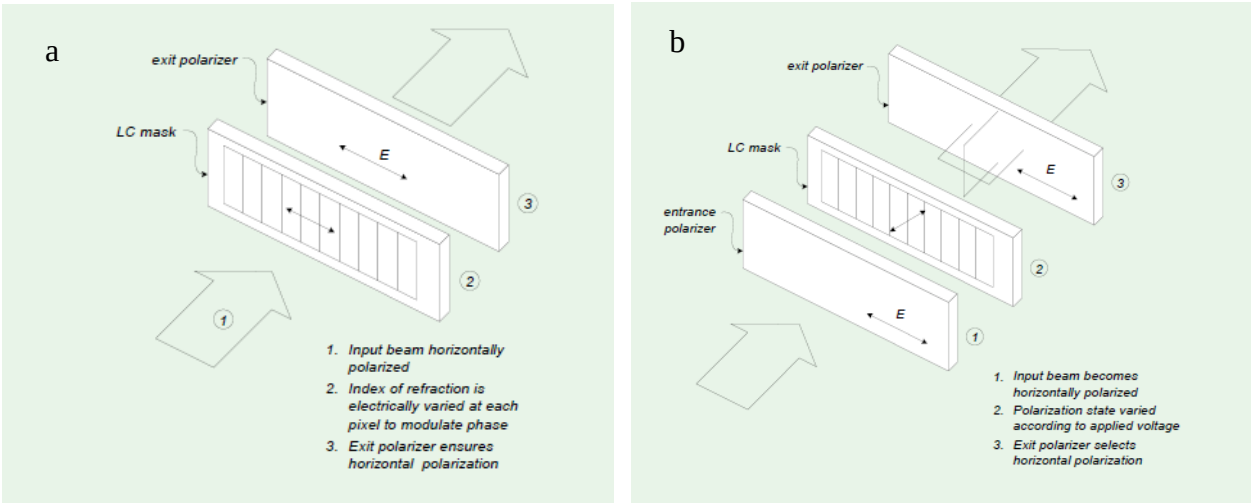

Fig. 2.3.2. (a) - Phase modulation transmissive mode, (b) - amplitude modulation transmissive mode.

The dual (D) models use a patented arrangement where a pair of liquid crystal masks is bonded together in precise pixel registration and proximity of 1.03 mm. The masks are oriented orthogonal to one another and 45 degrees to the polarization of incident light. To the extent that the aligned pixels vary together (common-mode signal), the phase is modulated. To the extent that these pixels differ (differential signal), the polarization is altered. Hence, this arrangement provides a way to independently alter phase and intensity (amplitude). This is shown in Fig.2.4.3. The dual-mask SLM can also be used as a pure phase modulator for arbitrarily polarized light by removing the entrance and exit polarizers and always driving both masks with the same patterns, so that the differential signal is zero.

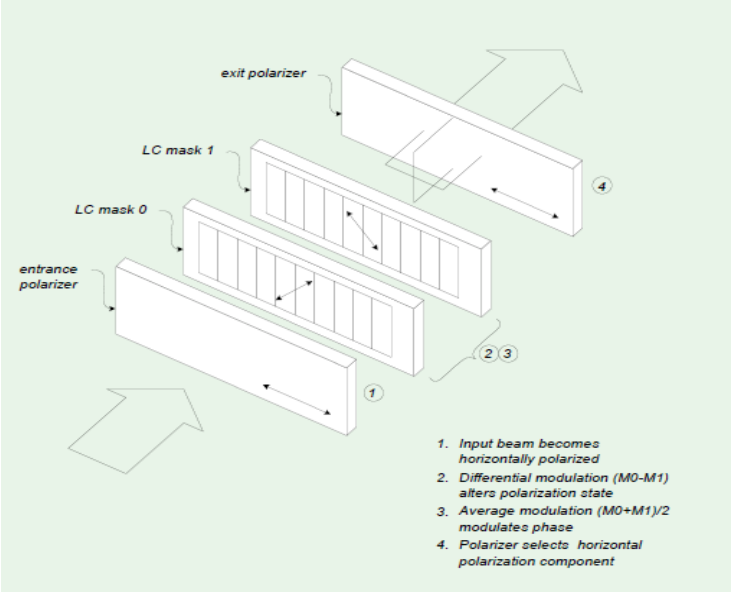

Fig. 2.3.3. Phase and amplitude modulation transmissive mode.

Any of the three optical modulation schemes can be exploited in reflective mode, by placing the optional mirror at the output face so the light passes through the system twice. In this case, the polarizer at the entrance face acts as an entrance polarizer for light on its way into the SLM, and as an exit polarizer or analyzer for light leaving the system. This doubles the optical action of the SLM, and greater phase modulation is achieved.

As an electronic device, the liquid crystal modulator is fully controllable with either a control programmable to load predefined patterns with values for each individual pixel or with high-level drivers for Matlab or LabVIEW. LabVIEW was preferred because it offers drivers for most equipment in the lab (such as spectrometers or power meters) and can therefore integrate parameters for an automated feedback design. Also, it is able to use Matlab scripts, when simple and fast

manipulation of data is required. LabVIEW is a graphical programming language in which devices can be placed and connected with elements from a virtual instrument screen, the Front Panel, where buttons, controls and graphs can be displayed. Data can be acquired, processed and sent back to the device.

As it was mentioned above, by using the SLM we can have simultaneous modulation of both the phase and amplitude. For our application, first we are looking for phase modulation by SLM to compensate the high orders of dispersion. The second and third orders of dispersion are compensated by the grism line. Thus we are inducing on the SLM the second, third and fourth orders phases. The influences of the application of these phases on the SLM are checked by the method of SPIRIT [56, 57]. SPIRIT is a passive and self-referencing pulse characterization technique that will be discussed in more details in next section. SPIRIT gives the access to the spectral phase of the pulse at the output of LMA PM fiber.

By the SLM we can apply the φ_i phase, where the index i is the order of phase. We are trying to adjust the second, third and higher orders of dispersion and to obtain maximum pulse compression at the exit of the fiber delivery scheme.

First of all we start by the second order phase. Without knowing the exact value of the phase that should be applied, we applied all possible phases, which we are able to apply by SLM. In Fig. 2.3.4 we can see the examples of second order phases which were applied on the SLM.

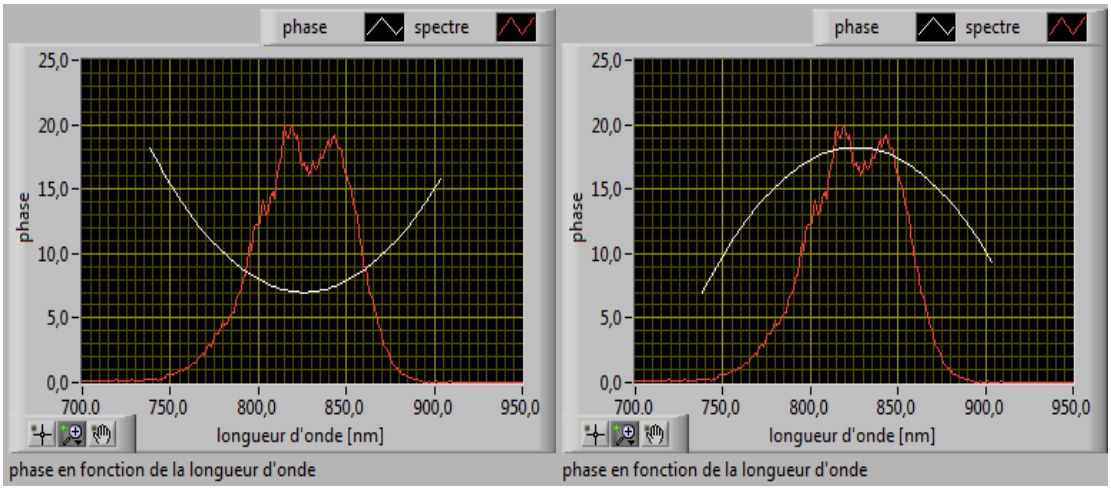

Fig. 2.3.4. Second order $\varphi_2 = 0.004$ rad/nm^{-2} and $\varphi_2 = -0.004$ rad/nm^{-2} phases applied on the SLM.

For the second order we have applied the phases in the range of [-0.004; 0.004] by the step of 0.0005 rad/nm^{-2} to find the good value. For each value we have registered the corresponding spectral phase. An analysis of each phase allows us to choose the value of the second order phase, which gives the most possible flat phase after LMA PM fiber. After finding the good coefficient for second order we pass to the third and fourth orders and we have done the same steps for these orders too. In Fig. 2.3.5 we can see examples of third and forth order phases applied on the SLM.

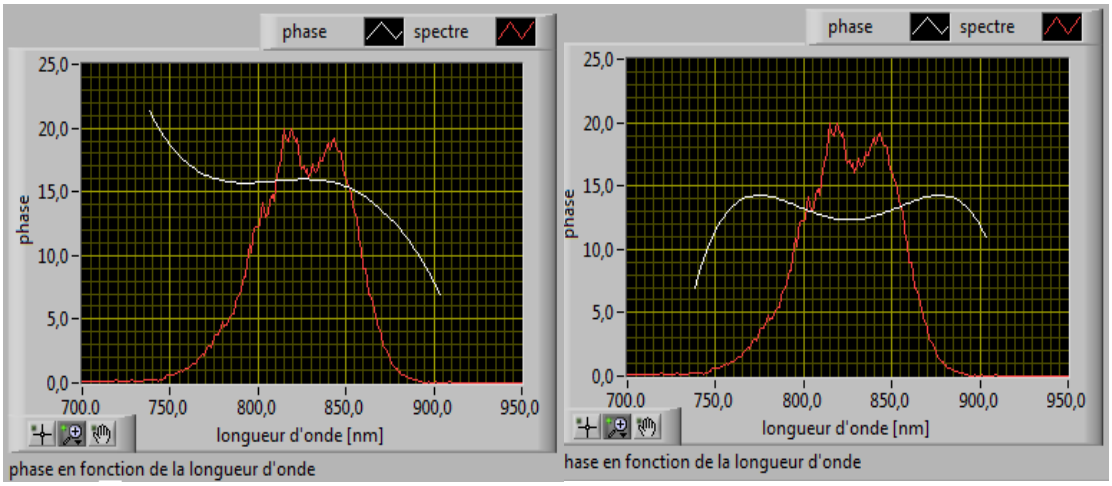

Fig. 2.3.5. Examples of third and fourth order phases applied on the SLM.

When we have found the good coefficients for each order of phases, by the next step we applied all those coefficients on the SLM to have flatter phase.

Unfortunately our first results of spectral phase modulation were not successful and for lack of time we stopped our investigations of the phase modulation. But we believe that we have identified the causes of this failure.

In order to show the capability of the SLM to generate arbitrarily shaped pulses, some examples, representing different applications, have been performed. Several examples of amplitude modulations obtained by SLM are presented in Fig. 2.3.6.

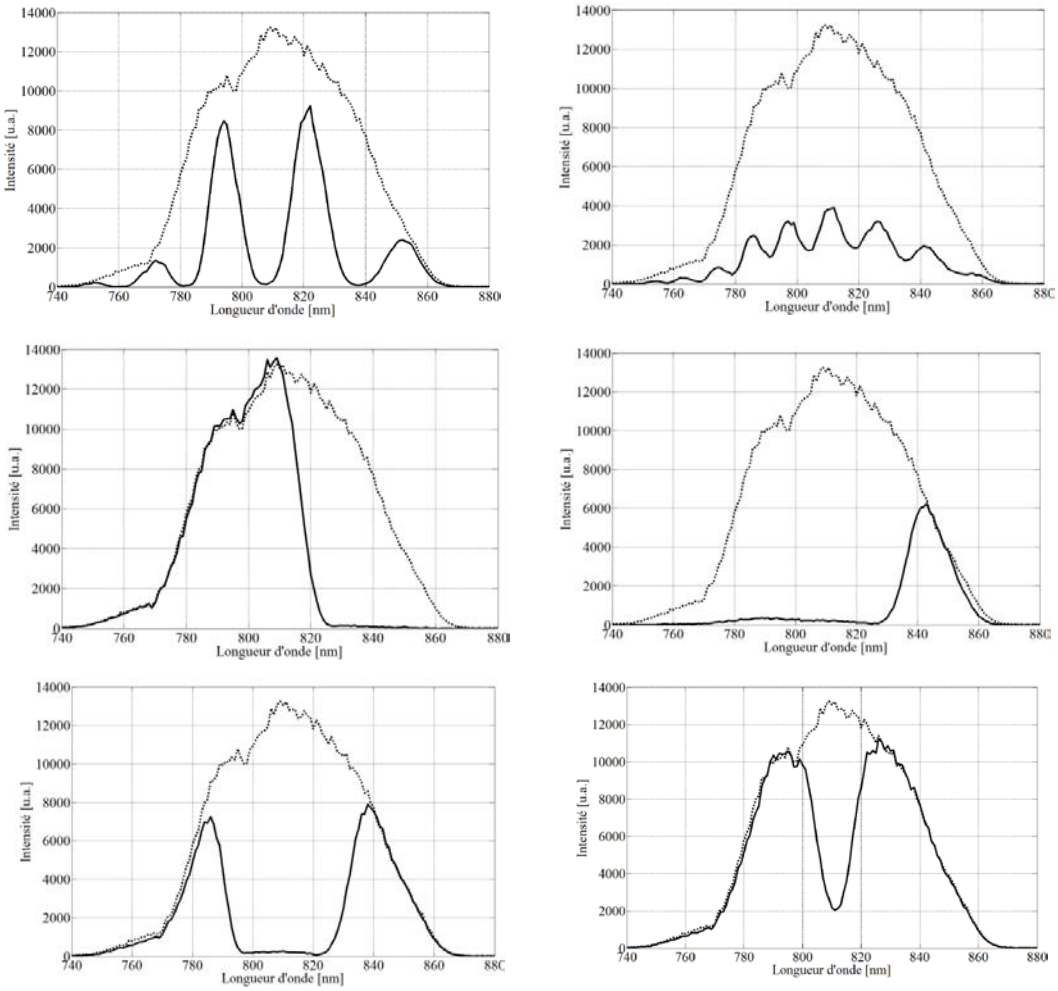

Fig. 2.3.6. Examples of modulated spectra.

For testing of the spectral shaping capabilities, triangular and rectangular functions were also chosen to be shaped, since they are comparatively easy waveforms. Obtained spectra are illustrated in Fig. 2.3.7.

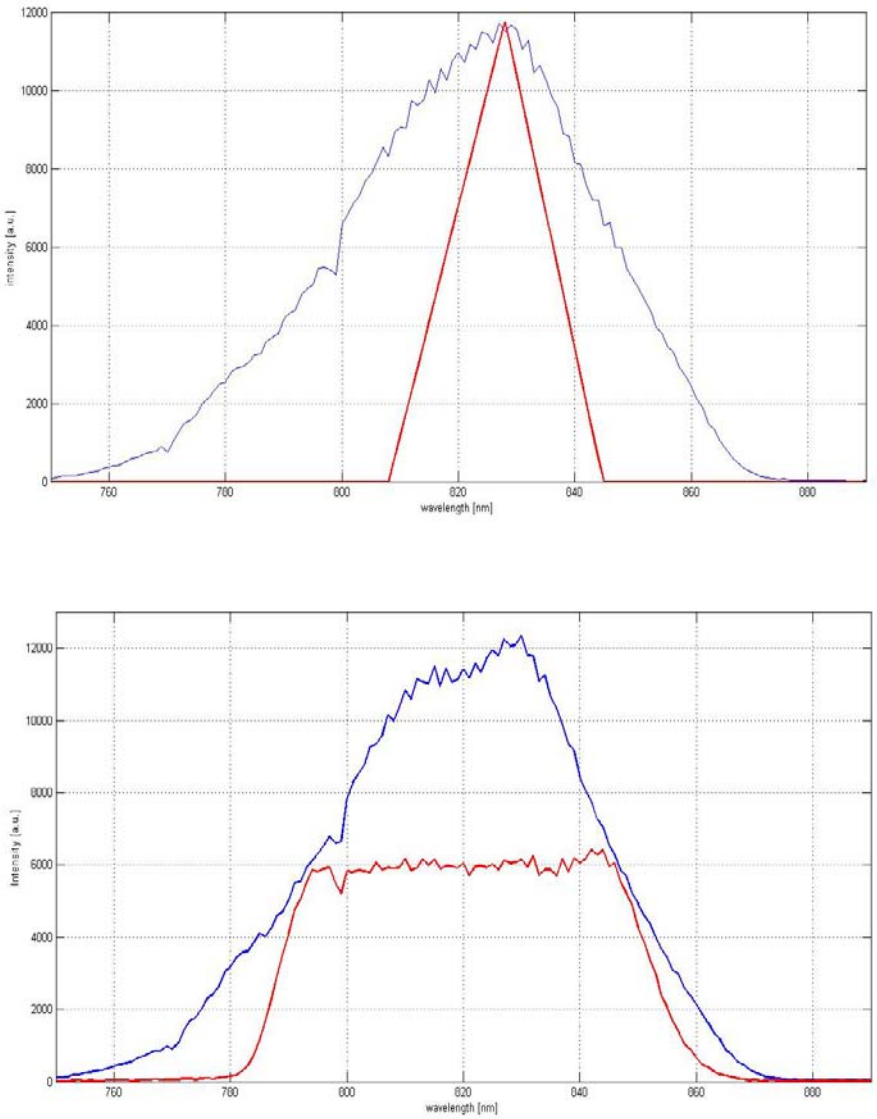

Fig. 2.3.7. Shaping of rectangular and triangular spectra.

Spectral shaping can be interesting when information is transmitted in the spectrum of the pulse, such as in optical communication.

In conclusion, to solve problems related to the uncompensated fourth order of dispersion, we experimentally demonstrated the SLM based fiber delivery scheme, for this we introduce a SLM in the grisms stretcher. This solution proved unsuccessful, but we believe that we have identified causes of this failure and future more detailed studies will give us better results in view to obtain shorter pulses at the output of LMA PM fiber. The capability of the SLM for arbitrarily shaped pulses generation is demonstrated by amplitude modulation.

Conclusion to chapter II

1. We experimentally demonstrate a compact and efficient arrangement for fiber delivery of sub-30 fs energetic light pulses at 800 nm. Pulses coming from a broadband Ti:Sapphire oscillator are negatively prechirped by a grism-pair stretcher that allows for the control of second and third orders of dispersion. At the direct exit of a 2.7-m long large mode area (LMA) photonic crystal fiber 1-nJ pulses are temporally compressed to 18 fs producing close to 30 kW of peak power. The tunability of the device is studied. Comparison between LMA fibers and standard SMF fibers is also discussed.

2. Evolution of the stretcher-compressor system was experimentally tested. We introduced a spatial light modulator in the grisms stretcher. The goal is to obtain more compressed pulses at the output of the LMA PM fiber. Unfortunately this solution was unsuccessful, and we have identified causes of this failure. To go further, it would be necessary to improve the system to have access to the complex phase by removing the limitations, which were related mainly to the low spectral resolution of the devices and the existence of spatial dispersion effect. The capability of the SLM for pulse shaping was demonstrated by amplitude modulation.

CHAPTER III.

WIDEBAND SPECTRAL INTERFEROMETRY RESOLVED IN TIME

During the past decade, continuous progress in the field of ultrashort pulse generation has lead to pulse durations below 10 fs in the visible and near-infrared spectral range [143]. These ultrashort pulses have been generated with a variety of different techniques, namely optical parametric amplification [144], compression of continua generated in either single-mode fibers [145] or hollow-core optical waveguides [146], second-harmonic generation, and directly from Ti:sapphire laser oscillators [147]. Despite the variety of methods, all these sources exhibit rather complex spectral and temporal structures, making characterization of their pulses a demanding task.

The main difficulty for the measurement of ultrashort optical pulses lies in the fact that in the optical spectral region only time-integrating or energy detectors exist. Even the fastest electronic detectors have response times that are orders of magnitude longer than state-of-the-art pulses. Therefore, all pulse characterization schemes have to build on slow detectors.

Classical pulse characterization relies on autocorrelation [31, 32]. Simple autocorrelation measurements, however, are often found not to be accurate and reliable enough in the sub-10-fs pulse duration regime. Even for only determining the duration of a pulse, simple autocorrelations are found to fail in the sub-10-fs pulse duration regime. The temporal parameters have usually been obtained by fitting an analytical pulse shape with constant phase to the autocorrelation data. The particular fitting function is motivated by theoretical models of the pulse formation process. For those passively mode-locked lasers, for example, that allow for parabolic approximation of these formation mechanisms one expects a sech^2 temporal and spectral pulse shape. For lasers obeying such a model the a priori assumption of a theoretically predicted pulse shape is well-motivated and leads to good estimates of the pulse duration. Therefore, autocorrelation is still a good standard diagnostic method.

In the sub-10-fs regime, however, theoretical models have to consider higher order effects and thus become more complicated. In this case, no simple analytical pulse shapes can be expected. Experimentally, this situation is clearly indicated by more complex pulse spectra, deviating from the ideal sech^2 shapes predicted by simpler models. Additionally, even after dispersion

compensation, broadband pulses usually deviate from the ideal transform-limited pulse. Chirped mirrors, for example, lead to a sinusoidal modulation of the spectral phase that cannot be completely compensated by conventional techniques. Although the resulting pulses can be close to the transform limit, they are distorted by the uncompensated phase structure.

For a more precise measurement with larger information content, several methods have been proposed allowing for a reconstruction of pulse amplitude and phase from measured data only. Every characterization technique reported presents particular assets and drawbacks.

Among the characterization methods supplying a complete description of the pulse (spectral or temporal amplitude and phase), two well-established techniques, FROG [40-42] and SPIDER [49] are more commercially available and widely spread. FROG is based on the spectral measurement of the pulse autocorrelation, as a function of delay. The pulse information is converted into a time-frequency representation, demanding an iterative algorithm in order to retrieve the pulse features. Advanced versions of FROG offer simpler optical set-ups and improved specifications, the case of GRENOUILLE (GRating-Eliminated No-nonsense Observation of Ultrafast Incident Laser Light E-fields), or modifications related to the nonlinear effect used [148].

On the other hand, SPIDER and its variations are based on spectral shearing interferometry. Unlike the previous schemes involving iterative algorithms, SPIDER provides complete real-time characterization of ultrashort optical signals. Since the interference of two spectrally sheared pulses contains the information about the original spectral phase, contributions to the phase other than the absolute phase and delay can be retrieved. To this goal, in SPIDER setup, a couple of replicas of the input pulse are first delayed in time with respect to one another. Next, these two replicas interacting with a stretched copy of the original pulse produce a pair of identical frequency-sheared pulses through a nonlinear up-conversion process. The frequency shear between the up-converted pulses depends on the delay introduced between the initial replicas and on the dispersion of the stretched pulse. Finally, the spectral interference fringes due to the coherent sum of the up-converted pulses are measured with a spectrometer.

SPIRIT (SPectral Interferometry Resolved In Time) [56-58] is a different characterization method, also based on spectral shearing interferometry, and passive and self-referencing as well. SPIRIT has shown to be suited to a variety of pulse and experimental conditions, such as the measurement of single pulses or high repetition rate trains. A two-dimensional interferogram

development, 2D-SPIRIT, offers a direct and intuitive characterization of short pulses. As it will be explained in detail below, in SPIRIT, the frequency shift between the spectra of the two replicas of the input pulse is based on a geometrical shear, and it does not depend on the frequency up-conversion process. In our technique the nonlinear effect is used only for temporal gating.

The knowledge of the pulse shape and/or phase is in certain experiments needed for the full understanding of the interactions in a medium under investigation. Several examples clearly demonstrate the need for accurate amplitude and phase characterization techniques. We have developed and analyzed such methods for measuring ultra broadband pulses in the sub-10-fs pulse duration regime.

¢3.1. Pulse measurement by time-to-frequency conversion with a quadratic nonlinearity

In this section we demonstrate a new method of aberration-free time-to-frequency conversion through temporal lensing in a wave-mixing process, for the spectrotemporal imaging (STI) and femtosecond pulse direct, real-time measurement. The nonlinear-spectronic reference pulse, self-shaped in a SMF, makes our technique a self-referencing one.

We report on studies aimed at designing a femtosecond optical oscilloscope / decoder of sub-PHz service band based on spectral imaging of pulse temporal profile through an aberration-free temporal lensing / spectral compression (SC). In the last decade, temporal Kerr lensing / SC demonstrated promising applications to signal analysis-synthesis problems in ultrafast optics, and particularly for time-to-frequency conversion and direct, real-time femtosecond pulse measurements. High order nonlinear (NL) and dispersive (D) effects, accompanying the femtosecond pulse self-phase modulation in fiber, lead to Kerr lens "aberrations" in SC. The cross-phase modulation technique of SC serves for the aberration-free temporal lensing with specially shaped reference pulse, involving the problems to differentiate the signal and reference radiation by frequency or polarization, to avoid the walk-off pulses, etc. We demonstrate a new method of aberration-free time-to-frequency conversion through optical frequency inter-modulation in a quadratic nonlinear process instead of self- or cross-modulations.

The principle of our method is following: we split the radiation under test (with the $A_{in}(t)$ complex temporal envelope) into low- and high-power parts. We direct the low-power pulse to a DDL with negative dispersion, to dispersively stretch the pulse under test (resulting in $A_d(t)$). We inject the second high-power pulse into a single-mode fiber, to have a NL+D self-interaction of the pulse, and shape a sub-parabolic reference pulse ($A_f(t)$). The nonlinear-spectronic nature of such a pulse makes its chirp linear and independent of the initial pulse parameters: only the fiber dispersion determines the chirp slope, and so the technique becomes a self-referencing one. Moreover, in the NL+D interaction process the pulse and spectrum become parabolic at their central energy-carrying parts. In both paths of setup, we have linearly chirped pulses, for which the pulse temporal profiles repeat the spectral ones, and so, we have time-to-frequency conversion for these pulses (with an accuracy of ~1/stretching factor). It permits to check qualitatively and control these D and NL+D processes. Afterwards, we direct these two pulses to a nonlinear crystal for non-collinear sum-frequency generation (SFG), and so multiply the complex fields:

$$A_{out}(t) \propto A_d(t) \times A_f(t) \tag{3.1.1}$$

The chirp cancellation, under the condition of a constant reference pulse during the stretched signal, results in spectral compression, and time-to-frequency conversion:

$$S_{out}(\omega) \propto I_{in}(t) \tag{3.1.2}$$

In the experiment, we use a Coherent Verdi V10+Mira 900F commercial femtosecond laser system with the following parameters of radiation: 100 fs pulse duration, 76 MHz repetition rate, 1.6 W average power, 800 nm central wavelength. At the input of the SFG-STI system (Fig.3.1.1), we shape the pulses under test and measure them by a standard autocorrelator (APE PulseCheck). Afterwards, we split the radiation under test into two parts by means of a beam splitter (80% + 20%). As a D-line, we use the SF11 dispersive prism pair (DP) with a reverse mirror (M). We form a nonlinear-spectronic similariton, as a reference pulse with a parabolic phase, in a piece of standard single-mode fiber (SMF) (Newport F-SPF at 820 nm). For non-collinear SFG, we use β-barium borate (BBO) type 1 (oo−e), 0.1 mm thick crystal, with 800 nm operating wavelength (θ=29.2°, φ=0°). To observe the spectral compression and STI, we measure the SFG spectrum at the output

of the system by the optical spectrum analyzer (OSA) Ando AQ 6315. Along with it, we also measure the spectra at the entrance of the SFG crystal.

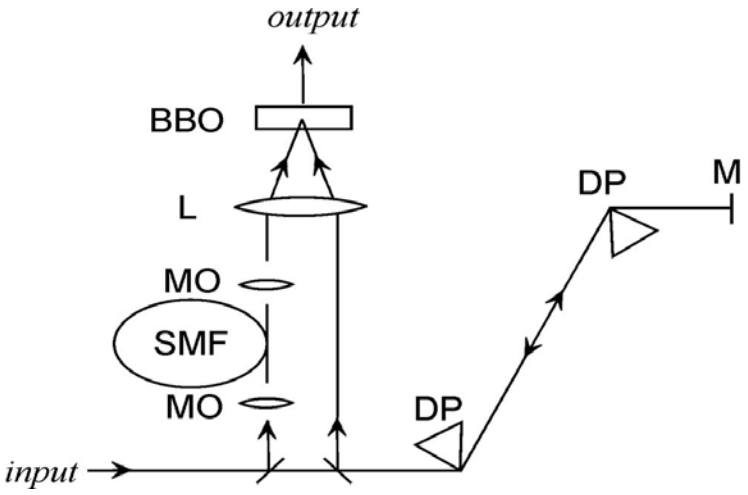

Fig. 3.1.1. Schematic of the SFG-STI setup.

Concerning the details of our experiment, first we widen and well collimate the laser beam at the input of the STI setup using a 5× telescope to avoid diffractive distortion of the beam. Afterwards, we carry out shaping of the pulse to be measured. We shape the pulses in three different ways. First, we simply place a thin glass plate in front of a part of the widened laser beam. The part of the beam passing through the glass plate obtains a time delay with respect to the other free-propagated part. This way we shape pulses with two- or three-peak structures. Moving the plate along the vertical axis, we adjust the power proportion. The thickness of the plate determines the time delay between the peaks. Second, a more traditional way for two-peak pulse shaping is the use of a Michelson interferometer. One arm of the interferometer is slightly longer than the other one; the difference gives the peak separation in time. Finally, we shape pulses by spectral phase masking in the spectrometer scheme which was discussed in Chapter I. This way we shape pulses with complex substructure.

When directing the radiation into our SFG-STI system, we split it with a beam splitter and inject the powerful part (80%) into the SMF; the low part we direct to the DDL. We slightly shift the back beam in the vertical plane by the reverse mirror of DDL, and direct it to the nonlinear BBO crystal for the SFG interaction with the beam from the fiber. We inject the radiation into the fiber and then collimate the beam after it by means of 10× microscope objectives (MOs). The beams from the DDL and fiber are approximately at a distance of 1.5 cm from each other. We focus these

two beams on a spot in the BBO crystal by a lens (L) with a 14 cm focal length. We record the spectrum of the resulting radiation with the OSA. To equalize the optical paths of the beams in the D-line and the fiber, we adjust the distance between the second DP and reverse mirror M of the DDL. First, we manage this by taking the feedback of the spectral interference pattern of two pulses at the OSA: we look for the maximal fringe period. Then we search for the central wavelength of the SFG signal. To achieve full chirp cancellation for a correct STI, we carry out fine adjustment of the prism separation for the given length of fiber and check the SFG spectrum for the maximal SFG spectral compression. We also carry out spectral measurements at the input of the BBO nonlinear crystal to check the fulfillment of the conditions necessary for spectral compression and FT and STI: the spectrotemporal similarity of the spectronic stretched signal and the nonlinear-spectronic reference allow us to check their temporal profiles via spectral measurements.

Fig. 3.1.2, with the experimental spectrograms, illustrates the performance of our method for a two-peak pulse shaped at the input of the system. First we make an autocorrelation measurement to check our shaped pulse. Afterwards, we measure the spectra of the stretched signal and self-shaped reference pulses to have an idea of their temporal behavior. One can see that despite the initial two-peak structure, the formed nonlinear-spectronic similariton obtains a bell shape with the tendency to be parabolic at the central energy-carrying part.

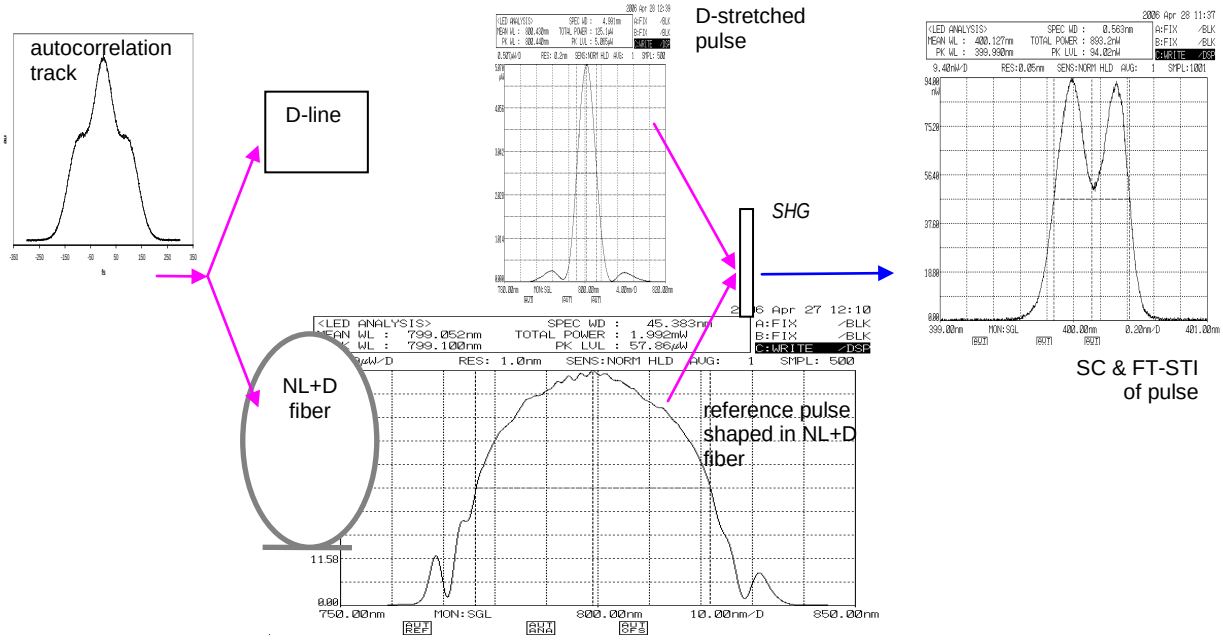

Fig. 3.1.2. Performance of the STI through parabolic temporal lensing in SFG.

Fig. 3.1.3(a) shows the images of the pulses stretched in glasses with different thickness. Comparison with the relevant autocorrelation tracks (on the right) shows a reasonable accordance. Figures 3.1.3(b)– 3.1.3(d) and 3.1.3(f) present the spectral images of two-peak pulses in the 12×, 2.5×, and 1.2× regimes of the spectral compression: the pulse and image autocorrelation tracks coincide practically for all regimes. In Fig. 3.1.3(e) the spectral image of the pulse with a substructure is shown: the pulse and image autocorrelation tracks are in quantitative accordance.

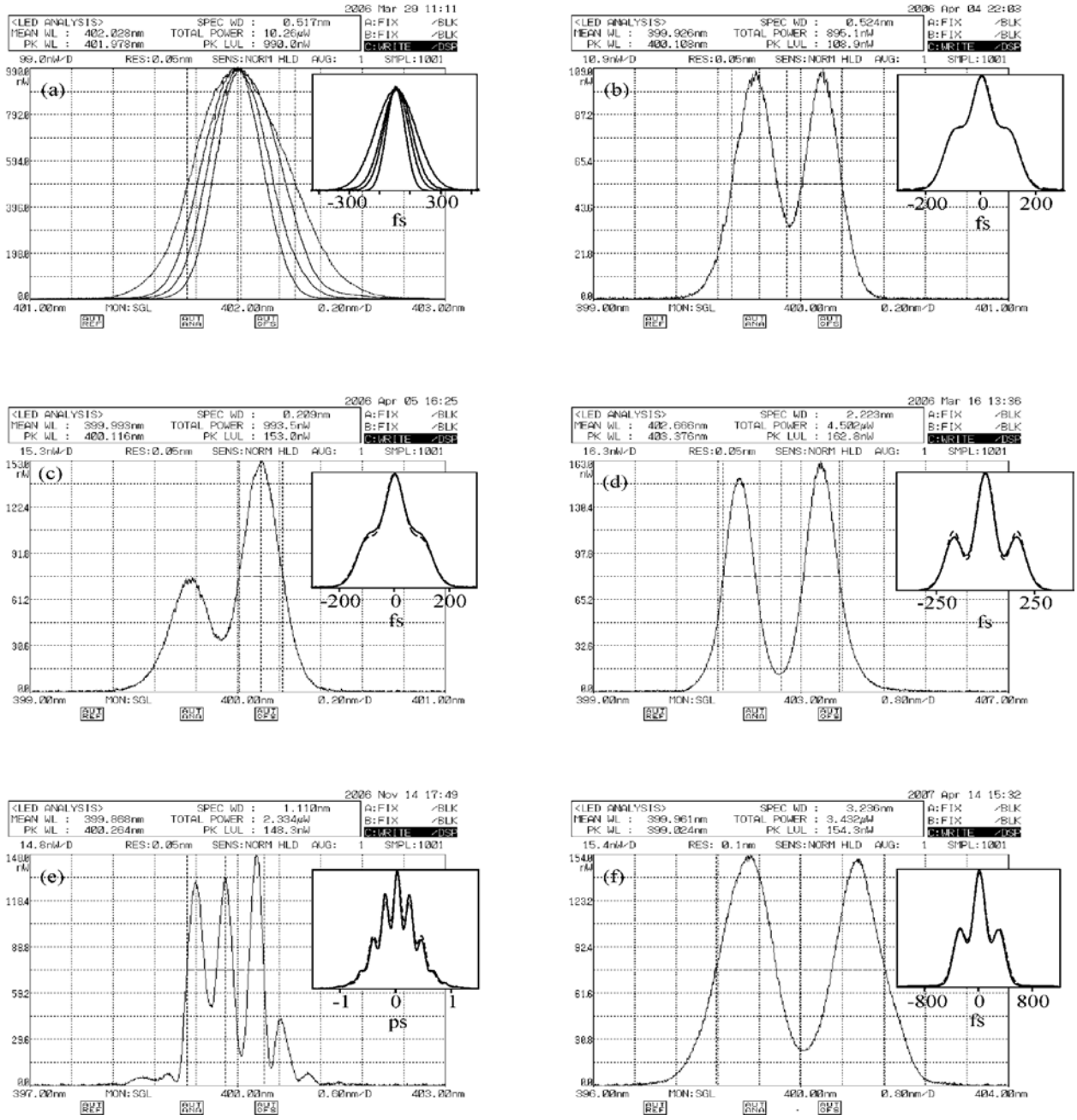

Fig. 3.1.3. STI of different pulses: (a) pulses stretched in glasses with different thickness; (b), (c), (d), (f) two-peak pulses in the 12×, 2.5×, and 1.2× regimes of spectral compression; (e) pulse with substructure. On the right, autocorrelation tracks of the signal pulses and their images are shown.

The principal resolution of the method is conditioned by the bandwidth of the reference pulse. Along with it, the spectral resolution of the spectrometer, which is 0.05 nm in our case, can also restrict the temporal resolution of our measurements. We have higher resolution in the case of a broadband spectral image, i.e., in the case of a small ratio of spectral compression. The advantages of the proposed technique are:

- it is free of demand to differentiate the reference and signal radiation by frequency or polarization,
- it is self-referencing (by the self-shaping of sub-parabolic/nonlinear-spectronic reference pulse),
- it permits to follow up the process steps (by spectrotemporal images of D and NL+D interactions of the pulse).

In conclusion, we have proposed and experimentally demonstrated a new method of aberration-free time-to-frequency conversion through temporal lensing by wave mixing process. This all-optical time-to-frequency imaging allows direct, real-time pulse characterization on the femtosecond time-scale. The self-shaping of the reference pulse in a SMF makes our technique a self-referencing one. The reference and signal pulses interact with each other in SHG nonlinear crystal. The spectral profile of the non-collinear SFG repeats the initial pulse temporal profile. For this technique there are no principal restrictions on the reference pulse polarization and wavelength.

Experiments on imaging simple and complex femtosecond pulses' by our technique show a good agreement between the measured and calculated autocorrelation tracks. The registered image is reliable in a wide range of intensity variation. Using a non-collinear interaction of the signal and reference pulses in nonlinear crystal allows background-free registrations. The separated D-line and NL+D media in the spectral compressor allow us to follow up and control the pulse imaging criterions by spectrotemporal images of the pulses passed through.

¢3.2. SPIRIT for characterization of few-cycle femtosecond pulses

SPIRIT (SPectral Interferometry Resolved In Time) is a characterization method, based on spectral shearing interferometry, and passive and self-referencing as well. Different SPIRIT configurations have shown the method to be convenient either for measurement of single pulses or high repetition rate trains [56, 57]. Also, 2D-SPIRIT offers a direct and intuitive characterization of ultra-short pulses [58]. As will be explained in detail below, in SPIRIT, the frequency shift between the spectra of the two replicas of the input pulse is based on a geometrical shear, and it does not depend on the frequency up-conversion process. The SPIRIT measurement is independent of the input pulse, in contrast to SPIDER [49], where the frequency conversion stage may depend on the pulse initial features, namely on its chirp. The SPIRIT arrangement is avoiding the use of expensive or intricate tools, such as the streak camera required for implementing SORBETS [54].

In this section, we present a version of SPIRIT for measuring very large spectral bandwidth pulses, Wideband-SPIRIT. The principles of Wideband SPIRIT and its configuration aiming at the characterization of pulses with just a few femtoseconds duration and a broad bandwidth are described in detail. Furthermore, the data processing allowing few-cycle pulse complete characterization are briefly explained, and experimental results are presented.

This experiment is done together with the Lluís Martínez-León and Tigran Mansuryan.

3.2.1. General description of SPIRIT

In describing the principle of SPIRIT, first one should create two delayed replicas of the tested pulse. These replicas are sent with a slight angle difference onto a spectroscope that displays two slightly shifted in space identical spectra. At each point of the spectral axis two different frequencies ω and $\omega+\Delta\omega$ interfere leading to temporal beatings, whose phases depend on the tested pulse spectral phase distribution. The resultant instantaneous distribution $I(\omega,t)$ collected at the exit of the spectroscope can be written as

$$I(\omega,t)=\left|E(\omega)\right|^2+\left|E(\omega+\Delta\omega)\right|^2+2\left|E(\omega)\times E(\omega+\Delta\omega)\right|\times\cos\left(\Delta\omega t+\omega\tau+\varphi'(\omega)\Delta\omega\right) \qquad (3.2.1)$$

ω is the frequency and *t* is the time. $E(\omega)$ denotes the electric field of tested pulse. $\Delta\omega$ is the spectral shear introduced between the two replicas. τ is the temporal delay. $\varphi'(\omega)=d\varphi(\omega)/d\omega$ is

the derivative of the spectral phase $\varphi(\omega)$ of the pulse under test ($\varphi'(\omega)\Delta\omega \approx \varphi(\omega+\Delta\omega)-\varphi(\omega)$). For the following step, one needs to have $\varphi'(\omega)$. The problem is that $I(\omega,t)$ cannot be measured with a slow integrating detector, because the beating time period $2\pi/\Delta\omega$ is typically in the range of few picoseconds. In order to avoid the use of an expensive streak camera, SPIRIT is taking a time sample of the space-time interference pattern using a nonlinear time gating technique. For this purpose a fraction of the initial ultrashort pulse has been extracted at the input of the setup. At the exit this non-dispersed ultrashort pulse is used for time gating so the method is passive and self-referencing. The gate pulse is synchronously mixed with the space-time beatings inside a type I nonlinear crystal. The nonlinear crystal is set for non-collinear sum-frequency generation leading to a second harmonic signal, which is the time sample of the studied space-time beatings. Along the spatial coordinate, the sampling step can have two configurations: (i) the spectral components can be sampled one by one using a localized gate (in time and space) or (ii) the spectral components can be sampled simultaneously using a spatially extended gate. In our case, we investigate the second configuration (ii) for which the whole spectrum can be sampled in a single shot working with a spatially wide gate.

3.2.2. Specificity of wideband SPIRIT

The SPIRIT principle is illustrated in Fig. 3.2.1. An input pulse is first split into a temporal gate pulse and a pulse under test, which is further split. These latter replicas are temporally delayed and angularly sheared through a Mach-Zehnder type interferometer, and then they are imaged into a dispersive element. The inset of Fig. 3.2.1 shows the effect of the angular shear at the Fourier plane of the dispersive element, where the angular deviation is transformed into a spatial shear between two spectra. Thus, two spatially shifted spectra of the input pulse are obtained. The interference between these spectra generates spatio-temporal beatings that cannot be discriminated with a slow detector. Instead, the spatio-temporal beatings are sampled thanks to the nonlinear mixing of the temporal gate pulse and the interfering spectra. This is possible by placing a nonlinear crystal at the Fourier plane of the dispersive element. A line detector captures the stationary interferogram, the second harmonic signal, which is processed in real-time. The complete information about the pulse

is retrieved from the interferogram. The method is robust and permits direct and fast pulse characterization.

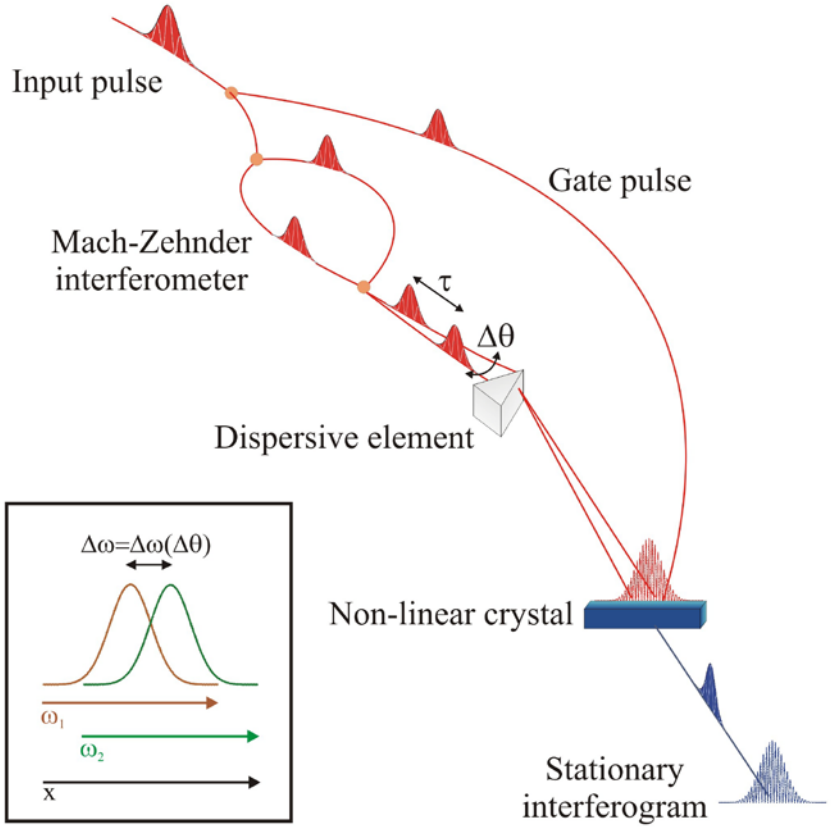

Fig. 3.2.1. Principal scheme of SPIRIT.

Wideband SPIRIT introduces several modifications comparing with previous SPIRIT versions, in order to deal with pulses of just a few femtoseconds duration and a broad bandwidth. Accurate management of the phase introduced by any optical element is required when dealing with broadband pulses. Therefore, lenses have been substituted by focusing mirrors, and a thorough optical design has been implemented. The dispersive element is now a prism. The gate beam is spatially broadened for overlapping the two sheared spectral signals upon the nonlinear crystal (type I BBO). A compact and moveable setup allows the characterization of ultrashort pulses. The setup is shown in Fig. 3.2.2. The real picture of SPIRIT setup is demonstrated in Fig. 3.2.3.

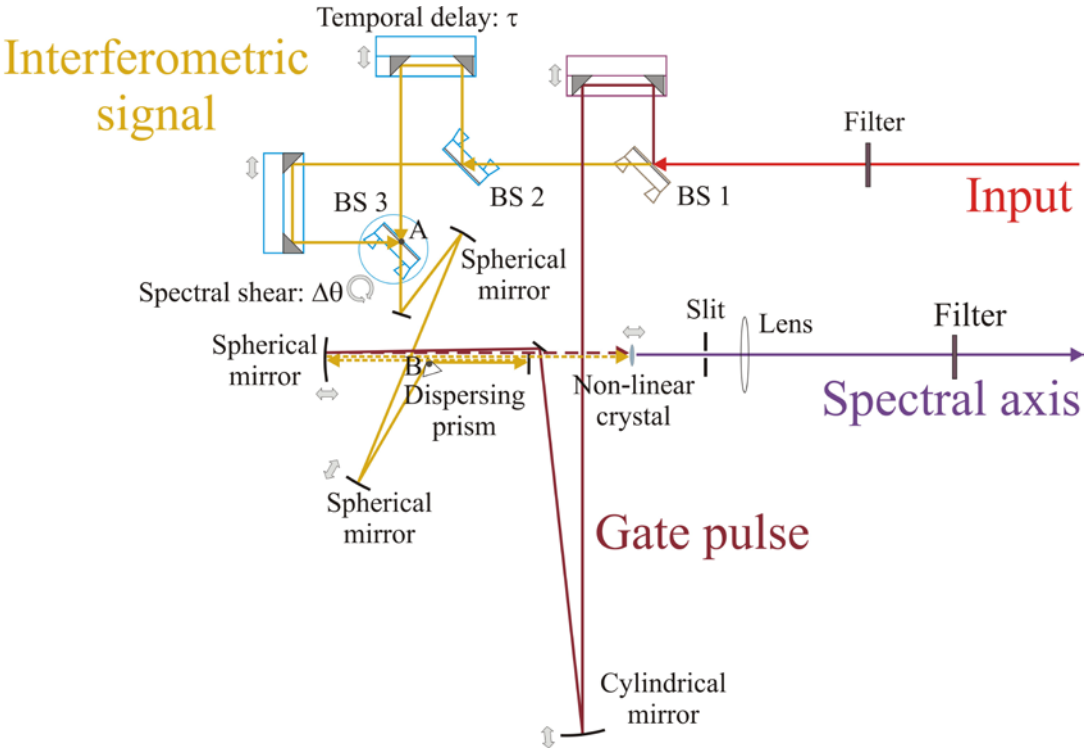

Fig. 3.2.2. Wideband SPIRIT setup.

Fig. 3.2.3. Picture of Wideband SPIRIT real setup.

3.2.3. Pulse reconstruction algorithm

In SPIRIT, the derivative of the input pulse phase is encoded in the recorded interferogram, as a function of the relative positions of the fringes. The gate pulse has just an effect in the second-order mixing, but it does not affect the phase information. An inversion algorithm reconstructs the pulse information from the experimental data [109]. Through few calculation steps, the spectral and temporal pulse profile and the spectral phase information are obtained. Fig. 3.2.4 illustrates that process, beginning with the capture of the one dimensional interference pattern by a linear detector (CCD).

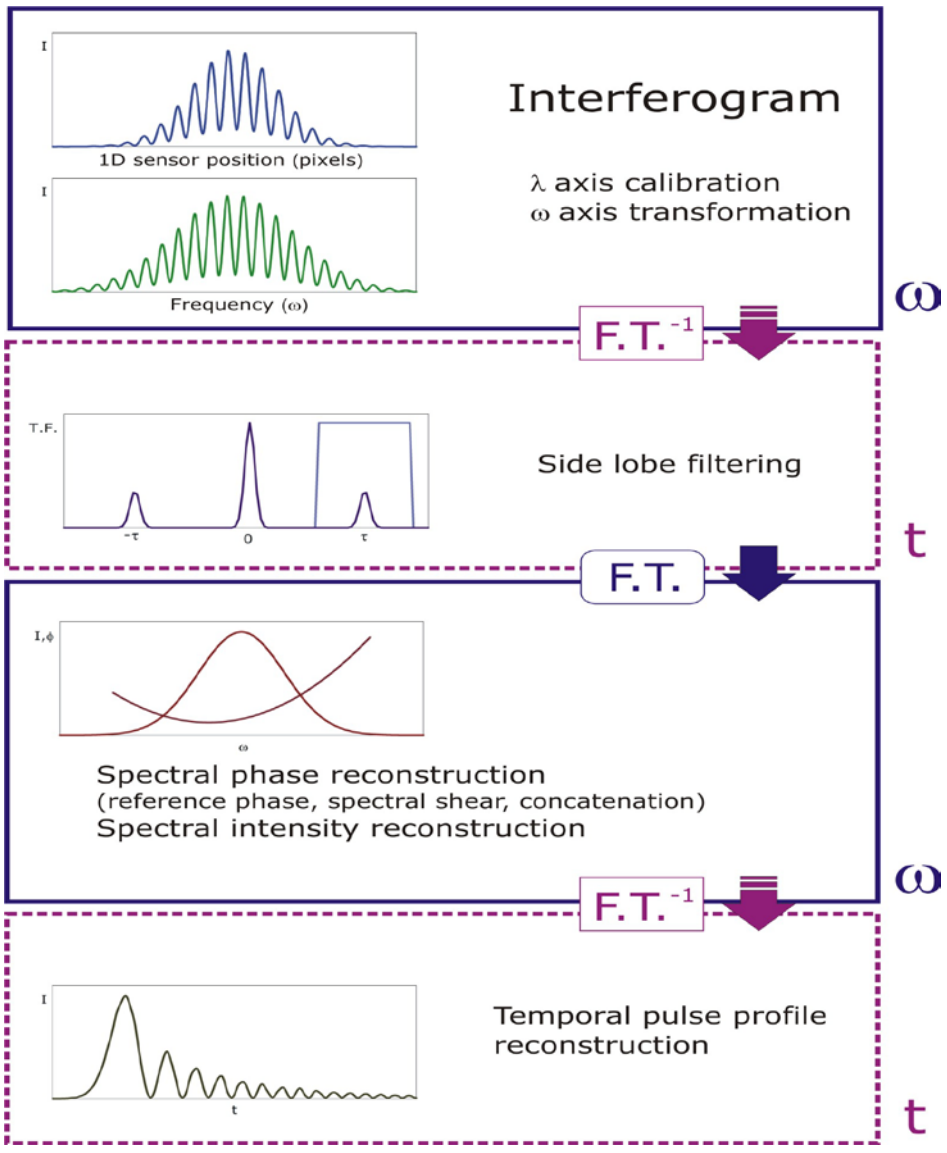

Fig. 3.2.4. Inversion algorithm for complete pulse reconstruction.

Once the data is associated to the proper frequency axis, and after a first Fourier transformation, a numerical filter is applied to isolate, in the temporal axis, the essential information for calculating the input pulse phase derivative. A second Fourier transformation and further calculations provide the spectral phase, once the delay τ and the angular shear are taken into account. A last Fourier transformation brings the data back to the temporal domain, resulting in the final temporal pulse reconstruction.

The method is passive and self-referencing. The time delay between the two pulse replicas and the angular shear are required parameters in order to reconstruct the pulse, but just a single calibration is necessary. This calibration is direct and simple with the actual Wideband SPIRIT arrangement because of the motorized components and monitoring devices included in the setup.

3.2.4. Experimental results

Preliminary experimental results have shown the capability of Wideband SPIRIT for the measurement of ultra-short pulses, like the pulses below 10 fs that have been characterized with our scheme. Low energy (0.25 nJ) pulses below 10 fs directly coming from a Rainbow oscillator (FEMTOLASERS GmbH, 200 nm bandwidth, 75 MHz, 300 mW average power, 810 nm central wavelength) have been measured by means of Wideband SPIRIT. An example of the complete characterization of a 8 fs pulse is shown in Fig. 3.2.5.

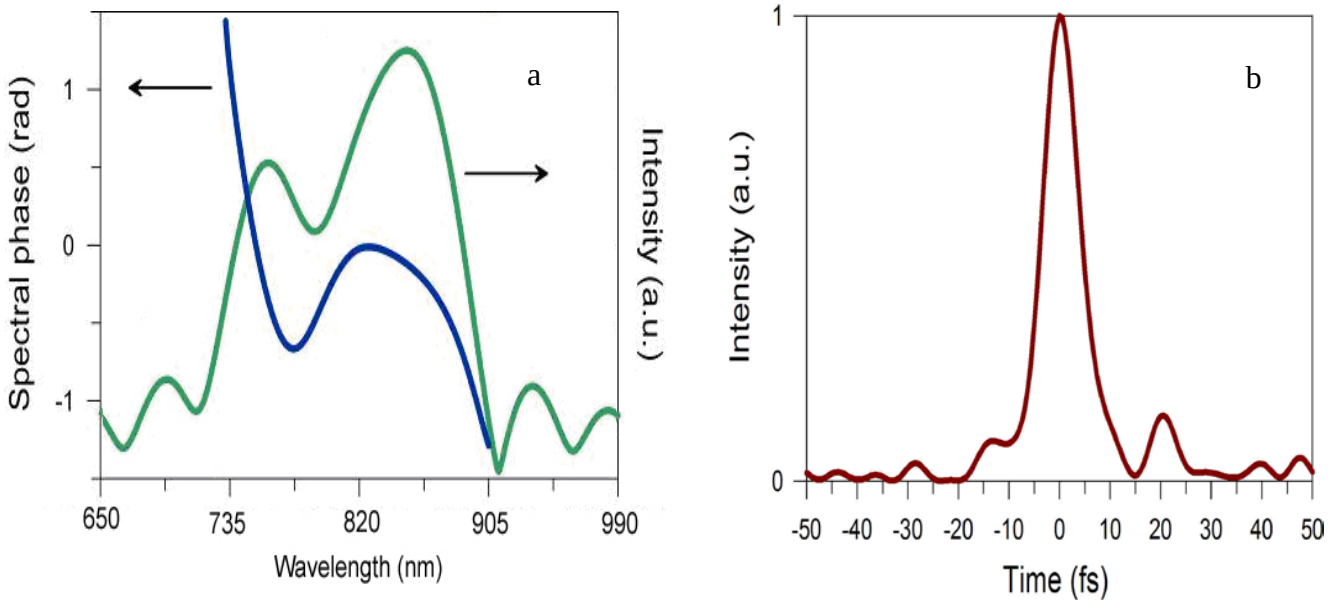

Fig. 3.2.5. 8 fs 0.25 nJ pulse characterization: (a) - spectral phase and spectrum of pulses, (b) - reconstructed pulse temporal profile.

Also, third order dispersion introduced by a piece of glass has been effectively measured. We have performed an experiment with pulses from a COHERENT Micra laser, with a bandwidth of 95 nm, in which TOD is introduced by 16 cm of SF11 glass, and second order dispersion has been compensated through a grism line. In this section, we present the characterization of those pulses mostly influenced by TOD. Fig. 3.2.6. shows the spectral phase, spectrum of the pulses and the reconstructed pulse temporal profile, which is compared in the inset with an additional interferometric autocorrelation trace registered with an independent system.

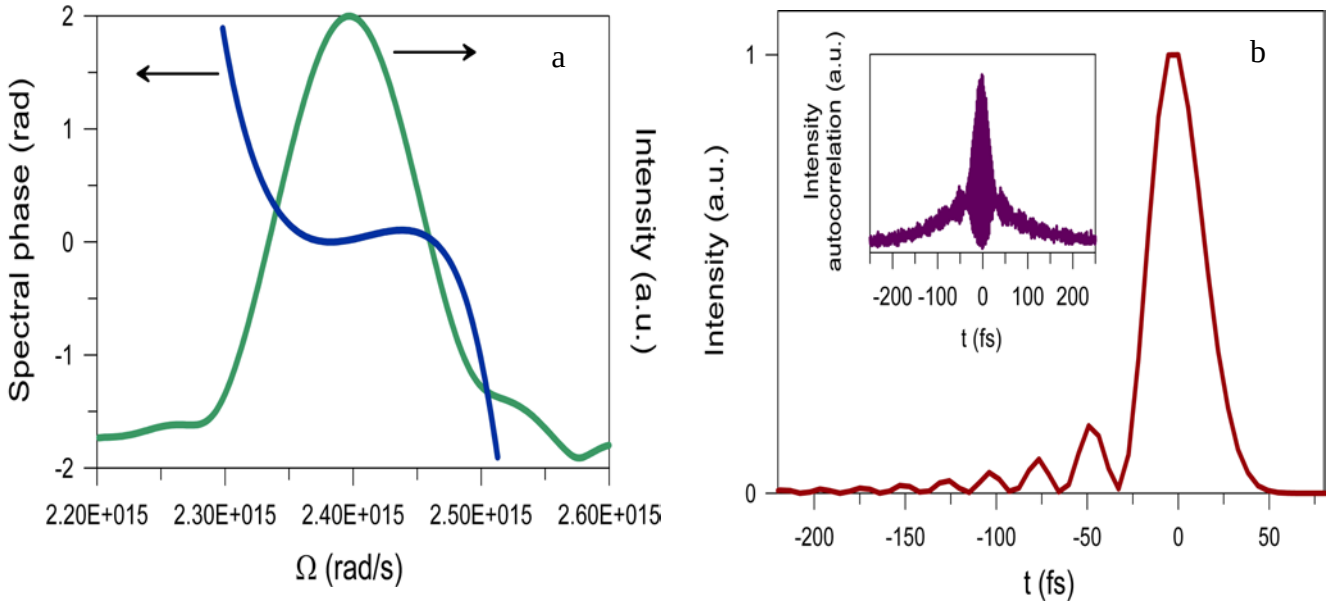

Fig. 3.2.6. Characterization of pulses with third order dispersion: (a) spectral phase and spectrum of pulses, (b) reconstructed temporal profile of pulse. The inset shows the interferometric autocorrelation trace of the same pulse.

3.2.5. Chirpogram

Besides the capabilities presented so far, SPIRIT easily provides data as a sonogram, which enables an intuitive representation of the pulse's dispersion. We have named this image as Chirpogram. According to the description by Walmsley and Dorrer, a sonogram is obtained in the result of applying first, a time-stationary filter, and then a time non-stationary filter, a spectrometer and a temporal gate, respectively, in our case. Thus, simply by scanning the delay of the temporal gate pulse, and using just a single measurement beam instead of the joint interferometric signal, it is possible to retrieve a meaningful picture of the dispersion of the pulse. Experimentally, temporal gating is accomplished by the interaction of the signal and the temporal gate pulses in the nonlinear

crystal. The signal beam has been spatially dispersed by the prism, so that each spectral component occupies a different position on the transversal axis. The gate pulse area has been enlarged in one dimension by a cylindrical lens, in order to overlap at the maximum extent with the spatially dispersed signal, and therefore generate a second harmonic signal containing information about the whole spectrum, as described in the general description of Wideband SPIRIT setup.

Unlike some types of spectrograms, a sonogram not only provides an intuitive representation of the chirp but furthermore, it is sensitive to its sign.

We present simulations and experimental results relating to Chirpogram. In our simulation, some amount of chirp and third order dispersion is introduced into a Fourier limited pulse. The different spectral components of the pulse, which have been at the dispersive prism, travel with a relative delay described by the group delay function, and in this way they interact with the temporal gate pulse in the nonlinear crystal. Finally, the resultant pulse is detected by the linear CCD. The passage through the spectrometer is simulated taking into account the spectrometer's time impulse response in both the time and the frequency domain. One example of our measured chirpograms is shown in Fig.3.2.7.

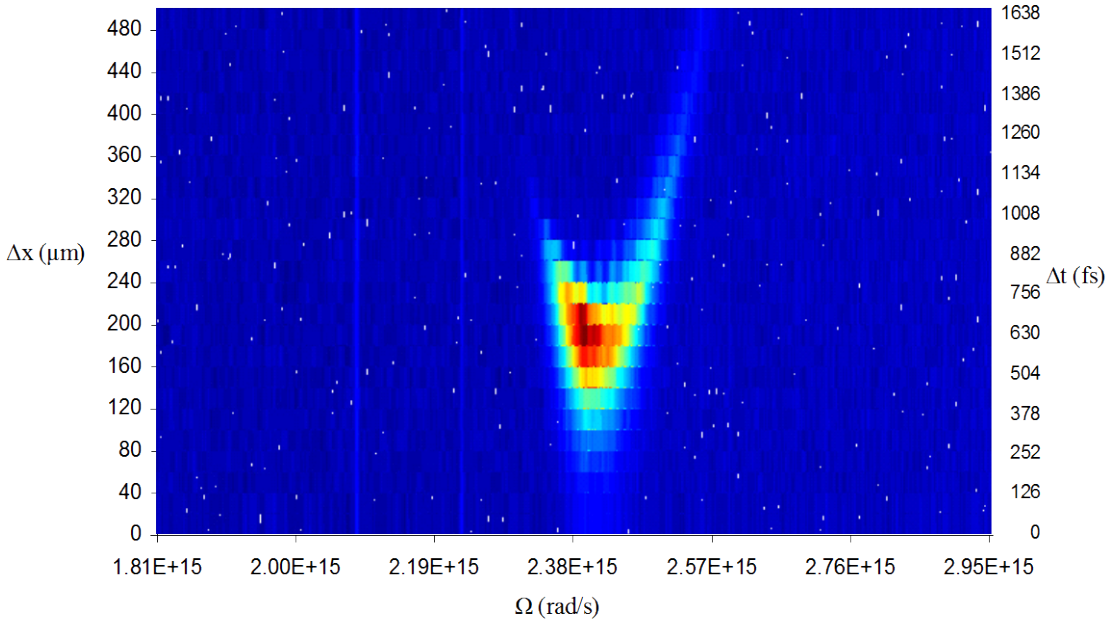

Fig. 3.2.7. Third order dispersion measurement: spectral chirp measured by simple gate scanning over the signal.

3.2.6. Pulse measurements at the exit of fiber delivery scheme

We have used also the Wideband SPIRIT for pulse measurements at the exit of fiber delivery scheme, which was reported in Chapter II. For this purpose we have combined the two experimental setups to be able to measure the compressed pulse at the exit of LMA fiber. Experimental setup is illustrated in Fig. 3.2.8. Using two mirrors we direct the beam after LMA fiber to the SPIRIT setup. We have done not only the measurement of the obtained short pulse, but also several measurements of pulses with different spectral phases. Fig.3.2.9 demonstrates the pulse characterization performed through Wideband SPIRIT at the exit of a 2.7-meter-long LMA fiber for 1-nJ pulses. Pulse duration amounted to 29 fs (FWHM) with 31.6-kW peak power. The delivered pulse has a clean shape with 29-fs-duration (FWHM) and more than 30-kW-peak power. During the experiments we have done also the autocorrelation measurements for comparison with the autocorrelation traces calculated from the pulse temporal profile measured by Wideband SPIRIT. The comparison of the registered and calculated autocorrelation traces is presented in Fig.3.2.10. As can be seen, we have obtained good quantitative and qualitative agreement.

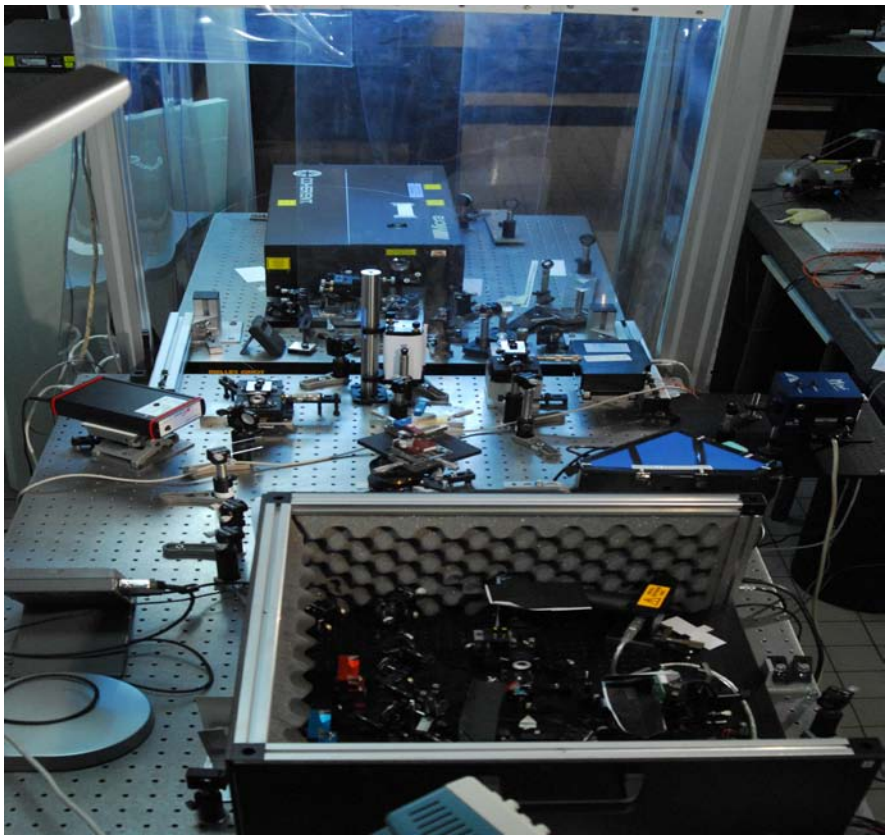

Fig. 3.2.8. Picture of fiber delivery and Wideband SPIRIT combined setups.

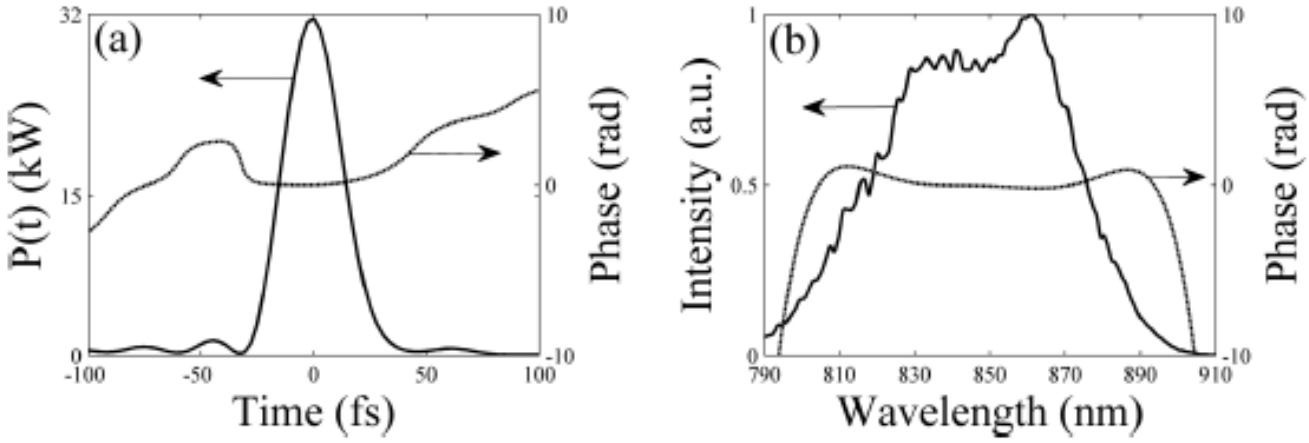

Fig. 3.2.9. Coherent pulse characterization performed through SPIRIT at the exit of a 2.7-meter-long LMA fiber for 1-nJ pulses. Pulse duration amounted to 29 fs (FWHM) with 31.6-kW peak power: (a) reconstructed temporal profile of pulse and temporal phase, (b) spectral phase and spectrum of pulse.

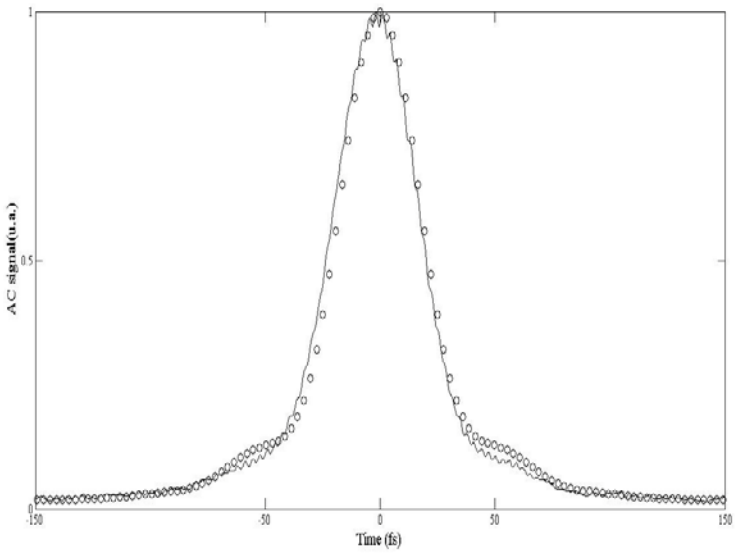

Fig. 3.2.10. Comparison of registered and calculated autocorrelation traces.

In conclusion we have experimentally demonstrated the measurements of low-energy 8 fs pulses with Wideband SPIRIT, a method for the measurement of ultrashort and wideband pulses based on spectral shearing interferometry. Experimental results demonstrate the capabilities of the method for the characterization of a few femtosecond pulses. Also, third order dispersion measurement has been possible with our system. Experiments for comparing Wideband SPIRIT measurements with other characterization techniques such as FROG or SPIDER are in progress.

Conclusion to chapter III

1. We have proposed and demonstrated experimentally an aberration-free method of parabolic temporal lensing and spectrotemporal imaging based on sum-frequency generation - spectral compression for direct femtosecond-scale temporal measurements. In contrast to contemporary techniques of FROG, SPIDER, SPIRIT, SORBETS, based on spectral phase determination and pulse retrieval, our method provides a direct, high-resolution measurement of the pulse in a standard spectrometer, serving as a basis to design an optical femtosecond oscilloscope, exceeding the bandwidth of the existing electronic oscilloscopes and streak cameras by several orders of magnitude.

2. Wideband SPIRIT, a method for the measurement of a few optical cycle pulses based on spectral shearing interferometry has been demonstrated. Experimental results demonstrate the capabilities of the method for the complete characterization of 0.25 nJ 8 fs pulses. Furthermore, Wideband SPIRIT easily provides data as a sonogram, which enables an intuitive representation of the pulse's dispersion. TOD measurement has been possible with our scheme. Chirpogram not only provides an intuitive representation of the chirp but furthermore, it is sensitive to its sign. Sub-30-fs pulse characterization at the exit of fiber delivery scheme performed through Wideband SPIRIT. For comparing Wideband SPIRIT measurements with other characterization techniques such as FROG or SPIDER a compact and moveable setup has been prepared.

SUMMARY

1. We proposed and experimentally demonstrated an alternative dispersive delay line for ultrashort pulse shaping with the following advantages:
    - compact and simple design, independent of the dispersive force;
    - possibility to induce both negative and positive dispersion;
    - easy tunable dispersion;
    - possibility to shape pulses with different temporal profiles;
    - applicable for picosecond pulses due to the compact design.

    The obtained results are in good accordance with the numerical simulation.

2. We experimentally demonstrated that the fiber group velocity dispersion together with the principal factor of Kerr nonlinearity becomes important for spectral compression. The group velocity dispersion impact is controllable, it can:
    - block spectral compression by temporal recompression of pulse in the fiber;
    - lead to an effective dispersive regime of spectral compression when rectangular Fourier transform pulses are formed along with the achievement of maximal spectral compression ratio.

    These pulses are Fourier transform limited, in contrast to the well known rectangular pulses generated in the fiber due to combined impacts of self-phase modulation and dispersion. Our results of pulse complete characterization obtained by spectral interferometry are in a good agreement with the numerical simulations.

3. We have numerically and experimentally demonstrated an efficient femtosecond fiber delivery setup with improved fiber dispersion precompensation thanks to a high throughput grism-pair stretcher. Sub-30-fs-duration 1-nJ-energy pulses were compressed at the direct exit of 2.7-meters-long large mode area fiber. The proposed device that involves only readily available commercial components is compact in addition of being wavelength tunable over a 100-nm-badwidth around 800 nm. Large mode area fibers gave the best performances in terms of pulse shortness and brightness. But surprisingly standard single mode fibers also gave short and powerful pulses despite their increased nonlinearity.

4. A new programmable direct space-to-time femtosecond pulse shaper using phase-only liquid crystal spatial light modulators has been demonstrated. The experimental setup is very simple and compact. The flexibility of the shaper for amplitude and phase control has been demonstrated by the generation of various pulse sequences with tailored intensity and phase (in the range of π).

5. Evolution of the stretcher-compressor system was experimentally tested. We introduced a spatial light modulator in the grisms stretcher. The goal is to obtain more compressed pulses at the output of the LMA PM fiber. Unfortunately this solution was unsuccessful, and we have identified causes of this failure. To go further, it would be necessary to improve the system to have access to the complex phase by removing the limitations, which were related mainly to the low spectral resolution of the devices and the existence of spatial dispersion effect. The capability of the SLM for pulse shaping was demonstrated by amplitude modulation.

6. We experimentally examine the method of aberration-free time-to-frequency conversion through temporal lensing by wave mixing process. This all-optical time-to-frequency imaging allows direct, real-time pulse characterization on the femtosecond time scale. The self-shaping of the reference pulse in a single-mode fiber makes our technique a self-referencing one. The reference and signal pulses interact with each other in SHG nonlinear crystal. The spectral profile of non-collinear sum-frequency generation repeats the initial pulse temporal profile. There are no principal restrictions on the reference pulse intensity, polarization and wavelength. Experiments on simple and complex femtosecond pulse imaging by our technique show a good agreement between the measured and calculated correlation tracks. The registered image is reliable in a wide range of intensity variation. Using the non-collinear interaction of the signal and reference pulses in nonlinear crystal allows background-free registrations. The separated D-line and NL+D media in the spectral compressor allow us to follow up and control the pulse imaging criterions by spectrotemporal images of the pulses passed through.

7. Wideband SPIRIT, a method for the measurement of a few optical cycle pulses based on spectral shearing interferometry has been demonstrated. Experimental results demonstrate the capabilities of the method for the complete characterization of 0.25 nJ 8 fs pulses. Furthermore, Wideband SPIRIT easily provides data as a sonogram, which enables an intuitive representation of the pulse's dispersion. TOD measurement has been possible with our scheme. Chirpogram not only provides an intuitive representation of the chirp but furthermore, it is sensitive to its sign. Sub-30-fs pulse characterization at the exit of fiber delivery scheme performed through Wideband SPIRIT.

REFERENCES

1. M.T. Asaki, C.P. Huang, D. Garvey, J. Zhou, H.C. Kapteyn M.M. Murnane, “Generation of 11-fs pulses from a self-mode-locked Ti:sapphire laser”, Opt Lett. **18**, 977 (1993)
2. J. Zhou, G. Taft, C.P. Huang, M.M. Murnane, H.C. Kapteyn, “Pulse evolution in a broad-bandwidth Ti:sapphire laser”, Opt. Lett. **19**, 1149 (1994).
3. D.E. Spence, P.N. Kean, W. Sibbett, “60-fsec pulse generation from a self-mode-locked Ti:sapphire laser”, Opt. Lett. **16**, 42 (1991).
4. R.L. Fork, C.H. Cruz, P.C. Becker, C.V. Shank, “Compression of optical pulses to six femtoseconds by using cubic phase compensation”, Opt. Lett. **12**, 483 (1987).
5. W.R. Zipfel, R.M. Williams, W.W. Webb, “Nonlinear magic: multiphoton microscopy in the biosciences”, Nat. Biotechnol. **21**(11), 1369-1377 (2003).
6. D.J. Kane, R. Trebino, “Characterization of arbitrary femtosecond pulses using frequency-resolved optical gating”, IEEE J. Quantum Electron. **29**, 571-579 (1993).
7. J. Heritage, R. Thurston, W. Tomlinson, A. Weiner, R. Stolen, “Spectral windowing of frequency-modulated optical pulses in a grating compressor”, Appl.Phys.Lett. **47**, 87 (1985).
8. P. Tian, D. Keusters, Y. Suzaki, W.S. Warren, “Femtosecond phase-coherent two-dimensional spectroscopy”, Science **300**, 1553-1555 (2003).
9. N. Dudovich, D. Oron, Y. Silberberg, “Single-pulse coherently-controlled nonlinear raman spectroscopy and microscopy”, Nature **418**, 512-514 (2002).
10. M. Shapiro, P. Brumer, “Principles of the Quantum Control of Molecular Processes”, Wiley-Interscience, New Jersey, 2003.
11. N. Karasawa, L. Li, A. Suguro, H. Shigekawa, R. Morita, M. Yamashita, “Optical pulse compression to 5.0 fs by use of only a spatial light modulator for phase compensation”, J. Opt. Soc. Am. B **18**, 1742-1746 (2001).
12. H. Saradesai, C. Chang, A. Weiner, “A Femtosecond Code-Division Multiple- Access Communication System Test Bed”, L. Lightwave Technol. **16**, 1953-1964 (1998).
13. F. Huang, W. Yang, W. Warren, “Quadrature spectral interferometric detection and pulse shaping”, Opt. Lett. **26**, 362-364 (2001).

14. F. Parmigiani, P. Petropoulos, M. Ibsen, D. Richardson, “All-optical pulse reshaping and retiming systems incorporating pulse shaping fiber Bragg grating”, J.Lightwave Technol. **19**, 746 (2001).
15. T. Otani, T. Miyajaki, S. Yamamoto, “Optical 3R regenerator using wavelength converters based on electroabsorption modulator for all-optical network applications”, IEEE Photon. Technol. Lett. **12**, 431 (2000).
16. F. Parmigiani, C. Finot, K. Mukasa, M. Ibsen, M.A. Roelens, P. Petropoulos, D.J. Richardson, “Ultra-flat SPM-broadened spectra in a highly nonlinear fiber using parabolic pulses formed in a fiber Bragg grating,” Opt. Express **14**, 7617 (2006).
17. A.M. Weiner, “Femtosecond optical pulse shaping and processing”, Prog. Quantum Electron. **19**, 161 (1995).
18. T. Kurokawa, H. Tsuda, K. Okamoto, K. Naganuma, H. Takenouchi, Y. Inoue, M. Ishii, “Time-space-conversion optical signal processing using arrayed-waveguide grating”, Electron. Lett. **33**, 1890 (1997).
19. P. Petropoulos, M. Ibsen, A.D. Ellis, D.J. Richardson, “Rectangular pulse generation based on pulse reshaping using a superstructured fiber Bragg grating,” J. Lightwave Technol. **19**, 746 (2001).
20. Y. Park, M. Kulishov, R. Slavík, J. Azaña, “Picosecond and sub-picosecond flat-top pulse generation using uniform long-period fiber gratings”, Opt. Express **14**, 12670 (2006).
21. Y. Park, M.H. Asghari, T.J. Ahn, J. Azaña, “Transform-limited picosecond pulse shaping based on temporal coherence synthesization”, Opt. Express **15**, 9584 (2007).
22. A.M. Weiner, “Programmable shaping of femtosecond optical pulses by use of 128-element liquid crystal phase modulator”, IEEE J. Quantum Electron. **28**, 908-920 (1992).
23. P. Tournois, “Acousto-optic programmable dispersive filter for adaptive compensation of group delay time dispersion in laser systems”, Opt. Commun. **140**, 245-349 (1997).
24. F. Verluise, V. Laude, Z. Cheng, Ch. Spielmann, P. Tournois, “Amplitude and phase control of ultrashort pulses by use of an acousto-optic programmable dispersive filter: pulse compression and shaping”, Opt. Lett. **25**, 575-577 (2000).
25. S. Coudreau, D. Kaplan, P. Tournois, “Ultraviolet acoustooptic programmable dispersive filter laser pulse shaping in KDP”, Opt. Lett. **31**, 1899-1901 (2006).

26. R. Ell, U. Morgner, F.X. Kartner, J.G. Fujimoto, E.P. Ippen, V. Scheuer, G. Angelow, T. Tschudi, M.J. Lederer, A. Boiko,B. Luther-Davies, “Generation of 5 fs pulses and octave-spanning spectra directly from a Ti:sapphire laser”, Opt. Lett. **26**, 373-375 (2001).
27. E. Matsubara, K. Yamane, T. Sekikawa, M. Yamashita, “Generation of 2:6 fs optical pulses using induced-phase modulation in a gas-filled hollow fiber”, J. Opt. Soc. Am. B **24**, 985-989 (2007).
28. K. Hazu, T. Sekikawa, M. Yamashita, “Spatial light modulator with an over-two-octave bandwidth from ultraviolet to near infrared”, Opt. Lett. **32**, 3318-3320 (2007).
29. T. Tanigawa, Y. Sakakibara, S. Fang, T. Sekikawa, M. Yamashita, “Spatial light modulator of 648 pixels with liquid crystal transparent from ultraviolet to near-infrared and its chirp compensation application”, Opt. Lett. **34**, 1696-1698 (2009).
30. G. Sansone, E. Benedetti, F. Calegari, C. Vozzi, L. Avaldi, R. Flammini, L. Poletto, P. Villoresi, C. Altucci, R. Velotta, S. Stagira, S. De Silvestri, M. Nisoli, “Isolated single-cycle attosecond pulses”, Science **314**, 443-446 (2006).
31. H.A. Haus, C.V. Shank, E.P. Ippen, “Shape of passively mode-locked laser pulses”, Opt. Comm. **15**, 29 (1975).
32. I.S. Ruddock, D.J. Bradley, “Bandwidth-limited subpicosecond pulse generation in modelocked cw dye lasers”, Appl. Phys. Lett. **29**, 296 (1976).
33. K.L. Sala, G.A. Kenney-Wallace, G.E. Hall, “CW Autocorrelation Measurements of Picosecond Laser Pulses”, IEEE J. Quantum Electron. **16**, 990 (1980).
34. H.A. Haus, J.G. Fujimoto, E.P. Ippen, “Structures for additive pulse modelocking”, J. Opt. Soc. Am. B **8**, 2068 (1991).
35. J.W. Nicholson, J. Jasapara, W. Rudolph, F.G. Omenetto, A.J. Taylor, “Full-field characterization of femtosecond pulses by spectrum and cross-correlation measurements”, Opt. Lett. **24**, 1774 (1999).
36. J.C. Diels, J.J. Fontaine, I.C. McMichael, F. Simoni, “Control and measurement of ultrashort pulse shapes (in amplitude and phase) with femtosecond accuracy”, Appl. Opt. **24**, 1270 (1985).
37. S. Prein, S. Diddams, J.C. Diels, “Complete characterization of femtosecond pulses using an all-electronic detector”, Opt. Comm. **123**, 567 (1996).

38. G. Steinmeyer, D.H. Sutter, L. Gallmann, N. Matuschek, U. Keller “Frontiers in Ultrashort Pulse Generation: Pushing the Limits in Linear and Nonlinear Optics”, Science **286**, 1507 (1999).
39. I.A. Walmsley, V. Wong, “Characterization of the electric field of ultrashort optical pulses”, J. Opt. Soc. Am. B **13**, 2453 (1996).
40. D.J. Kane, R. Trebino, “Characterization of Arbitrary Femtosecond Pulses Using Frequency-Resolved Optical Gating”, IEEE J. Quantum Electron. **29**, 571 (1993).
41. R. Trebino, K.W. DeLong, D.N. Fittinghoff, J. Sweetser, M.A. Krumbügel, B. Richman, “Measuring ultrashort laser pulses in the time-frequency domain using frequency resolved optical gating”, Rev. Sci. Instrum. **68**, 1 (1997).
42. R. Trebino, D.J. Kane, “Using phase retrieval to measure the intensity and phase of ultrashort pulses: frequency-resolved optical gating”, J. Opt. Soc. Am. A **10**, 1101 (1993).
43. K.W. DeLong, R. Trebino, J. Hunter, W.E. White, “Frequency-resolved optical gating with the use of second-harmonic generation”, J. Opt. Soc. Am. B **11**, 2206 (1994).
44. A. Baltuska, M.S. Pshenichnikov, D.A. Wiersma, “Amplitude and phase characterization of 4.5-fs pulses by frequency-resolved optical gating”, Opt. Lett. **23**, 1474 (1998).
45. S. Linden, H. Giessen, J. Kuhl, “XFROG - A New Method for Amplitude and Phase Characterization of Weak Ultrashort Pulses”, Phys. Stat. Sol. B **206**, 119 (1998).
46. S. Linden, J. Kuhl, H. Giessen, “Amplitude and phase characterization of weak blue ultrashort pulses by down conversion”, Opt. Lett. **24**, 569 (1999).
47. C. Froehly, A. Lacourt, J.C. Vienot, “Notions de réponse impulsionelle et de fonction de transfert temporelles des pupilles optiques, justifications expérimentales et applications”, Nouv. Rev. Optique **4**, 183 (1973).
48. J. Piasecki, B. Colombeau, M. Vampouille, C. Froehly, J.A. Arnaud, “Nouvelle méthode de mesure de la réponse impulsionelle des fibres optiques”, Appl. Opt. **19**, 3749 (1980).
49. C. Iaconis, I.A. Walmsley, “Spectral phase interferometry for direct electric-field reconstruction of ultrashort optical pulses”, Opt. Lett. **23**, 792 (1998).
50. V.A. Zubov, T.I. Kuznetsova, “Solution of the phase problem for time-dependent optical signals by an interference system”, Sov. J. Quantum Electron. **21**, 1285 (1991).

51. T.M. Shuman, M.E. Anderson, J. Bromage, C. Iaconis, L. Waxer, I.A. Walmsley, “Real-time SPIDER: ultrashort pulse characterization at 20 Hz”, Opt. Express **5**, 134 (1999)
52. C. Dorrer “Implementation of spectral phase interferometry for direct electric-field reconstruction using a simultaneously recorded reference interferogram”, Opt.Lett. **24**, 1532 (1999).
53. L. Gallmann, G. Steinmeyer, D.H. Sutter, T. Rupp, C. Iaconis, I.A. Walmsley, U. Keller, “Spatially resolved amplitude and phase characterization of femtosecond optical pulses”, Opt. Lett. **26**, 98 (2001).
54. P. Kockaert, M. Haelterman, Ph. Emplit, C. Froehly, “Complete characterization of ultrashort optical pulses using fast linear detectors”, IEEE J. Sel. Top. Quantum Electron. **10**, 206-212 (2004).
55. A. Zeytunyan, A. Muradyan, G. Yesayan, L. Mouradian, F. Louradour, A. Barthélémy “Generation of broadband similaritons for complete characterization of femtosecond pulses”, Opt. Commun. **284**, 3742-3747 (2011).
56. V. Messager, F. Louradour, C. Froehly, A. Barthélémy “Coherent measurement of short laser pulses based on spectral interferometry resolved in time”, Opt. Lett. **28**, 743-745 (2003).
57. M. Lelek, F. Louradour, A. Barthélémy, C. Froehly, “Time resolved spectral interferometry for single shot femtosecond characterization”, Opt. Commun. **261**, 124-129 (2006).
58. M. Lelek, F. Louradour, A. Barthélémy, C. Froehly, T. Mansuryan, L. Mouradian, J.P. Chambaret, G. Chériaux, B. Mercier, “Two-dimensional spectral shearing interferometry resolved in time for ultrashort optical pulse characterization”, J. Opt. Soc. Am. B **25**, A17-A24 (2008).
59. W.R Zipfel, R.M. Williams, W.W. Webb, “Nonlinear magic: multiphoton microscopy in the biosciences”, Nat. Biotechnol. **21**(11), 1369-1377 (2003).
60. B.A. Flusberg, E.D. Cocker, W. Piyawattanametha, J.C. Jung, E.L. Cheung, M.J. Schnitzer, “Fiberoptic fluorescence imaging”, Nat. Methods **2**(12), 941-950 (2005).
61. G.P. Agrawal, Nonlinear Fiber Optics (Academic, 2001).

62. S. Ramachandran, M.F. Yan, J. Jasapara, P. Wisk, S. Ghalmi, E. Monberg, F.V. Dimarcello, “High-energy (nanojoule) femtosecond pulse delivery with record dispersion higher-order mode fiber”, Opt. Lett. **30**(23), 3225-3227 (2005).
63. F. Luan, J.C. Knight, P.St.J. Russell, S. Campbell, D. Xiao, D.T. Reid, B.J. Mangan, D.P. Williams,P.J. Roberts, “Femtosecond soliton pulse delivery at 800nm wavelength in hollow-core photonic bandgap fibers”, Opt. Express **12**(5), 835–840 (2004).
64. J.S. Skibina, R. Iliew, J. Bethge, M. Brock, D. Fischer, V.I. Beloglasov, R. Wedell, G. Steinmeyer, “A chirped photonic-crystal fibre”, Nat. Photonics **2**(11), 679–683 (2008).
65. F. Helmchen, D.W. Tank, W. Denk, “Enhanced Two-Photon Excitation Through Optical Fiber by Single-Mode Propagation in a Large Core”, Appl. Opt. **41**, 2930 (2002).
66. L. Fu, X. Gan, M. Gu, “Use of a single-mode fiber coupler for second-harmonic-generation microscopy”, Opt. Lett. **30**, 385 (2005).
67. W. Göbel, A. Nimmerjahn, F. Helmchen, “Distortion-free delivery of nanojoule femtosecond pulses from a Ti:sapphire laser through a hollow-core photonic crystal fiber”, Opt. Lett. **29**, 1285 (2004).
68. S. Ramachandran, M.F. Yan, J. Jasapara, P. Wisk, S. Ghalmi, E. Monberg, F.V. Dimarcello, “High-energy (nanojoule) femtosecond pulse delivery with record dispersion higher-order mode fiber”, Opt. Lett. **30**, 3225 (2005).
69. A.M. Larson, A.T. Yeh, “Delivery of sub-10-fs pulses for nonlinear optical microscopy by polarization-maintaining single mode optical fiber”, Opt. Express **16**, 14723 (2008).
70. J.C. Knight, P.St.J. Russell, “New Ways to Guide Light”, Science **296**, 276 (2002).
71. J. Limpert, T. Schreiber, S. Nolte, H. Zellmer, A. Tunnermann, R. Iliew, F. Lederer, J. Broeng, G. Vienne, A. Petersson, C. Jakobsen, “High-power air-clad large-mode-area photonic crystal fiber laser”, Opt. Express **11**, 818 (2003).
72. L. Fu, X. Gan, M. Gu, “Nonlinear optical microscopy based on double-clad photonic crystal fibers”, Opt. Express **13**, 5528 (2005).
73. D. Bird, M. Gu, “Two-photon fluorescence endoscopy with a micro-optic scanning head”, Opt. Lett. **28**, 1552 (2003).
74. H. Wang, T.B. Huff, J.X. Cheng, “Coherent anti-Stokes Raman scattering imaging with a laser source delivered by a photonic crystal fiber”, Opt. Lett. **31**(10), 1417–1419 (2006).

75. E.T.J. Nibbering, G. Grillon, M.A. Franco, B.S. Prade, A. Mysyrowicz, “Determination of the inertial contribution to the nonlinear refractive index of air, N2, and O2 by use of unfocused high-intensity femtosecond laser pulses”, J. Opt. Soc. Am. B **14**(3), 650 (1997).
76. C. Brée, A. Demircan, G. Steinmeyer, “Method for Computing the Nonlinear Refractive Index via Keldysh Theory”, IEEE J. Quantum Electron. **46**(4), 433–437 (2010).
77. H. Garcia, A.M. Johnson, F.A. Oguama, S. Trivedi, “New approach to the measurement of the nonlinear refractive index of short (<25 m) lengths of silica and erbium-doped fibers”, Opt. Lett. **28**(19), 1796–1798 (2003).
78. D.G. Ouzounov, F.R. Ahmad, D. Müller, N. Venkataraman, M.T. Gallagher, M.G. Thomas, J. Silcox, K.W. Koch, A.L. Gaeta, “Generation of megawatt optical solitons in hollow-core photonic band-gap fibers”, Science **301**(5640), 1702–1704 (2003).
79. M.G. Welch, C.E. de Nobriga, R.A. Correa, W.J. Wadsworth, J.C. Knight, “Accurate measurement of the dispersion of hollow-core fibers using a scalable technique”, Opt. Express **17**, 9006 (2009).
80. W. Göbel, A. Nimmerjahn, F. Helmchen, “Distortion-free delivery of nanojoule femtosecond pulses from a Ti:sapphire laser through a hollow-core photonic crystal fiber”, Opt. Lett. **29**, 1285 (2004).
81. J.S. Skibina, R. Iliew, J. Bethge, M. Bock, D. Fischer, V.I. Beloglasov, R. Wedell, G. Steinmeyer, “A chirped photonic-crystal fibre”, Nat. Photon. **2**, 679 (2008).
82. S.L. Shapiro, “Ultrashort light pulses: picosecond techniques and applications”, Berlin, Germany: Springer-Verlag, (1977).
83. M. Haner, W.S. Warren, “Generation of arbitrarily shaped pico second optical pulses using an integrated electro optic waveguide modulator”, Applied Optices **26**(17), 3687 (1987).
84. J.P. Heritage, A.M. Weiner, R.N. Thurston, “Picosecond pulse shaping by spectral phase and amplitude manipulation”, Opti. Lett. **10**, 609-611 (1985).
85. A.M. Weiner, “Femtosecond pulse shaping using spatial light modulators”, Rev. Sci. Instrum. **71**, 1929–1960 (2000).
86. E.B. Treacy, “Optical Pulse Compression with. Diffraction Gratings”, IEEE J. of Quantum Electron. **5**(9), 454-458 (1969).

87. A.V. Weiner, J.P. Heritage, R.N. Thurston, “Synthesis of phase-coherent, picosecond optical square pulses”, Opt. Lett. **11**, 153 (1986).
88. H. Nakatsuka, D. Grischkowsky, “Recompression of optical pulses broadened by passage through optical fibers”, Opt. Lett. **6**, 13-15 (1981).
89. M.A. Duguay, J.W. Hansen, “Compression of pulses from a mode-locked He-Ne laser”, Appl. Phys. Lett. **14**, 14 (1969).
90. G. Lenz, B.J. Eggleton, C.K. Madsen, R.E. Slusher, “Optical delay lines based on optical filters”, IEEE J. Quant. Electron. **37**, 525 (2001).
91. J. van Howe, Ch. Xu, “Ultrafast optical delay line using a time-prism pair”, Opt. Lett. **30**, 99 (2005).
92. А.П. Сухоруков, А.К. Сухорукова, Изв. АН СССР, Сер. физ. **46**, 2017 (1982)
93. G.J. Tearney, B.E. Bouma, J.G. Fujimoto, “High-speed phase- and group-delay scanning with a grating-based phase control delay line”, Opt. Lett. **22**, 1811 (1997).
94. Р.Б. Алавердян, С.М. Аракелян, Л.П. Геворкян, В.А. Макаров, А.А. Оганян, Т.А. Папазян, Ю.С. Чилингарян. “Жидкокристаллический транспарант для широкоапертурной компрессии пикосекундных лазерных импульсов и получения спектрально-ограниченного излучения”, ЖТФ **61**, 118-125 (1991).
95. Z. Bor, B. Racz, “Group Velocity Dispersion in Prisms and its Application to Pulse Compression and Travelling-Wave Excitation”, Opt. Commun. **54**, 165 (1985).
96. S.A. Akhmanov, V.A. Vysloukh, A.S. Chirkin, Optics of Femtosecond Laser Pulses (Nauka, Moscow, 1988) [in Russian].
97. J.W. Goodman, Introduction to Fourier Optics (McGraw-Hill, New York, 1968).
98. V.V. Lebedeva, Optical Spectroscopy Techniques (Izdat. MGU, Moscow, 1986) [in Russian].
99. D.S. Citrin, “Self-pulse-shaping coherent control of excitons in a semiconductor microcavity”, Phys. Rev. Lett. **77**, 4596 (1996).
100. W. Ingo, K. Guido, “Generation of flat-top picosecond pulses by coherent pulse stacking in a multicrystal birefringent filter”, Optics Express **16**(19), 14922 (2008).

101. W. Wang, Y. Wang, K. Allaart, D. Lenstra, “Subpicosecond Rectangular Optical Pulse Generator Using Cascaded Nonlinear Directional Couplers”, Proceedings Symposium IEEE/LEOS 1. Benelux Chapter, 37 (2004).

102. S. Cialdi, I. Boscolo, A. Flacco, “Features of a phase-only shaper set for a long rectangular pulse”, J. Opt. Soc. Am. B **21**, 1693 (2004).

103. D. Wang, S. Fujioka, H. Chuen Lim, K. Thanakom, S.-Y. Kim, K. Kikuchi, “Rectangular Short Pulse Generation by Using Strong Unchirped Fiber Bragg Grating”, CLEO-2006, Conf. Digest, JThC105 (2006).

104. S.A. Akhmanov, V.A. Vysloukh, A.S. Chirkin, Optics of Femtosecond Laser Pulses (New York: AIP, 1991, Moscow: Nauka, 1998).

105. M. Oberthaler, R.A. Hopfel “Spectral Narrowing of Ultrashort Laser Pulses by Self-Phase Modulation in Optical Fibers”, Appl. Opt. **63**(8), 1017-1019 (1993).

106. N.L. Margaryan, L.Kh. Mouradian, T.A. Papazyan, “Spectral compression of ultrashort laser pulses”, Sov. J. Quantum Electron. **21**, 783-785 (1991).

107. A.A. Kutuzyan, T.G. Mansuryan, G.L. Yesayan, R.S. Akopyan, L.Kh. Muradian, “Dispersive regime of spectral compression”, Quantum Electron. **38**(4), 383 (2008).

108. C. Froehly, A. Lacourt, J.C. Vienot, “Time impulse response and time frequency response of optical pupils. Experimental confirmations and applications”, J. Opt. **4**, 183 (1973).

109. M. Takeda, H. Ina, S. Kobayashi, “Fourier-transform method of fringe-pattern analysis for computer-based topography and interferometry”, J. Opt. Soc. Am. **72**, 156-160 (1982).

110. AM. Weiner, “Femtosecond pulse shaping using spatial light modulators”, Rev Sci Imstrum **71**, 1929–1960 (2000).

111. F. Verluise, V. Laude, Z. Cheng, C. Spielmann, P. Tournois, “Amplitude and phase control of ultrashort pulses by use of an acousto-optic programmable dispersive filter: pulse compression and shaping”, Opt Lett **25**, 575–577 (2000).

112. J.A. Davis, K.O. Valadéz, D.M. Cottrell, “Encoding Amplitude and Phase Information onto a Binary Phase-Only Spatial Light Modulator”, Appl. Opt. **42**, 2003 (2003).

113. J. Bourderionnet, A. Brignon, J.P. Huignard, A. Delboulb, B. Loiseaux, “Spatial mode control of a diode-pumped NdYAG laser by an intracavity liquid-crystal light valve”, Optics Letters **26**, 1958-1960 (2001).

114. B. Wattelier, C. Sauteret, J.C. Chanteloup, A. Migus, “Beam-focus shaping by use of programmable phase-only filters: application to an ultralong focal line”, Optics Letters **27**, 213-215 (2002).

115. C. Kohler, X. Schwab, W. Osten, “Optimally tuned spatial modulators for digital holography”, Applied Optics **45**, 960-967 (2006).

116. L.P. Zhao, N. Bai, X. Li, L.S. Ong, Z.P. Fang, A.K. Asundi, “Efficient implementation of a spatial light modulator as a diffractive optical microlens array in a digital Shack-Hartmann wavefront sensor”, Applied Optics **45**, 90-94 (2006).

117. D.E. Leaird, A.M. Weiner, “Femtosecond optical packet generation by a direct space-to-time pulse shaper”, Opt. Lett. **24**, 853 (1999).

118. A. Vega, D.E. Leaird, A.M. Weiner, “High-speed direct space-to-time pulse shaping with 1 ns reconfiguration”, Opt. Lett. **35**, 1554 (2010).

119. D.E. Leaird, A.M. Weiner, “Femtosecond direct space-to-time pulse shaping”, IEEE J. Quantum Electron. **37**, 494 (2001).

120. W.R. Zipfel, R.M. Williams, W.W. Webb, “Nonlinear magic: multiphoton microscopy in the biosciences”, Nat. Biotechnol. **21**(11), 1369–1377 (2003).

121. M. Tonouchi, “Cutting-edge terahertz technology”, Nat. Photonics **1**(2), 97–105 (2007).

122. W.L. Chan, J. Deibel, D.M. Mittleman, “Imaging with terahertz radiation”, Rep. Prog. Phys. **70**(8), 1325–1379 (2007).

123. H. Wang, T.B. Huff, J.X. Cheng, “Coherent anti-Stokes Raman scattering imaging with a laser source delivered by a photonic crystal fiber”, Opt. Lett. **31**(10), 1417–1419 (2006).

124. A. Downes, R. Mouras, A. Elfick, “A versatile CARS microscope for biological imaging”, J. Raman Spectrosc. **40**(7), 757–762 (2009).

125. J.X. Cheng, X.S. Xie, “Coherent anti-Stokes Raman scattering microscopy: instrumentation, theory, and applications”, J. Phys. Chem. B **108**(3), 827–840 (2004).

126. F. Ganikhanov, C.L. Evans, B.G. Saar, X.S. Xie, “High-sensitivity vibrational imaging with frequency modulation coherent anti-Stokes Raman scattering (FM CARS) microscopy”, Opt. Lett. **31**(12), 1872–1874 (2006).

127. C.L. Evans, E.O. Potma, D. Côté, C.P. Lin, X.S. Xie, “Chemical imaging of tissue in vivo with video-rate coherent anti-Stokes Raman scattering microscopy,” Proc. Natl. Acad. Sci. U.S.A. **102**(46), 16807–16812 (2005).

128. L. Guittet, G. Launoy, F. Mohammed, D.A. Lieberman, “Screening for colorectal cancer”, N. Engl. J. Med. **362**(1), 84–85 (2010).

129. M. Suter, J. Tschirren, J. Reinhardt, M. Sonka, E. Hoffman, W. Higgins, G. McLennan, “Evaluation of the human airway with multi-detector x-ray-computed tomography and optical imaging”, Physiol. Meas. **25**(4), 837–847 (2004).

130. M.A. Eloubeidi, D. Provenzale, “Does this patient have Barrett’s esophagus? The utility of predicting Barrett’s esophagus at the index endoscopy,” Am. J. Gastroenterol. **94**(4), 937–943 (1999).

131. C.M. Brown, P.G. Reinhall, S. Karasawa, E.J. Seibel, “Optomechanical design and fabrication of resonant microscanners for a scanning fiber endoscope”, Opt. Eng. **45**, 043001-043010 (2006).

132. Y.C. Wu, Y.X. Leng, J.F. Xi, X.D. Li, “Scanning all-fiber-optic endomicroscopy system for 3D nonlinear optical imaging of biological tissues”, Opt. Express **17**(10), 7907–7915 (2009).

133. L. Fu, M. Gu, “Fibre-optic nonlinear optical microscopy and endoscopy”, J. Microsc. **226**, 195 (2007).

134. S.J. Im, A. Husakou, J. Herrmann, “Soliton delivery of few-cycle optical gigawatt pulses in Kagome-lattice hollow-core photonic crystal fibers”, Phys. Rev. A **82**, 025801 (2010).

135. T. Le, J. Bethge, J. Skibina, G. Steinmeyer, “Hollow fiber for flexible sub-20-fs pulse delivery”, Opt. Lett. **36**, 442 (2011).

136. J. Bethge, G. Steinmeyer, S. Burger, F. Lederer, R. Iliew, “Guiding properties of chirped photonic crystal fibers”, J. Lightwave Technol. **27**, 1698 (2009).

137. P. Tournois, “New diffraction grating pair with very linear dispersion for laser pulse compression”, Electron. Lett. **29**, 1414 (1993).

138. E.A. Gibson, D.M. Gaudiosi, H.C. Kapteyn, R. Jimenez, “Efficient reflection grisms for pulse compression and dispersion compensation of femtosecond pulses”, Opt. Lett. **31**, 3363 (2006).

139. T.H. Dou, R. Tautz, X. Gu, G. Marcus, T. Feurer, F. Krausz, L. Veisz, “Dispersion control with reflection grisms of an ultra-broadband spectrum approaching a full octave”, Opt. Express **18**, 27900 (2010).

140. C. Lefort, T. Mansuryan, F. Louradour, A. Barthelemy, “Pulse compression and fiber delivery of 45 fs Fourier transform limited pulses at 830 nm”, Opt. Lett. **36**, 292 (2011).

141. M. Moenster, G. Steinmeyer, R. Iliew, F. Lederer, K. Petermann, “Analytical relation between effective mode field area and waveguide dispersion in microstructure fibers”, Opt. Lett. **31**, 3249 (2006).

142. M. Oberthaler, R. A. Höpfel, “Spectral narrowing of ultrashort laser pulses by self-phase modulation in optical fibers”, Appl. Phys. Lett. **68**, 1017 (1993).

143. G. Steinmeyer, D.H. Sutter, L. Gallmann, N. Matuschek, U. Keller: “Frontiers in Ultrashort Pulse Generation: Pushing the Limits in Linear and Nonlinear Optics”, Science **286**, 1507 (1999).

144. A. Shirakawa, I. Sakane, M. Takasaka, T. Kobayashi: “Sub-5-fs visible pulse generation by pulse-front-matched noncollinear optical parametric amplification”, Appl. Phys. Lett. **74**, 2268 (1999).

145. A. Baltuska, Z. Wei, M.S. Pshenichnikov, D.A. Wiersma, R. Szipöcs: “All-solid- state cavity-dumped sub 5fs laser”, Appl. Phys. B **65**, 175 (1997).

146. M. Nisoli, S. Stagira, S.D. Silvestri, O. Svelto, S. Sartania, Z. Cheng, M. Lenzner, C. Spielmann, F. Krausz: “Compression of High-Energy Laser Pulses Below 5fs”, Appl. Phys. B **65**, 189 (1997).

147. U. Morgner, F.X. Kärtner, S.H. Cho, Y. Chen, H.A. Haus, J.G. Fujimoto, E.P. Ippen, V. Scheuer, G. Angelow, T. Tschudi: “Sub-two-cycle pulses from a Kerr-lens mode-locked Ti:sapphire laser”, Opt. Lett. **24**, 411 (1999).

148. S. Akturk, M. Kimmel, P.O. Shea, R. Trebino, “Measuring spatial chirp in ultrashort pulses using single shot frequency-resolved optical gating”, Opt. Express **11**, 68–78 (2003).

ACKNOWLEDGEMENTS

This thesis would not be possible without the help of many people. I have been very fortunate to work with bright, motivated and talented people.

First of all, I am particularly thankful to my supervisors, Prof. Frederic Louradour and Prof. Levon Mouradian, for their proper and constant wise guidance through my graduate research, and for maintaining an open and interactive environment for me to thrive in.

I would like to express my huge gratitude to Garegin Yesayan for his encouragement and support throughout the entire work. His expert guidance showed me the light at the end of every dark tunnel I encountered during this research.

I would especially like to thank all my colleagues of XLIM laboratory of the University of Limoges in France for offering me the opportunity to obtain a PhD in their research group.

I would like to thank also graduate students and postdocs of the Ultrafast Optics Laboratory group at YSU for all their help.

I would like to thank the examiners of my thesis; I appreciate their constructive suggestions and comments.

Finally I can not thank my family. It would be really difficult for me to complete this work without their immense support, encouragement and love.

MAIN DESIGNATIONS

SMF	single mode fiber
SPM	self-phase-modulation
GVD	group-velocity dispersion
PCF	photonic crystal fiber
DDL	dispersive delay line
OSA	optical spectrum analyzer
SOD	second order dispersion
TOD	third order dispersion
FOD	fourth order dispersion
SFG	sum-frequency generation
SC	spectral compression
NA	numerical aperture
SI	spectral interferometry
MMF	multimode fiber
CPCF	chirped photonic crystal fiber
LMA fiber	large mode area fiber
HOM fiber	higher-order-mode fiber
PBG fiber	photonic band gab fiber
HC-PBGF	hollow core photonic band-gap fiber
PM-SMF	polarization maintaining single mode fiber
DST-PS	direct space-to-time pulse shaping
LC-SLM	liquid crystal spatial light modulator
STI	spectrotemporal imaging
FROG	frequency-Resolved Optical Gating
XFROG	cross-correlation FROG
SPIDER	spectral phase interferometry for direct electric-field reconstruction
SORBETS	superposition of optical radiations and beatings to extract the time signal
SPIRIT	spectral interferometry resolved in time